EQUIVALENT CIRCUITS FOR JUNCTIONS OF LOSSY AND DISPERSIVE VLSI INTERCONNECTS

By

Man-chung SUEN

A Thesis

submitted in partial fulfillment of the requirements

for the Degree of Master of Philosophy

Division of Computer Science

The Chinese University of Hong Hong

November 1994

Acknowledgement

First of all, I would like to express my greatest gratitude to my supervisor, Prof. Omar Wing. His advice and supervision throughout the course of this research project and during the preparation of this dissertation has been indispensable and most valuable. Thanks are also to Dr. K. Y. Lai, Mr. C. M. Fung, Mr. H. K. Yau, and Mr. Angus Siu for their technical help. Finally, I would like to extend my thanks to Dr. F. Y. Chang for his valuable advice to my research.

Abstract

Advances in MOS technology allow VLSI circuits to operate at higher and higher speeds. As a result, VLSI interconnects become lossy transmission lines and the propagated signal will be reflected at the microstrip discontinuities such as bends and junctions. A good CAD package should include accurate models of discontinuities so that VLSI designers can take into account of these high frequency effects during the design stage, and equivalent circuits for these microstrip discontinuities must be developed. To find the equivalent circuits, our approach is firstly to obtain the scattering parameters of the microstrip discontinuities. Then the scattering parameters of the proposed equivalent circuits, which are in terms of the model parameters, are calculated. Finally, the model parameters are determined by optimization.

In this thesis, several wideband equivalent circuits are proposed to model the right-angle bend, T-junction, and tapered line. The equivalent circuits consist of segments of transmission lines and lumped circuit elements. Both TEM and non-TEM lines are used in the models. It is found that the non-TEM models are the best to model the microstrip discontinuities but the TEM models are also adequate in the modelling of the 90^{o} bend and T-junction. The percentage errors of the equivalent circuits are shown to be less than or equal to 10% which is tolerable in the engineering sense. So the TEM models can be used in the CAD software such as SPICE and no FFT or convolution is required in the simulation of circuits that include microstrip discontinuities as circuit elements.

Contents

List of Tables

List of Figures

Chapter 1

Introduction

Due to advances in VLSI technology in recent years, more and more circuitry can be fabricated on a single wafer. To increase the packing density, both at the chip and package level, the cross section of the interconnects is reduced and they are packed closer together. At the same time the propagated signals switch from one value to another with faster rise time. For these reasons, VLSI circuit design can no longer be done by simply applying static digital logic theory as in the design of digital circuits at the SSI level with slow clock rate.

As the wiring cross section is being reduced, the dimension of the interconnects becomes comparable to the wavelengths of the propagated signal, and the interconnects can no longer be regarded as simple metal wires. They must be treated as transmission lines and should be analyzed by applying microwave techniques. These lines are dispersive and lossy and are usually characterized by frequency dependent parameters. Several electromagnetic phenomena, such as pulse dispersion, skin effects, crosstalks and the presence of discontinuities in transmission lines, that are insignificant in previous VLSI design should now be modelled and included in CAD packages in order to be good design tools. One area of interest is to develop frequency dependent equivalent circuits for junctions of interconnects. In VLSI circuits, interconnect junctions include bends, T-junctions, and crossings. A lot of work has been done to find the equivalent inductance and/or capacitance of right-angle bends, mitered

bends with arbitrary angle, T-junctions, and crossings. Benedek and Silvester calculated the equivalent capacitances for right-angle bends, T-junctions, and crossings [SB73]. This was also done by Farrar and Adams using another approach [FA72]. Gopinath, Neale, Easter, and Thomson [GE74, TG75, NG78] extended the analysis to the equivalent inductance. Anders and Arndt used moment method to find the equivalent capacitances and inductances for asymmetric right-angle bends [AA80]. Recently, interest is focused in finding equivalent circuits for multiconductor microstrip bend discontinuities [HM93].

The basic idea of the previous work is to investigate the field behaviour inside the microstrip structure by using some numerical techniques such as moment method. The circuit elements of the equivalent circuit are then calculated to obtain the scattering parameters. All of the above approaches are to find the equivalent lumped circuit elements of the microstrip discontinuities. However, with today's high speed picosecond rise time signal in VLSI circuit design, the lumped equivalent circuits are no longer accurate enough to model the microstrip discontinuities [JY92]. This is demonstrated in Chapter 4. Distributed elements such as uniform microstrip lines have to be incorporated into the model for it to be accurate at frequencies above 20GHz (in order to support the picosecond rise time signal). This CAD model can then be included in any circuit simulation package so that the package is able to describe the high frequency behaviour of the microstrip discontinuities as accurate as possible.

In VLSI design, the time domain response of a circuit is desired. Strictly speaking, if the scattering parameters of a 2-port network are known, one can compute the time response by FFT or similar techniques. However, if it is possible to model a junction by sections of transmission lines plus possibly a few lumped elements, then circuit simulation may proceed directly in the time domain using such standard simulator as SPICE. For this purpose, we investigate how best to represent a junction by a network of transmission lines and

lumped elements. Our approach is to first compute the scattering parameters of a junction using a software called High Frequency Structure Simulator (HFSS) [Hew92]. Then an equivalent circuit is postulated and its parameters are found by optimization. This approach can also be applied if the measured values of the scattering parameters are available. It will be shown later that the equivalent circuits consisting of TEM lines and lumped circuit element are able to model the right-angled bend and T-junction. This implies that their transient responses can be obtained entirely in the time domain by using SPICE because SPICE can only accept constant $RLGC$ values. In this way, there is no need to do FFT and inverse FFT or convolution when finding the transient response.

This thesis consists of eight chapters. In Chapter 2, the method which is used to find the wideband equivalent circuits is discussed. To use this method, scattering parameters which correctly characterize the microstrip discontinuities must firstly be obtained. Scattering parameters are well suited for the characterization and the modelling of linear high-frequency devices. So, in this research project, they are obtained by the HFSS software. In this software, finite element method is used to solve the Maxwell's equations of the microstrip structure with suitable boundary conditions. The scattering parameters are then calculated from the field solutions. The detailed description of the finite element method can be found in [Jac89, Jin93].

Three types of microstrip discontinuities are analyzed: right-angled bend (90^o bend), T-junction, and tapered line. Since the aim of this research project is to show that equivalent circuits with distributed elements are superior in modelling the microstrip discontinuities to the lumped equivalent circuits, only one type of substrate and metal strip material is employed. The substrate used is a lossy alumina with relative permittivity 9.8 and electric loss tangent 0.0003. The metal strip is first assumed to be perfect conductor and then be aluminium (electrical conductivity is 3.5×10^7 S/m) later with skin effects included.

In Chapter 3, the geometry of the three microstrip discontinuities will be firstly described. Then, in Chapter 4, a known lumped equivalent circuit called T-network is used to illustrate that it cannot model the microstrip bend with the frequency range beyond 20GHz. Several new equivalent circuits are then proposed in Chapter 5 for the three types of microstrip discontinuities being analyzed. The modelling performance is recorded in Chapter 6. In this chapter, the new equivalent circuits are called non-TEM wideband equivalent circuits because the microstrip lines in those equivalent circuits are non-TEM dispersive and lossy model. The transmission parameters, $RLGC$, are frequency dependent. In Chpater 7, we use TEM transmission lines instead of the non-TEM ones in those proposed equivalent circuits to test whether they can also be used to model the microstrip discontinuities. In fact, we find models consisting of TEM lines and lumped circuit element for the right-angled bend and T-junction are quite adequate. Finally, a conclusion is made in Chapter 8.

Chapter 2

Approach to Find the Equivalent Models

In this Chapter, the method used to find the circuit elements of the equivalent circuits are described in detail. It is actually a numerical optimization method which minimizes the difference between two sets of scattering parameters of the microstrip structure, one obtained from the HFSS software [Hew92] and one calculated from the equivalent circuits.

2.1 Scattering Parameters of the Microstrip Structure

The scattering parameters associated with a microstrip discontinuity (90° bend, T-junction, and tapered line) are obtained from the software called High Frequency Structure Simulator (HFSS) [Hew92]. Since the interface between any object and the background[1] is assumed to be a thin perfect conductor surface, sufficient distance of the side walls, except the surfaces to be defined as ports, from the microstrip is needed in order to avoid the sidewall field effects[2]. Besides, the air layer should also be thick enough for the same reason (to avoid the field effect from the top surface).

[1]The background is the region that surrounds the geometric model and fills any space not occupied by an object. No material characteristics are assigned to the background.

[2]Sidewalls may become important if the operating frequency is near a resonant frequency of the enclosure. All parts of the circuit will couple to one another through the resonant mode when the circuit is operated near these frequencies.

The material alumina is used as substrate. Its dielectric constant is 9.8 and the electric loss tangent is 0.0003. On the other hand, both perfect conductor and aluminium are used as metal strip in the analysis.

To calculate the scattering parameters of the microstrip structure, HFSS does the followings:

- divides the microstrip structure into a finite element mesh.
- assumes that each port of the structure is excited with a wave travelling along a uniform wave-guiding structure or shielded transmission line that has the same cross section as the port.
- computes the full electromagnetic field pattern (mode) inside the structure resulting from the excitation waves.
- computes the generalized scattering matrix (S-matrices) from the amount of reflection and transmission that occurs.

To find a suitable size of finite element mesh which can accurately describe the electromagnetic field inside the microstrip structure, HFSS first does an adaptive analysis at a particular frequency (usually the median of a range of frequencies is used). After that, it uses that finite element mesh size to calculate the scattering parameters at other frequency points. The frequency range covered is up to 25GHz.

The scattering parameters obtained from the HFSS software[3] are normalized by the natural port impedances[4], so they are called generalized scattering parameters according to the definition given in [Hew92]. This definition is slightly different from that given in [Med92], which states that generalized scattering parameters are the scattering parameters referenced to arbitrary terminations

[3]They will be called simulated scattering parameters later in separation from those calculated from the equivalent circuits, which are called calculated scattering parameters.

[4]Impedance values represent the characteristic impedance of a transmission structure having the same cross section as the port.

at each port. However, we will use the definition given in [Hew92] as our generalized scattering parameters. To renormalize them to a fixed impedance such as 50 ohms, the following formulae are used [Hew92]:

$$\mathbf{Z} = \sqrt{\mathbf{Z_o}}(\mathbf{I}+\mathbf{S})(\mathbf{I}-\mathbf{S})^{-1}\sqrt{\mathbf{Z_o}} \tag{2.1}$$

$$\mathbf{S_\Omega} = \sqrt{\mathbf{Y_\Omega}}(\mathbf{Z}-\mathbf{Z_\Omega})(\mathbf{Z}+\mathbf{Z_\Omega})^{-1}\sqrt{\mathbf{Z_\Omega}} \tag{2.2}$$

where

- $\mathbf{Z}$ is a unique impedance matrix associated with the structure
- $\mathbf{S}$ is the $n \times n$ generalized S-matrix
- $\sqrt{\mathbf{Z_o}}$ is a diagonal matrix having the square root of the characteristic impedance of each port as a diagonal value
- $\mathbf{S_\Omega}$ is the renormalized S-matrix
- $\mathbf{Z_\Omega}$ and $\mathbf{Y_\Omega}$ are diagonal matrices with the desired impedance and admittance as diagonal values

2.2 Optimization Process

After finding the scattering parameters of the microstrip structure by the HFSS software, they are fitted by the calculated scattering parameters. This optimization process is done by calling the *leasqr.m* function of Matlab which is available from the Mathworks ftp site. Levenberg-Marquardt non-linear least squares optimization algorithm [Mar63] is employed. The cost function which is to be minimized is defined as:

$$err(\mathbf{X}) = \frac{1}{N_\omega}\sum_{\omega}\sum_{i,j}\left|\frac{s_{ij}(j\omega) - s_{ij}^{N}(j\omega,\mathbf{X})}{s_{ij}(j\omega)}\right|^2 \tag{2.3}$$

where

- N_ω is the number of frequency points

- $s_{ij}(j\omega)$ is the scattering parameters of the microstrip structure
- $s_{ij}^{N}(j\omega, \mathbf{X})$ is the scattering parameters of the equivalent circuits
- $\mathbf{X}$ is a vector of parameters to be tuned so that $err(\mathbf{X})$ is minimized

or

$$err(\mathbf{X}) = \frac{\| \mathbf{S}(j\omega) - \mathbf{S^N}(j\omega, \mathbf{X}) \|}{\| \mathbf{S}(j\omega) \|} \tag{2.4}$$

where

- $\mathbf{S}(j\omega)$ is a vector of the scattering parameters of the microstrip structure
- $\mathbf{S^N}(j\omega, \mathbf{X})$ is a vector of the scattering parameters of the equivalent circuits
- $\| v \|$ is the 2-norm of a vector v

In this research, Eq. 2.4 will be used because it avoids the possibility of dividing by zero or by a small number.

2.3 Summary

The approach to find the wideband equivalent circuits for the microstrip discontinuities can be summarized in the following steps:

- obtains the simulated scattering parameters from the HFSS software;
- minimizes the value of the cost function (Eq. 2.4) by using the Levenberg-Marquardt non-linear least square algorithm.

Chapter 3

Microstrip Discontinuities Being Modelled

In VLSI circuits, the interconnection network is composed of interconnects (microstrip lines) and junctions, which can be bends, T-junctions, and crossings. Right-angled bends and T-junctions are chosen to be analyzed because they are rather simple and are important components in the interconnection network. Crossings are not considered because they are 4-port networks and it is time-consuming for the HFSS software to calculate the scattering parameters. Tapered lines are considered because they are often used as impedance matching sections in high-speed chip-packages and multichip modules.

The geometry and dimension of the three types of microstrip discontinuities are shown in this chapter. Their dimensions are so chosen because the values are comparable to the typical values in the current packaging technologies [DKR+90]. The air layer of the microstrip structure is supposed to be 10 times the thickness of the substrate to avoid the top-wall field effects.

3.1 Right-Angled Bend

When the metal strip is treated as a perfect metal, the width, w, of the microstrip is $250\mu m$ (Fig. 3.1). The thickness of the substrate, h, is in turn $50\mu m$, $100\mu m$, $150\mu m$, $200\mu m$, and $250\mu m$ so that the $\frac{h}{w}$ ratio is 0.2, 0.4, 0.6, 0.8,

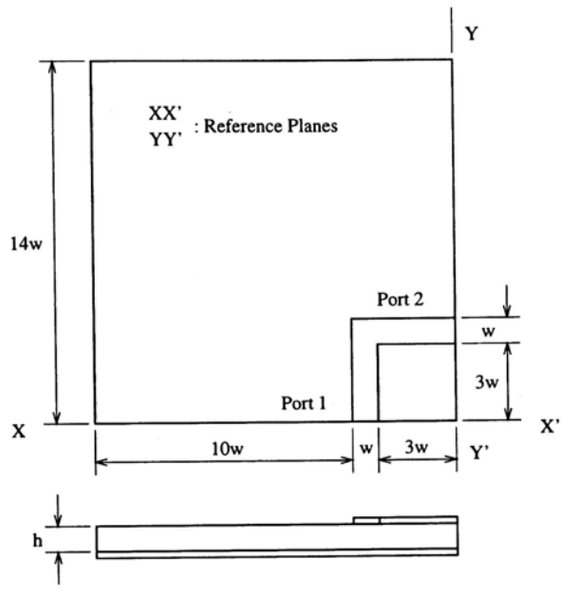

Figure 3.1: The geometry of the right-angle bend to be investigated.

and 1.0 respectively. $100\mu m$ width of the metal strip is used when it is treated as a lossy metal (aluminium) and only one kind of geometry is analyzed. The thickness of the substrate is $100\mu m$ and that of the metal strip is $1\mu m$.

3.2 T-Junction

The geometry of the T-junction is shown in Fig. 3.2. The width, w, of the microstrip is $250\mu m$ and the same set of $\frac{h}{w}$ values from the right-angled bend is used when the metal strip is a perfect metal. For the case of lossy metal strip, only one type of geometry, where the width of the metal strip and the substrate thickness are $100\mu m$, is analyzed. The thickness of the metal strip is $1\mu m$.

3.3 Tapered Line

The layout of the tapered line is shown in Fig. 3.3. The ratio $\frac{w_2-w_1}{l}$ is used to measure the slope of a tapered line. In this research project, only one value of this ratio of the tapered line is analyzed. It is a 20% tapered line. For this

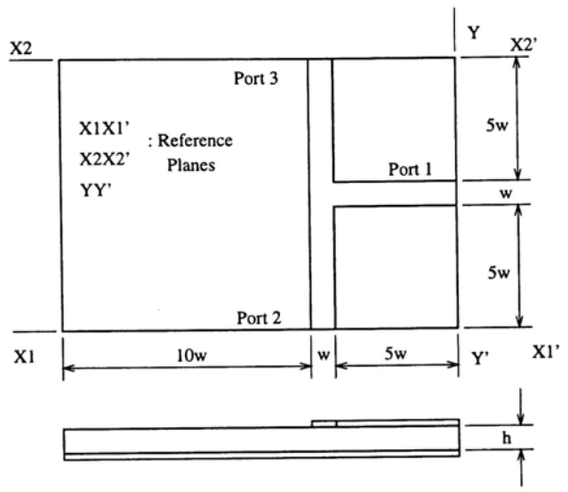

Figure 3.2: The geometry of the T-junction to be investigated.

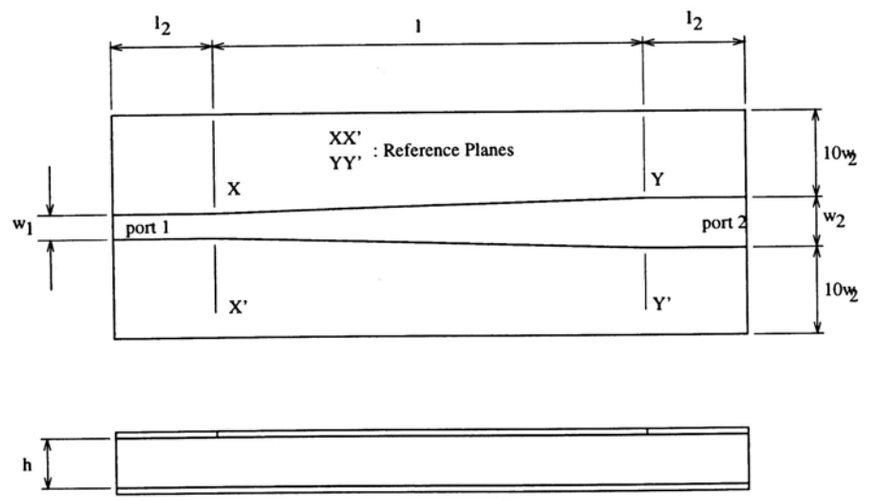

Figure 3.3: The geometry of the Tapered Line to be investigated.

20% tapered line, $w_1 = 10\mu m$, $w_2 = 100\mu m$, $l = 450\mu m$, $l_2 = 100\mu m$, $h = 100\mu m$, and $t = 1\mu m$. Both lossless and lossy cases use the same configuration (geometry).

Chapter 4

Deficiency of Lumped Equivalent Circuits

In this chapter, an example is used to show that the lumped equivalent circuits are not capable of modelling the microstrip discontinuities when the frequency range is beyond 20GHz for the picosecond rise time signal. The example used is the modelling of the right-angled bend by the well-known T-network (Fig. 4.1) consisting of two lumped inductors and a capacitor. In [JY92], it shows that the T-network can only model the right-angled bend with frequency up to about 1 to 2 GHz. Empirical expressions for the inductor and capacitor [JY92] are used to calculate their values. These expressions were developed by Gupta et al [GGC81] which were based on graphical values presented by Silvester et al [SB73, SB75] and Thomson et al [TG75]. On the other hand, we will use the approach developed in chapter 2 to show the deficiency of lumped equivalent circuits in modelling the microstrip discontinuities with picosecond rise time signal.

4.1 Scattering Parameter of the T-Network

The scattering parameters of the T-network is derived by the usual technique and is recorded as follows.

$$Z_1 = \frac{Z_C\,(Z_L + Z_{r2})}{Z_C + Z_L + Z_{r2}} \tag{4.1}$$

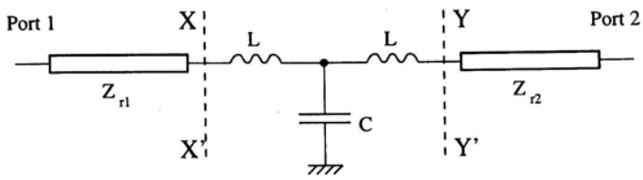

Figure 4.1: A T-network

$$Z_2 = Z_L + Z_1 \tag{4.2}$$

$$Z_3 = \frac{Z_C\,(Z_L + Z_{r1})}{Z_C + Z_L + Z_{r1}} \tag{4.3}$$

$$Z_4 = Z_L + Z_3 \tag{4.4}$$

$$s_{11} = \frac{Z_2 - Z_{r1}^*}{Z_2 + Z_{r1}} \tag{4.5}$$

$$s_{21} = \frac{Z_1\,(Z_{r1}^* + Z_{r1}s_{11})}{Z_2\,(Z_L + Z_{r2})}\sqrt{\frac{ReZ_{r2}}{ReZ_{r1}}} \tag{4.6}$$

$$s_{22} = \frac{Z_4 - Z_{r2}^*}{Z_4 + Z_{r2}} \tag{4.7}$$

$$s_{12} = \frac{Z_3\,(Z_{r2}^* + Z_{r2}s_{22})}{Z_4\,(Z_L + Z_{r1})}\sqrt{\frac{ReZ_{r1}}{ReZ_{r2}}} \tag{4.8}$$

where

- $Z_L = j\omega L$ and $Z_C = \frac{1}{j\omega C}$
- Z^* denotes the complex conjugate of a complex number Z
- $Re(Z)$ denotes the real part of a complex number Z
- Z_{r1} and Z_{r2} are the reference port impedances of port 1 and port 2 respectively.

4.2 Optimization Result for the T-Network

As said before, Levenberg-Marquardt non-linear least square algorithm is used to minimize the cost function in Eq. 2.4. The optimization result is plotted

in Fig. 4.2. The solid curve represents the simulated scattering parameters of the right-angled bend with $\frac{h}{w}$ ratio equal to 0.6 and the dotted curve the calculated scattering parameters of the T-network. Since $s_{21} = s_{12}$, only s_{11}, s_{21}, and s_{s22} will be shown. It is seen that the T-network basically is not able to model the right-angled bend with the operating frequency beyond 20GHz. The reason is due to the nature of the T-network itself. With reference to Fig.4.1, it is not difficult to see that the T-network is a low pass filter because the inductors become open-circuited and the capacitor becomes short-circuited when the operating frequency is sufficiently high. So the T-network is valid in modelling the right-angled bend only at low frequency. If the maximum operating frequency, f_{max}, is decreased to 5GHz, 4GHz, and 3GHz in turn, the relative error of s_{11}, s_{21}, and s_{22} are tabulated in Table 4.1. It is observed that the T-network are able to model the right-angled bend with the relative error less than 5% only when the operating frequency is constrained below 3GHz, which matches the result stated in [JY92].

f_{max} /GHz	err of S_{11} /%	err of s_{21}/%	err of s_{22} /%
3	4.9936	0.075882	4.9776
4	6.3253	0.087420	6.3132
5	8.4742	0.14884	8.4774

Table 4.1: Relative error between the simulated and calculated scattering parameters, $\frac{h}{w} = 0.6$ (lossless metal strip)

4.3 Summary

It is evidenced from the above example that the lumped circuit element equivalent circuits are not able to model the microstrip discontinuities when the frequency is beyond 20GHz. To obtain an accurate model, wideband equivalent circuits are required.

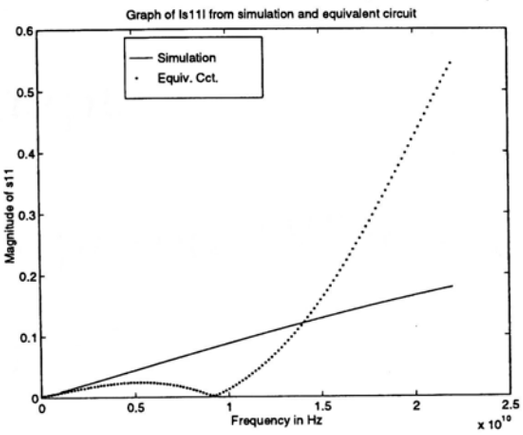

Magnitude of s_{11}

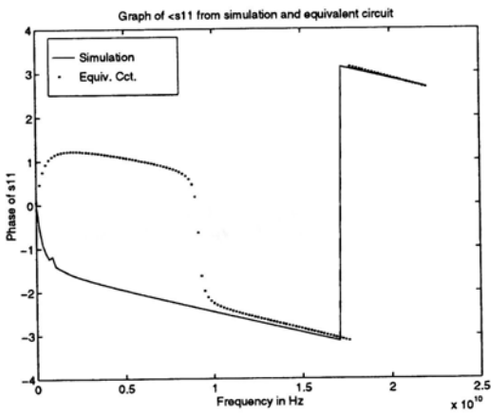

Phase of s_{11}

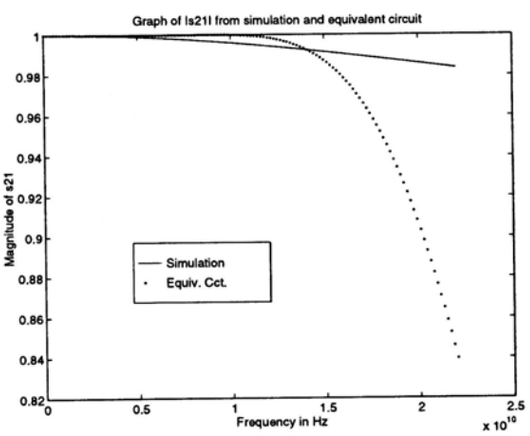

Magnitude of s_{21}

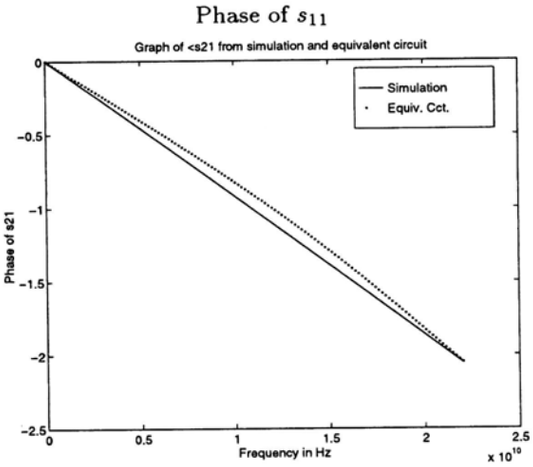

Phase of s_{21}

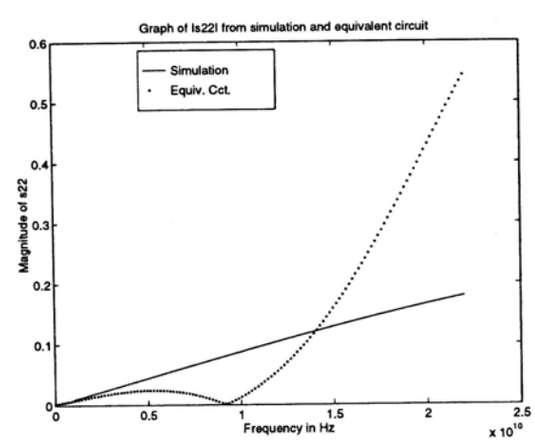

Magnitude of s_{22}

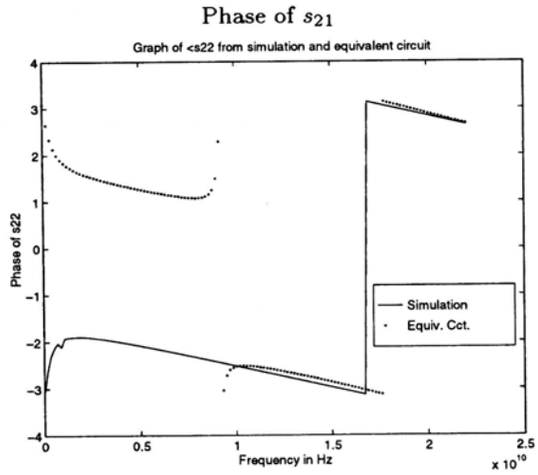

Phase of s_{22}

Figure 4.2: Difference of S parameters between 90^o bend and T-network.

Chapter 5

Proposed Wideband Equivalent Circuits

Several new distributed equivalent circuits for the three types of the microstrip discontinuities are proposed in this chapter. Most of the proposed circuits are constructed by modifying the existing lumped equivalent circuits. For example, one of the wideband equivalent circuits is modified from the T-network by adding two uniform microstrip lines to it. Besides, there are also equivalent circuits which contains no lumped circuit element.

5.1 Model of a Uniform Non-Homogeneous Microstrip Line

As there are wideband equivalent circuits proposed by adding uniform non-homogeneous microstrip lines to the existing lumped equivalent circuits, so a model of this lossy and dispersive microstrip line is necessary. The model developed here is based on [Dwo79, PB83, Bog90, YEL90, DCC90, HNR93, Hof87].

For a simple interconnect with a single substrate (Fig. 5.1), its equivalent circuit model per unit length of the structure is shown in Fig. 5.2. In Fig. 5.2, R represents the interconnection line series skin effect impedance, L is the interconnect line inductance resulting from the propagating electromagnetic field, G is the substrate shunt conductance, and C is the substrate capacitance. These

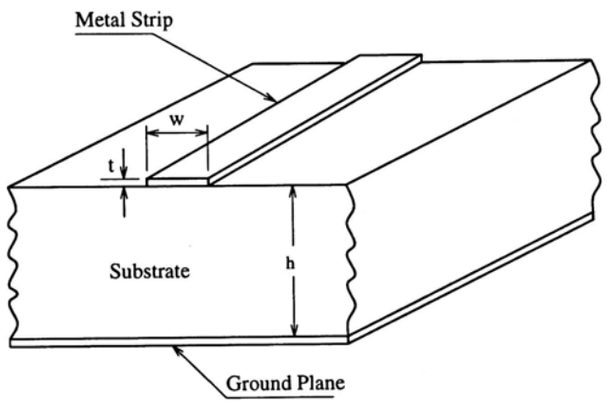

Figure 5.1: The geometry of an interconnect line

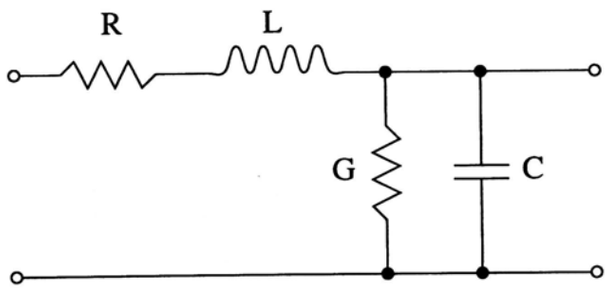

Figure 5.2: The equivalent circuit model per unit length of a uniform non-homogeneous interconnect.

circuit elements are derived in terms of the width w, thickness t, of the microstrip line, and the thickness h of the substrate.

To find the capacitance per unit length of a microstrip line, we must first know the field distribution beneath the strip. The field distribution is usually accounted for by the effective permittivity of the substrate. Under the static condition, the effective permittivity, ϵ_r', is between

$$\frac{1}{2}(\epsilon_r + 1) \leq \epsilon_r' \leq \epsilon_r \tag{5.1}$$

where ϵ_r is the dielectric constant of the substrate. It is to consider the case of the microstrip line with a very wide line[1] and that with a very narrow line[2]. Hammerstad [Ham75] derived a closed-form formula for the effective permittivity under the static condition. It is quoted as:

$$\epsilon_r' = \frac{\epsilon_r + 1}{2} + \frac{\epsilon_r - 1}{2\left(1 + \frac{12h}{w_{eff}}\right)^{\frac{1}{2}}} \tag{5.2}$$

where w_{eff} is the effective width of the microstrip line. The reason for introducing the effective width is as follows. As the thickness of the strip increases, electric field lines from the ground plane will reorient and terminate along the vertical edge of the strip. This reorientation causes the capacitance of a given width strip to increase with increasing metal strip thickness. To account for this effect, a formula for the effective width with zero thickness metal strip is derived [Dwo79]:

$$w_{eff} = \begin{cases} w + \frac{t}{\pi}\left(1 + \ln\frac{2h}{t}\right), & for\ \frac{h}{w} \leq 2\pi \\ w + \frac{t}{\pi}\left(1 + \ln\frac{4\pi w}{t}\right), & for\ \frac{h}{w} \geq 2\pi \end{cases} \tag{5.3}$$

As the operating frequency is increased, the mode-coupling effect increases and the fields become more concentrated in the region beneath the strip. Consequently the effective permittivity increases as the frequency increases. This

[1]When the strip line is very wide, the microstrip structure is like a parallel capacitor. Therfore, all the electric field is confined to the substrate dielectric.

[2]When the strip line is very narrow, the field is almost equally shared by the air and the substrate.

phenomenon is called the dielectric dispersion in microstrip. Much previous work has been done to derive the expression for the frequency-dependent effective permittivity. Pramanick and Bhartia [PB83] expressed the dispersion in microstrip by considering that this is the frequency at which the quasi-TEM mode couples with the lowest order TE wave mode. The frequency-dependent effective permittivity, ϵ_{eff}, developed yields close agreement with experimental results.

$$\epsilon_{eff}(f) = \epsilon_r - \frac{\epsilon_r - \epsilon_r'}{1 + \frac{f^2}{f_c^2}} \tag{5.4}$$

where f_c is the cutoff frequency of the lowest order TE mode of the microstrip and is defined as

$$f_c = \frac{c^2 \epsilon_o Z_o \epsilon_r^{\frac{1}{2}}}{2h\epsilon_r'^{\frac{1}{2}}} \tag{5.5}$$

with c is the light velocity and ϵ_o the permittivity of free space. Z_o denotes the microstrip characteristic impedance at dc and is given by

$$Z_o = \frac{120\pi F(w,h)}{\epsilon_r'^{\frac{1}{2}}} \tag{5.6}$$

Here $F(w,h)$ is the geometrical factor which accounts for the geometry of the microstrip line.

$$F(w,h) = \begin{cases} \frac{1}{2\pi} \ln\left(\frac{8h}{w_{eff}} + \frac{w_{eff}}{4h}\right), & for\ \frac{h}{w} \geq 1 \\ \frac{1}{\frac{w_{eff}}{h} + 1.393 + 0.667 \ln\left(\frac{w_{eff}}{h} + 1.444\right)}, & for\ \frac{h}{w} < 1 \end{cases} \tag{5.7}$$

With the above equations, Yuan et al [YEL90] derived an expression for the capacitance per unit length of a microstrip line:

$$C(f) = \frac{\epsilon_o \epsilon_{eff}(f)}{F(w,h)} \tag{5.8}$$

The expression of the inductance per unit length, L, is obtained by temporarily setting $\epsilon_r = 1$, finding $C(\epsilon_r = 1)$, and then finding L by using the formula

$$L = \frac{\mu_o \epsilon_o}{C(\epsilon_r = 1)} \tag{5.9}$$

So, the formula of L is given by

$$L = \mu_o F(w,h) \tag{5.10}$$

By neglecting the effect of frequency-dependent polarization of the substrate material[3], Yuan et al [YEL90] derived the expression for the conductance per unit length which was dependent only on the substrate conductivity, σ_{sub}, and the geometry of the microstrip line.

$$G = \frac{\sigma_{sub}\left(1 + \frac{1}{\sqrt{1+12\frac{h}{w_{eff}}}}\right)}{F(w,h)} \tag{5.11}$$

Three of the four microstrip line parameters have been found. The remaining one is the resistance per unit length of the microstrip line. Much research has been done to find R so as to include the skin effect at high frequency. Nahman et al [NH72] approximated the resistance (with skin effect) with the form $A+B\sqrt{s}$. With suitable choices of A and B, the expression $A+B\sqrt{s}$ can approximate the resistance in the whole frequency range. Dinh et al [DCC90] modelled the series resistance by

$$R(f) = \begin{cases} \frac{1}{\sigma_M wt}, & for\ f \le f_{crn} \\ \frac{1}{\sigma_M wt}\sqrt{\frac{f}{f_{crn}}}, & for\ f > f_{crn} \end{cases} \tag{5.12}$$

where σ_M is the electrical conductivity of the metal strip, f_{crn} is the corner frequency and is defined as the point where the skin depth equals the half of the strip thickness

$$f_{crn} = \frac{4}{\pi\sigma_M\mu_o t^2} \tag{5.13}$$

This approach is easily implemented but Eq. 5.12 gives a lower-estimate of the series resistance at the transition region (from low frequency to high frequency) and does not consider the internal inductance due to the skin effect. On the

[3]It is acceptable because alumina is a non-polar material and the frequency-dependent effect of the polarization occurs only in the optical frequency range.

other hand, He et al [HNR93] considered the internal inductance and the internal reactance is equal to the skin effect resistance due to the causality of the microstrip line (The term $\sqrt{s} = \sqrt{j\omega}$ instead of considering $\sqrt{\omega}$ only.) In [Bog90], Bogatin used the concept of effective thickness, t_{eff}, of the strip line to account for the variation of the series resistance (from dc resistance to skin-effect resistance) in the whole frequency range (Bogatin did not consider the internal reactance as well). Since the effective thickness of the strip line is equal to the physical thickness, t, at low frequency and the skin depth, δ, at high frequency, the effective thickness is derived by integrating the transverse current density, which drops off exponentially moving into the depth of the strip. With those boundary conditions, the effective thickness is approximated by

$$t_{eff} = \delta\left(1 - e^{-\frac{t}{\delta}}\right) \tag{5.14}$$

where $\delta = 1/\sqrt{(\pi\mu_o\sigma_M f)}$ is the skin depth. By considering the above different methods in approximating the series resistance as well as trial and error in the optimization, the resistance per unit length of the microstrip line, which considers the internal inductance and the dc resistance, is found as:

$$R(f) = \frac{1+j}{\sigma_M w t_{eff}} \tag{5.15}$$

Equations Eq. 5.8, 5.10, 5.11, and 5.15 are used to model a lossy (conductor loss and dielectric loss) and dispersive (geometrical or modal dispersion) microstrip line.

5.2 Right-Angled Bend

Four equivalent circuits are suggested for the right-angled bend (Fig. 5.3). The first two equivalent circuits (Circuit 1L and 2L) are the result of the modification of the lumped equivalent circuits. Circuit 3L and 4L are purely distributed equivalent circuits because each transmission (microstrip) line is modelled by

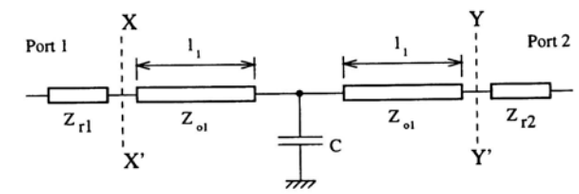

Equivalent Circuit 1L

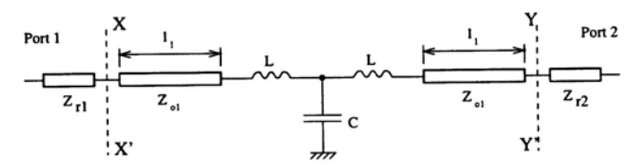

Equivalent Circuit 2L

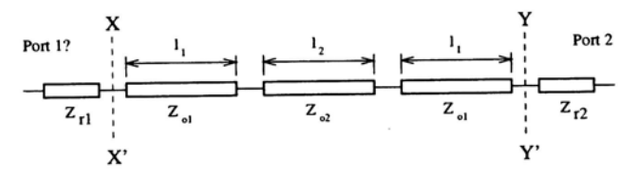

Equivalent Circuit 3L

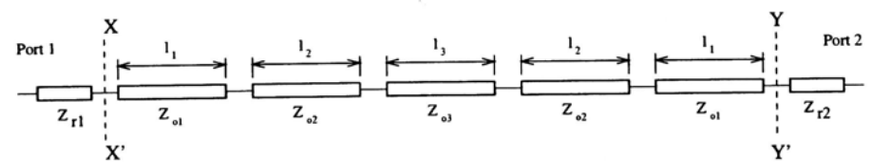

Equivalent Circuit 4L

Figure 5.3: Proposed equivalent circuits to model right-angled bend.

the interconnect model just developed. Their derived formulae of scattering parameters are recorded as follows. From these formulae, the symbols γ_i and Z_{oi}, where $i \in \aleph$, represent the propagation constant and characteristic impedance of the *ith* transmission (microstrip) line respectively. They can be in turn defined in terms of the *RLGC* transmission line parameters as:

$$\gamma_i = \sqrt{(R_i + j\omega L_i)(G_i + j\omega C_i)} \tag{5.16}$$

$$Z_{oi} = \sqrt{\frac{R_i + j\omega L_i}{G_i + j\omega C_i}} \tag{5.17}$$

However when the metal strip of the microstrip structure is assumed to be a perfect conductor in the analysis, R_i is equal to zero.

5.2.1 Circuit 1L

We first compute

$$Z_C = \frac{1}{j\omega C} \tag{5.18}$$

$$Z_1 = Z_{o1}\frac{Z_{r2} + Z_{o1}\tanh(\gamma_1 l_1)}{Z_{o1} + Z_{r2}\tanh(\gamma_1 l_1)} \tag{5.19}$$

$$Z_2 = \frac{Z_1 Z_C}{Z_1 + Z_C} \tag{5.20}$$

$$Z_3 = Z_{o1}\frac{Z_2 + Z_{o1}\tanh(\gamma_1 l_1)}{Z_{o1} + Z_2\tanh(\gamma_1 l_1)} \tag{5.21}$$

$$Z_4 = Z_{o1}\frac{Z_{r1} + Z_{o1}\tanh(\gamma_1 l_1)}{Z_{o1} + Z_{r1}\tanh(\gamma_1 l_1)} \tag{5.22}$$

$$Z_5 = \frac{Z_4 Z_C}{Z_4 + Z_C} \tag{5.23}$$

$$Z_6 = Z_{o1}\frac{Z_5 + Z_{o1}\tanh(\gamma_1 l_1)}{Z_{o1} + Z_5\tanh(\gamma_1 l_1)} \tag{5.24}$$

The above equations Eq. 5.19 – 5.21 are found when the port 2 is terminated by Z_{r2} whereas Eq. 5.22 – 5.24 are calculated when the port 1 is terminated by Z_{r1}. Then the scattering parameters are:

$$s_{11} = \frac{Z_3 - Z_{r1}^*}{Z_3 + Z_{r1}} \tag{5.25}$$

$$s_{21} = \frac{Z_2(Z_{r1}^* + Z_{r1}s_{11})}{\cosh^2(\gamma_1 l_1)(Z_2 + Z_{o1}\tanh(\gamma_1 l_1))} \times \frac{1}{Z_{r2} + Z_{o1}\tanh(\gamma_1 l_1)}\sqrt{\frac{ReZ_{r2}}{ReZ_{r1}}} \quad (5.26)$$

$$s_{22} = \frac{Z_6 - Z_{r2}^*}{Z_6 + Z_{r2}} \quad (5.27)$$

$$s_{12} = \frac{Z_5(Z_{r2}^* + Z_{r2}s_{22})}{\cosh^2(\gamma_1 l_1)(Z_5 + Z_{o1}\tanh(\gamma_1 l_1))} \times \frac{1}{Z_{r1} + Z_{o1}\tanh(\gamma_1 l_1)}\sqrt{\frac{ReZ_{r1}}{ReZ_{r2}}} \quad (5.28)$$

5.2.2 Circuit 2L

Compute

$$Z_L = j\omega L \quad (5.29)$$

$$Z_C = \frac{1}{j\omega C} \quad (5.30)$$

$$Z_1 = Z_{o1}\frac{Z_{r2} + Z_{o1}\tanh(\gamma_1 l_1)}{Z_{o1} + Z_{r2}\tanh(\gamma_1 l_1)} \quad (5.31)$$

$$Z_2 = Z_L + Z_1 \quad (5.32)$$

$$Z_3 = \frac{Z_C Z_2}{Z_C + Z_2} \quad (5.33)$$

$$Z_4 = Z_L + Z_3 \quad (5.34)$$

$$Z_5 = Z_{o1}\frac{Z_4 + Z_{o1}\tanh(\gamma_1 l_1)}{Z_{o1} + Z_4\tanh(\gamma_1 l_1)} \quad (5.35)$$

$$Z_6 = Z_{o1}\frac{Z_{r1} + Z_{o1}\tanh(\gamma_1 l_1)}{Z_{o1} + Z_{r1}\tanh(\gamma_1 l_1)} \quad (5.36)$$

$$Z_7 = Z_L + Z_6 \quad (5.37)$$

$$Z_8 = \frac{Z_C Z_7}{Z_C + Z_7} \quad (5.38)$$

$$Z_9 = Z_L + Z_8 \quad (5.39)$$

$$Z_{10} = Z_{o1}\frac{Z_9 + Z_{o1}\tanh(\gamma_1 l_1)}{Z_{o1} + Z_9\tanh(\gamma_1 l_1)} \quad (5.40)$$

Eq. 5.31 – 5.35 are obtained by terminating the port 2 with Z_{r2} and Eq. 5.36 – 5.40 by Z_{r1}. Then we have

$$s_{11} = \frac{Z_5 - Z_{r1}^*}{Z_5 + Z_{r1}} \quad (5.41)$$

$$s_{21} = \frac{Z_1 Z_3 (Z_{r1}^* + Z_{r1} s_{11})}{\cosh^2(\gamma_1 l_1)(Z_4 + Z_{o1}\tanh(\gamma_1 l_1))Z_2} \times \frac{1}{Z_{r2} + Z_{o1}\tanh(\gamma_1 l_1)} \sqrt{\frac{ReZ_{r2}}{ReZ_{r1}}} \quad (5.42)$$

$$s_{22} = \frac{Z_{10} - Z_{r2}^*}{Z_{10} + Z_{r2}} \quad (5.43)$$

$$s_{12} = \frac{Z_6 Z_8 (Z_{r2}^* + Z_{r2} s_{22})}{\cosh^2(\gamma_1 l_1)(Z_9 + Z_{o1}\tanh(\gamma_1 l_1))Z_7} \times \frac{1}{Z_{r1} + Z_{o1}\tanh(\gamma_1 l_1)} \sqrt{\frac{ReZ_{r1}}{ReZ_{r2}}} \quad (5.44)$$

5.2.3 Circuit 3L

Compute

$$Z_1 = Z_{o1} \frac{Z_{r2} + Z_{o1}\tanh(\gamma_1 l_1)}{Z_{o1} + Z_{r2}\tanh(\gamma_1 l_1)} \quad (5.45)$$

$$Z_2 = Z_{o2} \frac{Z_1 + Z_{o2}\tanh(\gamma_2 l_2)}{Z_{o2} + Z_1\tanh(\gamma_2 l_2)} \quad (5.46)$$

$$Z_3 = Z_{o1} \frac{Z_2 + Z_{o1}\tanh(\gamma_1 l_1)}{Z_{o1} + Z_2\tanh(\gamma_1 l_1)} \quad (5.47)$$

$$Z_4 = Z_{o1} \frac{Z_{r1} + Z_{o1}\tanh(\gamma_1 l_1)}{Z_{o1} + Z_{r1}\tanh(\gamma_1 l_1)} \quad (5.48)$$

$$Z_5 = Z_{o2} \frac{Z_4 + Z_{o2}\tanh(\gamma_2 l_2)}{Z_{o2} + Z_4\tanh(\gamma_2 l_2)} \quad (5.49)$$

$$Z_6 = Z_{o1} \frac{Z_5 + Z_{o1}\tanh(\gamma_1 l_1)}{Z_{o1} + Z_5\tanh(\gamma_1 l_1)} \quad (5.50)$$

Eq. 5.45 – 5.47 are obtained by terminating the port 2 with Z_{r2} whereas Eq. 5.48 – 5.50 are derived by terminating the port 1 with Z_{r1}. Then

$$s_{11} = \frac{Z_3 - Z_{r1}^*}{Z_3 + Z_{r1}} \quad (5.51)$$

$$s_{21} = \frac{Z_1 Z_2 (Z_{r1}^* + Z_{r1} s_{11})}{\cosh^2(\gamma_1 l_1)\cosh(\gamma_2 l_2)(Z_2 + Z_{o1}\tanh(\gamma_1 l_1))} \times \frac{1}{(Z_1 + Z_{o2}\tanh(\gamma_2 l_2))(Z_{r2} + Z_{o1}\tanh(\gamma_1 l_1))} \sqrt{\frac{ReZ_{r2}}{ReZ_{r1}}} \quad (5.52)$$

$$s_{22} = \frac{Z_6 - Z_{r2}^*}{Z_6 + Z_{r2}} \quad (5.53)$$

$$s_{12} = \frac{Z_4 Z_5 (Z_{r2}^* + Z_{r2} s_{22})}{\cosh^2(\gamma_1 l_1)\cosh(\gamma_2 l_2)(Z_5 + Z_{o1}\tanh(\gamma_1 l_1))} \times \frac{1}{(Z_4 + Z_{o2}\tanh(\gamma_2 l_2))(Z_{r1} + Z_{o1}\tanh(\gamma_1 l_1))} \sqrt{\frac{ReZ_{r1}}{ReZ_{r2}}} \quad (5.54)$$

5.2.4 Circuit 4L

Compute

$$Z_1 = Z_{o1}\frac{Z_{r2} + Z_{o1}\tanh(\gamma_1 l_1)}{Z_{o1} + Z_{r2}\tanh(\gamma_1 l_1)} \quad (5.55)$$

$$Z_2 = Z_{o2}\frac{Z_1 + Z_{o2}\tanh(\gamma_2 l_2)}{Z_{o2} + Z_1\tanh(\gamma_2 l_2)} \quad (5.56)$$

$$Z_3 = Z_{o3}\frac{Z_2 + Z_{o3}\tanh(\gamma_3 l_3)}{Z_{o3} + Z_2\tanh(\gamma_3 l_3)} \quad (5.57)$$

$$Z_4 = Z_{o2}\frac{Z_3 + Z_{o2}\tanh(\gamma_2 l_2)}{Z_{o2} + Z_3\tanh(\gamma_2 l_2)} \quad (5.58)$$

$$Z_5 = Z_{o1}\frac{Z_4 + Z_{o1}\tanh(\gamma_1 l_1)}{Z_{o1} + Z_4\tanh(\gamma_1 l_1)} \quad (5.59)$$

$$Z_6 = Z_{o1}\frac{Z_{r1} + Z_{o1}\tanh(\gamma_1 l_1)}{Z_{o1} + Z_{r1}\tanh(\gamma_1 l_1)} \quad (5.60)$$

$$Z_7 = Z_{o2}\frac{Z_6 + Z_{o2}\tanh(\gamma_2 l_2)}{Z_{o2} + Z_6\tanh(\gamma_2 l_2)} \quad (5.61)$$

$$Z_8 = Z_{o3}\frac{Z_7 + Z_{o3}\tanh(\gamma_3 l_3)}{Z_{o3} + Z_7\tanh(\gamma_3 l_3)} \quad (5.62)$$

$$Z_9 = Z_{o2}\frac{Z_8 + Z_{o2}\tanh(\gamma_2 l_2)}{Z_{o2} + Z_8\tanh(\gamma_2 l_2)} \quad (5.63)$$

$$Z_{10} = Z_{o1}\frac{Z_9 + Z_{o1}\tanh(\gamma_1 l_1)}{Z_{o1} + Z_9\tanh(\gamma_1 l_1)} \quad (5.64)$$

Eq. 5.55 – 5.59 are derived by matching the port 2 with Z_{r2} and Eq. 5.60 – 5.64 with Z_{r1}. Then we get

$$s_{11} = \frac{Z_5 - Z_{r1}^*}{Z_5 + Z_{r1}} \quad (5.65)$$

$$s_{21} = \frac{Z_1 Z_2 Z_3 Z_4 (Z_{r1}^* + Z_{r1} s_{11})}{\cosh^2(\gamma_1 l_1)\cosh^2(\gamma_2 l_2)\cosh(\gamma_3 l_3)(Z_4 + Z_{o1}\tanh(\gamma_1 l_1))} \times \frac{1}{(Z_3 + Z_{o2}\tanh(\gamma_2 l_2))(Z_2 + Z_{o3}\tanh(\gamma_3 l_3))} \times$$

$$\frac{1}{(Z_1 + Z_{o2}\tanh(\gamma_2 l_2))(Z_{r2} + Z_{o1}\tanh(\gamma_1 l_1))}\sqrt{\frac{ReZ_{r2}}{ReZ_{r1}}} \tag{5.66}$$

$$s_{22} = \frac{Z_{10} - Z_{r2}^*}{Z_{10} + Z_{r2}} \tag{5.67}$$

$$s_{12} = \frac{Z_6 Z_7 Z_8 Z_9 (Z_{r2}^* + Z_{r2} s_{22})}{\cosh^2(\gamma_1 l_1)\cosh^2(\gamma_2 l_2)\cosh(\gamma_3 l_3)(Z_9 + Z_{o1}\tanh(\gamma_1 l_1))} \times$$
$$\frac{1}{(Z_8 + Z_{o2}\tanh(\gamma_2 l_2))(Z_7 + Z_{o3}\tanh(\gamma_3 l_3))} \times$$
$$\frac{1}{(Z_6 + Z_{o2}\tanh(\gamma_2 l_2))(Z_{r1} + Z_{o1}\tanh(\gamma_1 l_1))}\sqrt{\frac{ReZ_{r1}}{ReZ_{r2}}} \tag{5.68}$$

5.3 T-Junction

For the T-junction type microstrip discontinuity, there are four equivalent circuits being proposed (Fig. 5.4). Since a T-junction can be regarded as a structure consisting of a main line (port 2 and port 3 in Fig. 3.2) and a stub (port 1), the equivalent circuits are designed as in Fig. 5.4. Only port 2 and port 3 are symmetrical but not for port 1. Their scattering parameters formulae are derived and quoted as follows. The symbols γ_i and Z_{oi} have the same meaning defined as in section 5.2.

5.3.1 Circuit 1T

$$Z_1 = Z_{o1}\frac{Z_{r3} + Z_{o1}\tanh(\gamma_1 l_1)}{Z_{o1} + Z_{r3}\tanh(\gamma_1 l_1)} \tag{5.69}$$

$$Z_2 = Z_{o2}\frac{Z_{r1} + Z_{o2}\tanh(\gamma_2 l_2)}{Z_{o2} + Z_{r1}\tanh(\gamma_2 l_2)} \tag{5.70}$$

$$Z_3 = \frac{Z_1 Z_2}{Z_1 + Z_2} \tag{5.71}$$

$$Z_4 = Z_{o1}\frac{Z_3 + Z_{o1}\tanh(\gamma_1 l_1)}{Z_{o1} + Z_3\tanh(\gamma_1 l_1)} \tag{5.72}$$

The above equations (Eq. 5.69 – 5.72) are derived when the port 1 and port 3 of the equivalent circuit (Fig. 3.2) are terminated by the reference characteristic

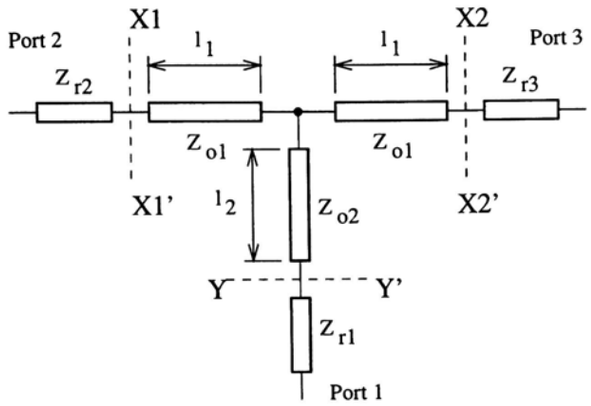

Equivalent Circuit 1T

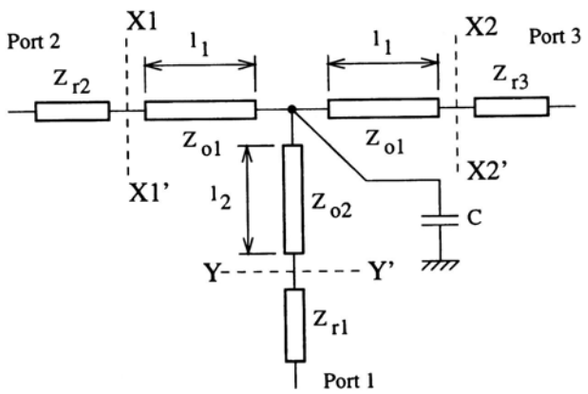

Equivalent Circuit 2T

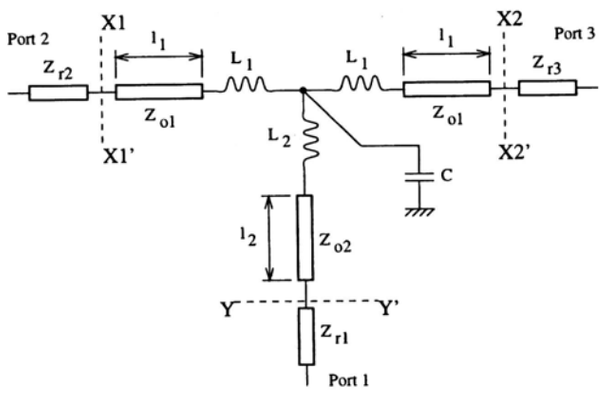

Equivalent Circuit 3T

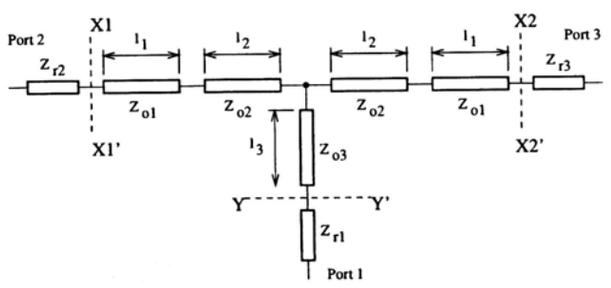

Equivalent Circuit 4T

Figure 5.4: Proposed equivalent circuits for T-junction.

impedances Z_{r1} and Z_{r3} respectively.

$$Z_5 = Z_{o1}\frac{Z_{r2} + Z_{o1}\tanh(\gamma_1 l_1)}{Z_{o1} + Z_{r2}\tanh(\gamma_1 l_1)} \tag{5.73}$$

$$Z_6 = Z_{o2}\frac{Z_{r1} + Z_{o2}\tanh(\gamma_2 l_2)}{Z_{o2} + Z_{r1}\tanh(\gamma_2 l_2)} \tag{5.74}$$

$$Z_7 = \frac{Z_5 Z_6}{Z_5 + Z_6} \tag{5.75}$$

$$Z_8 = Z_{o1}\frac{Z_7 + Z_{o1}\tanh(\gamma_1 l_1)}{Z_{o1} + Z_7\tanh(\gamma_1 l_1)} \tag{5.76}$$

Eq. 5.73 – 5.76 are found when the port 1 and port 2 of the equivalent circuit (Fig. 3.2) are terminated by the characteristic impedances Z_{r1} and Z_{r2} respectively.

$$Z_9 = Z_{o1}\frac{Z_{r2} + Z_{o1}\tanh(\gamma_1 l_1)}{Z_{o1} + Z_{r2}\tanh(\gamma_1 l_1)} \tag{5.77}$$

$$Z_{10} = Z_{o1}\frac{Z_{r3} + Z_{o1}\tanh(\gamma_1 l_1)}{Z_{o1} + Z_{r3}\tanh(\gamma_1 l_1)} \tag{5.78}$$

$$Z_{11} = \frac{Z_9 Z_{10}}{Z_9 + Z_{10}} \tag{5.79}$$

$$Z_{12} = Z_{o2}\frac{Z_{11} + Z_{o2}\tanh(\gamma_2 l_2)}{Z_{o2} + Z_{11}\tanh(\gamma_2 l_2)} \tag{5.80}$$

Eq. 5.77 – 5.80 are found when the port 2 and port 3 of the equivalent circuit (Fig. 3.2) are terminated by the characteristic impedances Z_{r2} and Z_{r3} respectively. The scattering parameters are:

$$s_{22} = \frac{Z_4 - Z_{r2}^*}{Z_4 + Z_{r2}} \tag{5.81}$$

$$s_{32} = \frac{Z_3(Z_{r2}^* + Z_{r2}s_{22})}{\cosh^2(\gamma_1 l_1)(Z_3 + Z_{o1}\tanh(\gamma_1 l_1))} \times \frac{1}{Z_{r3} + Z_{o1}\tanh(\gamma_1 l_1)}\sqrt{\frac{ReZ_{r3}}{ReZ_{r2}}} \tag{5.82}$$

$$s_{12} = \frac{Z_3(Z_{r2}^* + Z_{r2}s_{22})}{\cosh(\gamma_1 l_1)\cosh(\gamma_2 l_2)(Z_3 + Z_{o1}\tanh(\gamma_1 l_1))} \times \frac{1}{(Z_{r1} + Z_{o2}\tanh(\gamma_2 l_2))}\sqrt{\frac{ReZ_{r1}}{ReZ_{r2}}} \tag{5.83}$$

$$s_{33} = \frac{Z_8 - Z_{r3}^*}{Z_8 + Z_{r3}} \tag{5.84}$$

$$s_{23} = \frac{Z_7(Z_{r3}^* + Z_{r3}s_{33})}{\cosh^2(\gamma_1 l_1)(Z_7 + Z_{o1}\tanh(\gamma_1 l_1))} \times \frac{1}{Z_{r2} + Z_{o1}\tanh(\gamma_1 l_1)}\sqrt{\frac{ReZ_{r2}}{ReZ_{r3}}} \quad (5.85)$$

$$s_{13} = \frac{Z_7(Z_{r3}^* + Z_{r3}s_{33})}{\cosh(\gamma_1 l_1)\cosh(\gamma_2 l_2)(Z_7 + Z_{o1}\tanh(\gamma_1 l_1))} \times \frac{1}{(Z_{r1} + Z_{o2}\tanh(\gamma_2 l_2))}\sqrt{\frac{ReZ_{r1}}{ReZ_{r3}}} \quad (5.86)$$

$$s_{11} = \frac{Z_{12} - Z_{r1}^*}{Z_{12} + Z_{r1}} \quad (5.87)$$

$$s_{31} = \frac{Z_{11}(Z_{r1}^* + Z_{r1}s_{11})}{\cosh(\gamma_1 l_1)\cosh(\gamma_2 l_2)(Z_{11} + Z_{o2}\tanh(\gamma_2 l_2))} \times \frac{1}{(Z_{r3} + Z_{o1}\tanh(\gamma_1 l_1))}\sqrt{\frac{ReZ_{r3}}{ReZ_{r1}}} \quad (5.88)$$

$$s_{21} = \frac{Z_{11}(Z_{r1}^* + Z_{r1}s_{11})}{\cosh(\gamma_1 l_1)\cosh(\gamma_2 l_2)(Z_{11} + Z_{o2}\tanh(\gamma_2 l_2))} \times \frac{1}{(Z_{r2} + Z_{o1}\tanh(\gamma_1 l_1))}\sqrt{\frac{ReZ_{r2}}{ReZ_{r1}}} \quad (5.89)$$

5.3.2 Circuit 2T

Since Circuit 2T differs from Circuit 1T by adding a capacitor only (Fig. 3.2), the expressions of their scattering parameters are similar except for Z_3, Z_7, and Z_{11}, which are

$$Z_3 = \frac{1}{\frac{1}{Z_1} + \frac{1}{Z_2} + \frac{1}{Z_C}} \quad (5.90)$$

$$Z_7 = \frac{1}{\frac{1}{Z_5} + \frac{1}{Z_6} + \frac{1}{Z_C}} \quad (5.91)$$

$$Z_{11} = \frac{1}{\frac{1}{Z_9} + \frac{1}{Z_{10}} + \frac{1}{Z_C}} \quad (5.92)$$

where $Z_C = \frac{1}{j\omega C}$.

5.3.3 Circuit 3T

$$Z_{L1} = j\omega L_1 \quad (5.93)$$

$$Z_{L2} = j\omega L_2 \tag{5.94}$$

$$Z_C = \frac{1}{j\omega C} \tag{5.95}$$

$$Z_1 = Z_{o1}\frac{Z_{r3} + Z_{o1}\tanh(\gamma_1 l_1)}{Z_{o1} + Z_{r3}\tanh(\gamma_1 l_1)} \tag{5.96}$$

$$Z_2 = Z_{L1} + Z_1 \tag{5.97}$$

$$Z_3 = Z_{o2}\frac{Z_{r1} + Z_{o2}\tanh(\gamma_2 l_2)}{Z_{o2} + Z_{r1}\tanh(\gamma_2 l_2)} \tag{5.98}$$

$$Z_4 = Z_{L2} + Z_3 \tag{5.99}$$

$$Z_5 = \frac{1}{\frac{1}{Z_2} + \frac{1}{Z_4} + \frac{1}{Z_C}} \tag{5.100}$$

$$Z_6 = Z_{L1} + Z_5 \tag{5.101}$$

$$Z_7 = Z_{o1}\frac{Z_6 + Z_{o1}\tanh(\gamma_1 l_1)}{Z_{o1} + Z_6\tanh(\gamma_1 l_1)} \tag{5.102}$$

The above equations (Eq. 5.96 – 5.102) are derived when the port 1 and port 3 of the equivalent circuit (Fig. 3.2) are terminated by the reference characteristic impedances Z_{r1} and Z_{r3} respectively.

$$Z_8 = Z_{o1}\frac{Z_{r2} + Z_{o1}\tanh(\gamma_1 l_1)}{Z_{o1} + Z_{r2}\tanh(\gamma_1 l_1)} \tag{5.103}$$

$$Z_9 = Z_{L1} + Z_8 \tag{5.104}$$

$$Z_{10} = Z_{o2}\frac{Z_{r1} + Z_{o2}\tanh(\gamma_2 l_2)}{Z_{o2} + Z_{r1}\tanh(\gamma_2 l_2)} \tag{5.105}$$

$$Z_{11} = Z_{L2} + Z_{10} \tag{5.106}$$

$$Z_{12} = \frac{1}{\frac{1}{Z_9} + \frac{1}{Z_{11}} + \frac{1}{Z_C}} \tag{5.107}$$

$$Z_{13} = Z_{L1} + Z_{12} \tag{5.108}$$

$$Z_{14} = Z_{o1}\frac{Z_{13} + Z_{o1}\tanh(\gamma_1 l_1)}{Z_{o1} + Z_{13}\tanh(\gamma_1 l_1)} \tag{5.109}$$

Eq. 5.103 – 5.109 are found when the port 1 and port 2 of the equivalent circuit (Fig. 3.2) are terminated by the characteristic impedances Z_{r1} and Z_{r2} respectively.

$$Z_{15} = Z_{o1}\frac{Z_{r2} + Z_{o1}\tanh(\gamma_1 l_1)}{Z_{o1} + Z_{r2}\tanh(\gamma_1 l_1)} \tag{5.110}$$

$$Z_{16} = Z_{L1} + Z_{15} \tag{5.111}$$

$$Z_{17} = Z_{o1}\frac{Z_{r3} + Z_{o1}\tanh(\gamma_1 l_1)}{Z_{o1} + Z_{r3}\tanh(\gamma_1 l_1)} \tag{5.112}$$

$$Z_{18} = Z_{L1} + Z_{17} \tag{5.113}$$

$$Z_{19} = \frac{1}{\frac{1}{Z_{16}} + \frac{1}{Z_{18}} + \frac{1}{Z_C}} \tag{5.114}$$

$$Z_{20} = Z_{L2} + Z_{19} \tag{5.115}$$

$$Z_{21} = Z_{o2}\frac{Z_{20} + Z_{o2}\tanh(\gamma_2 l_2)}{Z_{o2} + Z_{20}\tanh(\gamma_2 l_2)} \tag{5.116}$$

Eq. 5.110 – 5.116 are found when the port 2 and port 3 of the equivalent circuit (Fig. 3.2) are terminated by the characteristic impedances Z_{r2} and Z_{r3} respectively. The scattering parameters are:

$$s_{22} = \frac{Z_7 - Z_{r2}^*}{Z_7 + Z_{r2}} \tag{5.117}$$

$$s_{32} = \frac{Z_1 Z_5 (Z_{r2}^* + Z_{r2} s_{22})}{Z_2 \cosh^2(\gamma_1 l_1)(Z_6 + Z_{o1}\tanh(\gamma_1 l_1))} \times \frac{1}{Z_{r3} + Z_{o1}\tanh(\gamma_1 l_1)} \sqrt{\frac{ReZ_{r3}}{ReZ_{r2}}} \tag{5.118}$$

$$s_{12} = \frac{Z_3 Z_5 (Z_{r2}^* + Z_{r2} s_{22})}{Z_4 \cosh(\gamma_1 l_1)\cosh(\gamma_2 l_2)(Z_6 + Z_{o1}\tanh(\gamma_1 l_1))} \times \frac{1}{(Z_{r1} + Z_{o2}\tanh(\gamma_2 l_2))} \sqrt{\frac{ReZ_{r1}}{ReZ_{r2}}} \tag{5.119}$$

$$s_{33} = \frac{Z_{14} - Z_{r3}^*}{Z_{14} + Z_{r3}} \tag{5.120}$$

$$s_{23} = \frac{Z_8 Z_{12} (Z_{r3}^* + Z_{r3} s_{33})}{Z_9 \cosh^2(\gamma_1 l_1)(Z_{13} + Z_{o1}\tanh(\gamma_1 l_1))} \times \frac{1}{Z_{r2} + Z_{o1}\tanh(\gamma_1 l_1)} \sqrt{\frac{ReZ_{r2}}{ReZ_{r3}}} \tag{5.121}$$

$$s_{13} = \frac{Z_{10} Z_{12} (Z_{r3}^* + Z_{r3} s_{33})}{Z_{11} \cosh(\gamma_1 l_1)\cosh(\gamma_2 l_2)(Z_{13} + Z_{o1}\tanh(\gamma_1 l_1))} \times \frac{1}{(Z_{r1} + Z_{o2}\tanh(\gamma_2 l_2))} \sqrt{\frac{ReZ_{r1}}{ReZ_{r3}}} \tag{5.122}$$

$$s_{11} = \frac{Z_{21} - Z_{r1}^*}{Z_{21} + Z_{r1}} \tag{5.123}$$

$$s_{31} = \frac{Z_{17} Z_{19} (Z_{r1}^* + Z_{r1} s_{11})}{Z_{18} \cosh(\gamma_1 l_1)\cosh(\gamma_2 l_2)(Z_{20} + Z_{o2}\tanh(\gamma_2 l_2))} \times$$

$$\frac{1}{(Z_{r3}+Z_{o1}\tanh(\gamma_1 l_1))}\sqrt{\frac{ReZ_{r3}}{ReZ_{r1}}} \tag{5.124}$$

$$s_{21} = \frac{Z_{15}Z_{19}(Z_{r1}^{*}+Z_{r1}s_{11})}{Z_{16}\cosh(\gamma_1 l_1)\cosh(\gamma_2 l_2)(Z_{20}+Z_{o2}\tanh(\gamma_2 l_2))} \times$$

$$\frac{1}{(Z_{r2}+Z_{o1}\tanh(\gamma_1 l_1))}\sqrt{\frac{ReZ_{r2}}{ReZ_{r1}}} \tag{5.125}$$

5.3.4 Circuit 4T

$$Z_1 = Z_{o1}\frac{Z_{r3}+Z_{o1}\tanh(\gamma_1 l_1)}{Z_{o1}+Z_{r3}\tanh(\gamma_1 l_1)} \tag{5.126}$$

$$Z_2 = Z_{o2}\frac{Z_1+Z_{o2}\tanh(\gamma_2 l_2)}{Z_{o2}+Z_1\tanh(\gamma_2 l_2)} \tag{5.127}$$

$$Z_3 = Z_{o3}\frac{Z_{r1}+Z_{o3}\tanh(\gamma_3 l_3)}{Z_{o3}+Z_{r1}\tanh(\gamma_3 l_3)} \tag{5.128}$$

$$Z_4 = \frac{Z_2 Z_3}{Z_2+Z_3} \tag{5.129}$$

$$Z_5 = Z_{o2}\frac{Z_4+Z_{o2}\tanh(\gamma_2 l_2)}{Z_{o2}+Z_4\tanh(\gamma_2 l_2)} \tag{5.130}$$

$$Z_6 = Z_{o1}\frac{Z_5+Z_{o1}\tanh(\gamma_1 l_1)}{Z_{o1}+Z_5\tanh(\gamma_1 l_1)} \tag{5.131}$$

Eq. 5.126 – 5.131 are derived by terminating the port 1 and port 3 with their reference characteristic impedances Z_{r1} and Z_{r3} respectively.

$$Z_7 = Z_{o1}\frac{Z_{r2}+Z_{o1}\tanh(\gamma_1 l_1)}{Z_{o1}+Z_{r2}\tanh(\gamma_1 l_1)} \tag{5.132}$$

$$Z_8 = Z_{o2}\frac{Z_7+Z_{o2}\tanh(\gamma_2 l_2)}{Z_{o2}+Z_7\tanh(\gamma_2 l_2)} \tag{5.133}$$

$$Z_9 = Z_{o3}\frac{Z_{r1}+Z_{o3}\tanh(\gamma_3 l_3)}{Z_{o3}+Z_{r1}\tanh(\gamma_3 l_3)} \tag{5.134}$$

$$Z_{10} = \frac{Z_8 Z_9}{Z_8+Z_9} \tag{5.135}$$

$$Z_{11} = Z_{o2}\frac{Z_{10}+Z_{o2}\tanh(\gamma_2 l_2)}{Z_{o2}+Z_{10}\tanh(\gamma_2 l_2)} \tag{5.136}$$

$$Z_{12} = Z_{o1}\frac{Z_{11}+Z_{o1}\tanh(\gamma_1 l_1)}{Z_{o1}+Z_{11}\tanh(\gamma_1 l_1)} \tag{5.137}$$

Eq. 5.132 – 5.137 are derived by terminating the port 1 and port 2 with their reference characteristic impedances Z_{r1} and Z_{r2} respectively.

$$Z_{13} = Z_{o1}\frac{Z_{r2} + Z_{o1}\tanh(\gamma_1 l_1)}{Z_{o1} + Z_{r2}\tanh(\gamma_1 l_1)} \tag{5.138}$$

$$Z_{14} = Z_{o2}\frac{Z_{13} + Z_{o2}\tanh(\gamma_2 l_2)}{Z_{o2} + Z_{13}\tanh(\gamma_2 l_2)} \tag{5.139}$$

$$Z_{15} = Z_{o1}\frac{Z_{r3} + Z_{o1}\tanh(\gamma_1 l_1)}{Z_{o1} + Z_{r3}\tanh(\gamma_1 l_1)} \tag{5.140}$$

$$Z_{16} = Z_{o2}\frac{Z_{15} + Z_{o2}\tanh(\gamma_2 l_2)}{Z_{o2} + Z_{15}\tanh(\gamma_2 l_2)} \tag{5.141}$$

$$Z_{17} = \frac{Z_{14}Z_{16}}{Z_{14} + Z_{16}} \tag{5.142}$$

$$Z_{18} = Z_{o3}\frac{Z_{17} + Z_{o3}\tanh(\gamma_3 l_3)}{Z_{o3} + Z_{17}\tanh(\gamma_3 l_3)} \tag{5.143}$$

Eq. 5.138 – 5.143 are obtained by terminating the port 2 and port 3 with their reference characteristic impedances Z_{r2} and Z_{r3} respectively. The scattering parameters are:

$$s_{22} = \frac{Z_6 - Z_{r2}^*}{Z_6 + Z_{r2}} \tag{5.144}$$

$$\begin{aligned} s_{32} = {} & \frac{Z_1 Z_4 Z_5 (Z_{r2}^* + Z_{r2} s_{22})}{\cosh^2(\gamma_1 l_1)\cosh^2(\gamma_2 l_2)(Z_5 + Z_{o1}\tanh(\gamma_1 l_1))} \times \\ & \frac{1}{(Z_4 + Z_{o2}\tanh(\gamma_2 l_2))(Z_1 + Z_{o2}\tanh(\gamma_2 l_2))} \times \\ & \frac{1}{Z_{r3} + Z_{o1}\tanh(\gamma_1 l_1)}\sqrt{\frac{ReZ_{r3}}{ReZ_{r2}}} \end{aligned} \tag{5.145}$$

$$\begin{aligned} s_{12} = {} & \frac{Z_4 Z_5 (Z_{r2}^* + Z_{r2} s_{22})}{\cosh(\gamma_1 l_1)\cosh(\gamma_2 l_2)\cosh(\gamma_3 l_3)(Z_5 + Z_{o1}\tanh(\gamma_1 l_1))} \times \\ & \frac{1}{(Z_4 + Z_{o2}\tanh(\gamma_2 l_2))(Z_{r1} + Z_{o3}\tanh(\gamma_3 l_3))}\sqrt{\frac{ReZ_{r1}}{ReZ_{r2}}} \end{aligned} \tag{5.146}$$

$$s_{33} = \frac{Z_{12} - Z_{r3}^*}{Z_{12} + Z_{r3}} \tag{5.147}$$

$$\begin{aligned} s_{23} = {} & \frac{Z_7 Z_{10} Z_{11} (Z_{r3}^* + Z_{r3} s_{33})}{\cosh^2(\gamma_1 l_1)\cosh^2(\gamma_2 l_2)(Z_{11} + Z_{o1}\tanh(\gamma_1 l_1))} \times \\ & \frac{1}{(Z_{10} + Z_{o2}\tanh(\gamma_2 l_2))(Z_7 + Z_{o2}\tanh(\gamma_2 l_2))} \times \end{aligned}$$

$$\frac{1}{Z_{r2}+Z_{o1}\tanh(\gamma_1 l_1)}\sqrt{\frac{ReZ_{r2}}{ReZ_{r3}}} \tag{5.148}$$

$$s_{13} = \frac{Z_{10}Z_{11}(Z_{r3}^{*}+Z_{r3}s_{33})}{\cosh(\gamma_1 l_1)\cosh(\gamma_2 l_2)\cosh(\gamma_3 l_3)(Z_{11}+Z_{o1}\tanh(\gamma_1 l_1))} \times$$

$$\frac{1}{(Z_{10}+Z_{o2}\tanh(\gamma_2 l_2))(Z_{r1}+Z_{o3}\tanh(\gamma_3 l_3))}\sqrt{\frac{ReZ_{r1}}{ReZ_{r3}}} \tag{5.149}$$

$$s_{11} = \frac{Z_{18}-Z_{r1}^{*}}{Z_{18}+Z_{r1}} \tag{5.150}$$

$$s_{31} = \frac{Z_{15}Z_{17}(Z_{r1}^{*}+Z_{r1}s_{11})}{\cosh(\gamma_1 l_1)\cosh(\gamma_2 l_2)\cosh(\gamma_3 l_3)(Z_{17}+Z_{o3}\tanh(\gamma_3 l_3))} \times$$

$$\frac{1}{(Z_{15}+Z_{o2}\tanh(\gamma_2 l_2))(Z_{r3}+Z_{o1}\tanh(\gamma_1 l_1))}\sqrt{\frac{ReZ_{r3}}{ReZ_{r1}}} \tag{5.151}$$

$$s_{21} = \frac{Z_{13}Z_{17}(Z_{r1}^{*}+Z_{r1}s_{11})}{\cosh(\gamma_1 l_1)\cosh(\gamma_2 l_2)\cosh(\gamma_3 l_3)(Z_{17}+Z_{o3}\tanh(\gamma_3 l_3))} \times$$

$$\frac{1}{(Z_{13}+Z_{o2}\tanh(\gamma_2 l_2))(Z_{r2}+Z_{o1}\tanh(\gamma_1 l_1))}\sqrt{\frac{ReZ_{r2}}{ReZ_{r1}}} \tag{5.152}$$

5.4 Tapered Line

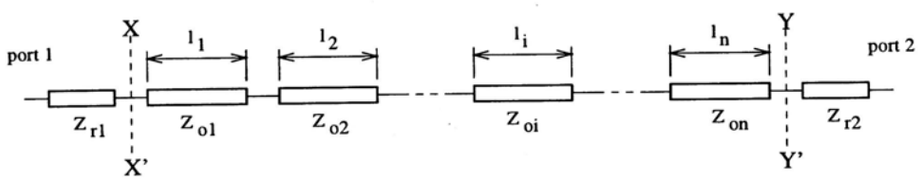

Figure 5.5: Proposed equivalent circuit for tapered line.

As a tapered line can be regarded as consisting of a number of uniform transmission lines with different cross-sectional areas connected in series, so the suggested equivalent circuits are basically designed in this way (Fig. 5.5). In Fig. 5.5, the equivalent circuit consists of n uniform microstrip line concatenated with one another, each of which has different length as well as microstrip width (hence different characteristic impedance). In this research project, the equivalent circuits with $n = 3$, 4, 5, 7, 10, and 20 are used to model the tapered

line. However, the optimization is only done for the case of $n = 3$. The reason will be shown in later chapters. Since the derivation of the scattering parameters for different n is similar, only the scattering parameter formulae for $n = 3$ is shown as follows.

5.4.1 Circuit 1t – $n = 3$

Compute

$$Z_1 = Z_{o3}\frac{Z_{r2} + Z_{o3}\tanh(\gamma_3 l_3)}{Z_{o3} + Z_{r2}\tanh(\gamma_3 l_3)} \tag{5.153}$$

$$Z_2 = Z_{o2}\frac{Z_1 + Z_{o2}\tanh(\gamma_2 l_2)}{Z_{o2} + Z_1\tanh(\gamma_2 l_2)} \tag{5.154}$$

$$Z_3 = Z_{o1}\frac{Z_2 + Z_{o1}\tanh(\gamma_1 l_1)}{Z_{o1} + Z_2\tanh(\gamma_l l_1)} \tag{5.155}$$

$$Z_4 = Z_{o1}\frac{Z_{r1} + Z_{o1}\tanh(\gamma_1 l_1)}{Z_{o1} + Z_{r1}\tanh(\gamma_1 l_1)} \tag{5.156}$$

$$Z_5 = Z_{o2}\frac{Z_4 + Z_{o2}\tanh(\gamma_2 l_2)}{Z_{o2} + Z_4\tanh(\gamma_2 l_2)} \tag{5.157}$$

$$Z_6 = Z_{o3}\frac{Z_5 + Z_{o3}\tanh(\gamma_3 l_3)}{Z_{o3} + Z_5\tanh(\gamma_3 l_3)} \tag{5.158}$$

The equations Eq. 5.153 – 5.155 are derived when the port 2 of the equivalent circuit is terminated by the reference impedance Z_{r2}, whereas Eq. 5.156 – 5.158 are obtained by terminating the port 1 with Z_{r1}. Then

$$s_{11} = \frac{Z_3 - Z_{r1}^*}{Z_3 + Z_{r1}} \tag{5.159}$$

$$\begin{aligned} s_{21} = {} & \frac{Z_1 Z_2 (Z_{r1}^* + Z_{r1} s_{11})}{\cosh(\gamma_1 l_1)\cosh(\gamma_2 l_2)\cosh(\gamma_3 l_3)} \times \\ & \frac{1}{(Z_2 + Z_{o1}\tanh(\gamma_1 l_1))(Z_1 + Z_{o2}\tanh(\gamma_2 l_2))} \times \\ & \frac{1}{Z_{r2} + Z_{o3}\tanh(\gamma_3 l_3)}\sqrt{\frac{ReZ_{r2}}{ReZ_{r1}}} \end{aligned} \tag{5.160}$$

$$s_{22} = \frac{Z_6 - Z_{r2}^*}{Z_6 + Z_{r2}} \tag{5.161}$$

$$s_{12} = \frac{Z_4 Z_5 (Z_{r2}^* + Z_{r2} s_{22})}{\cosh(\gamma_1 l_1)\cosh(\gamma_2 l_2)\cosh(\gamma_3 l_3)} \times$$

$$\frac{1}{(Z_5 + Z_{o3}\tanh(\gamma_3 l_3))(Z_4 + Z_{o2}\tanh(\gamma_2 l_2))} \times \frac{1}{Z_{r1} + Z_{o1}\tanh(\gamma_1 l_1)} \sqrt{\frac{ReZ_{r1}}{ReZ_{r2}}} \tag{5.162}$$

5.5 Summary

In this chapter, several wideband equivalent circuits are suggested for the three types of microstrip discontinuities. All circuits are proposed to compensate the deficiency of lumped equivalent circuits at high frequency. Their performance will be shown in Chapter 6 and 7.

Chapter 6

Performance of the Equivalent Circuits

The performance results of the equivalent circuits proposed in Chapter 5 are recorded in this chapter. By using the technique described in Chapter 2, it will be seen that wideband equivalent circuits are superior to the lumped equivalent circuit models for picosecond rise time signals. The maximum operating frequency that we use to obtain the scattering parameters of a geometry from the HFSS software is beyond 20GHz. This corresponds to about 18ps rise time signal[1]. So this frequency range is enough to analyze circuits with this kind of speed.

Since the plots of the performance result of an equivalent circuit among the different types of the microstrip discontinuities (e.g. the right-angled bend with different $\frac{h}{w}$ values) are similar in shape, only selected figures of the degree of fitness between the simulated and calculated scattering parameters are shown in this chapter for illustrating purpose. A table of the relative (percentage) error, err, between the simulated scattering parameters and the calculated ones (of different equivalent circuits) for each microstrip discontinuity is used to summarize the performance. The formula of err is similar as Eq. 2.4 except that each vector contains one of the components of the scattering parameters only (e.g. s_{11}, s_{21}, s_{22}, etc).

As the metal strip has been regarded as a perfect metal and aluminium type

[1]Here we employ a simple formula to relate the rise time, t_r, and the bandwidth, BW: $t_r BW \approx 2.2$, where t_r is in second and BW is in radian.

material during the analysis, the result will be recorded separately.

6.1 Right-Angled Bend

The performance results of the equivalent circuits without conductor loss are firstly recorded followed by those with conductor loss. It will be seen that the performance results having considered the conductor loss are slightly worse than those without taking the conductor loss in consideration. It is expected because the more physical factor is taken into account, the more difficult the optimization is to be done.

6.1.1 Without Conductor Loss

For each of the equivalent circuits for modelling the right-angled bend, its unknown parameters (e.g. the equivalent inductance and capacitance) obtained from optimization are tabulated for different values of $\frac{h}{w}$ ratio (Table 6.1 to 6.4). Several phenomena are observed (refer to Fig. 5.3):

- for the Circuit 1L and 2L, the equivalent capacitance values decreases as the ratio $\frac{h}{w}$ increases. Since the width of the right-angled bend is kept unchanged whereas the substrate thickness is varied, the decrease in the capacitor value is expected because the capacitance is inversely proportional to thickness of the dielectric.

- for the Circuit 2L, the values of the equivalent inductor is found to increase with the $\frac{h}{w}$ ratio. It shows that the value of the equivalent inductor depends on the geometry of the right-angled bend and its value increases as the $\frac{h}{w}$ value increases. From another point of view, since $LC = \mu_o \epsilon_{eff}(f)$ and $\epsilon_{eff}(f)$ increases with frequency while C decreases with increasing the $\frac{h}{w}$ value, L increases.

- for all equivalent circuits, it is observed that the matching results of the magnitudes plots between the simulated and calculated scattering parameters is better in the low frequency region than in the high frequency region. When the operating frequency is low, it can assume that only quasi-TEM mode wave is transmitted in the microstrip structure[2]. However, when frequency increases, more hybrid mode waves are generated and our model of the microstrip line assumes that a quasi-TEM mode wave couples with the lowest order TE mode wave only.

- for all equivalent circuits, the relative error increases when the $\frac{h}{w}$ ratio increases, i.e., the modelling result becomes worse when $\frac{h}{w}$ is larger. When the substrate thickness becomes thicker, the cutoff frequency of the lowest TE mode (Eq. 5.5) is decreased. It can imply that more hyrbid mode waves are generated at lower frequency and therfore the mode-coupling effect is increased; hence increasing the difficulty in the modelling.

The geometry of the right-angled bend with $\frac{h}{w} = 0.6$ is used to illustrate the degree of fitness between the simulated and calculated scattering parameters (Fig. 6.1 – 6.4). From the figures, it is observed that the phases of the scattering parameters between the simulated result and the calculated one match very well; whereas the magnitudes show some deviation when frequency increases. The phase plots match well because the effective length of the right-angled bend should be equal to that of the equivalent circuits. For example, the effective length of the right-angled bend ($\frac{h}{w} = 0.6$), which is calculated from the phase shift of s_{21}, is approximatedly found to be 1.524mm and that of the Circuit 1L is 1.6037mm. It can be seen that their values are close together.

Table 6.5 – 6.9 tabulate the relative error of the scattering parameters for different geometries. From the tables, it is seen that, for the same equivalent

[2]The higher order mode waves generated in the discontinuity region is not considered because they are evanescent mode and attenuate quickly from the discontinuity region.

circuit, the relative errors of the scattering parameters become larger when the $\frac{h}{w}$ value is increased. It is because of increasing mode-coupling effect just explained.

It is seen that all of the equivalent circuits can model the right-angled bend with the frequency up to and above 20GHz. Among them, Circuit 2L and Circuit 4L both are better to model the 90° bend for all the values of $\frac{h}{w}$ ratio within the valid frequency range. Since Circuit 4L gives such acceptable modelling result, we restrict the number of microstrip lines used up to 5. The more number of microstrip lines is used, the longer optimization time is required. Moreover, it is experienced that it will be very easy to trap into local minimum if large number of microstrip lines is used.

Besides, an interesting phenomenon has been observed. For the equivalent Circuit 2L and 4L, the values of the parameters show some trends (either monotonic increasing or decreasing) with respect to the ratio $\frac{h}{w}$ (Table 6.2 and 6.4). It shows that we can find some empirical formulae to relate the parameters of the equivalent circuits to the geometry of the right-angled bend within the valid frequency range.

$\frac{h}{w}$	w_1/mm	l_1/mm	C/F	err
0.2	0.27102	0.80603	7.8489×10^{-14}	4.2395×10^{-3}
0.4	0.28152	0.80618	4.5978×10^{-14}	6.3466×10^{-3}
0.6	0.29234	0.80185	2.8876×10^{-14}	8.5550×10^{-3}
0.8	0.30825	0.81158	8.6769×10^{-15}	1.1846×10^{-2}
1.0	0.32421	0.81638	1.8495×10^{-15}	1.3695×10^{-2}

Table 6.1: Parameter values of the equivalent circuit 1L (lossless metal strip)

$\frac{h}{w}$	w_1/mm	l_1/mm	L/H	C/F	err
0.2	0.30535	0.45276	5.9501×10^{-11}	4.1647×10^{-13}	2.7944×10^{-3}
0.4	0.36345	0.36961	1.1677×10^{-10}	2.8047×10^{-13}	3.1708×10^{-3}
0.6	0.44333	0.30782	1.6525×10^{-10}	2.2578×10^{-13}	4.0670×10^{-3}
0.8	0.57354	0.25304	2.1159×10^{-10}	1.9391×10^{-13}	6.7054×10^{-3}
1.0	0.72132	0.21796	2.4577×10^{-10}	1.7699×10^{-13}	6.8507×10^{-3}

Table 6.2: Parameter values of the equivalent circuit 2L (lossless metal strip)

$\frac{h}{w}$	w_1/mm	l_1/mm	w_2/mm	l_2/mm	err
0.2	0.27145	0.79619	0.88062	0.053921	4.0674×10^{-3}
0.4	0.28246	0.79264	0.84789	0.064198	6.0503×10^{-3}
0.6	0.29369	0.79016	0.89959	0.054215	8.2033×10^{-3}
0.8	0.30881	0.79975	0.62506	0.037027	1.1711×10^{-2}
1.0	0.32420	0.81386	0.75404	0.0079369	1.3632×10^{-2}

Table 6.3: Parameter values of the equivalent circuit 3L (lossless metal strip)

$\frac{h}{w}$	w_1/mm	l_1/mm	w_2/mm	l_2/mm	w_3/mm	l_3/mm	err
0.2	0.67894	0.080042	0.16016	0.35282	0.39299	0.66920	1.4279×10^{-3}
0.4	0.69758	0.11021	0.12246	0.36300	0.54182	0.51006	1.8824×10^{-3}
0.6	0.72141	0.13140	0.090388	0.33765	0.66202	0.45094	3.6529×10^{-3}
0.8	0.74967	0.14719	0.071162	0.31859	0.71183	0.43322	6.9630×10^{-3}
1.0	0.80858	0.16457	0.035979	0.26613	0.80293	0.43069	7.3928×10^{-3}

Table 6.4: Parameter values of the equivalent circuit 4L (lossless metal strip)

$\frac{h}{w} = 0.2$	s_{11}	s_{21}	s_{22}
Circuit 1L: $err/\%$	2.5749	0.32154	2.4497
Circuit 2L: $err/\%$	1.3541	0.22885	1.5673
Circuit 3L: $err/\%$	2.5652	0.29875	2.4488
Circuit 4L: $err/\%$	1.0130	0.082063	1.0998

Table 6.5: Relative error between the simulated and calculated scattering parameters, $\frac{h}{w} = 0.2$ (lossless metal strip)

$\frac{h}{w} = 0.4$	s_{11}	s_{21}	s_{22}
Circuit 1L: $err/\%$	3.0185	0.51103	2.8820
Circuit 2L: $err/\%$	1.4408	0.24977	1.6124
Circuit 3L: $err/\%$	3.0108	0.47327	2.8863
Circuit 4L: $err/\%$	0.99433	0.12951	1.1273

Table 6.6: Relative error between the simulated and calculated scattering parameters, $\frac{h}{w} = 0.4$ (lossless metal strip)

$\frac{h}{w} = 0.6$	s_{11}	s_{21}	s_{22}
Circuit 1L: $err/\%$	3.2481	0.69372	3.5021
Circuit 2L: $err/\%$	2.4788	0.19463	2.2473
Circuit 3L: $err/\%$	3.2568	0.64886	3.4929
Circuit 4L: $err/\%$	2.3568	0.11373	2.2311

Table 6.7: Relative error between the simulated and calculated scattering parameters, $\frac{h}{w} = 0.6$ (lossless metal strip)

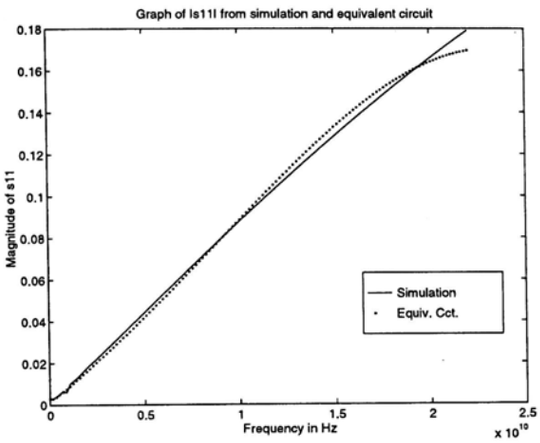

Magnitude of s_{11}

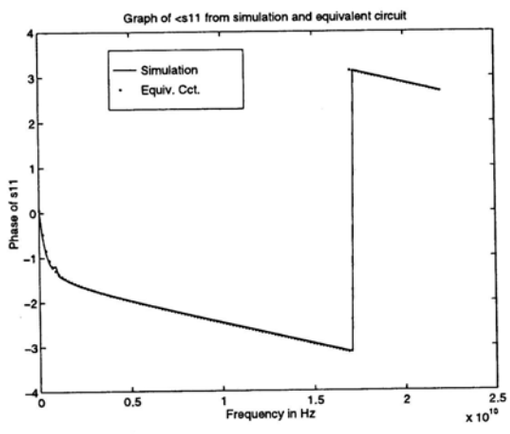

Phase of s_{11}

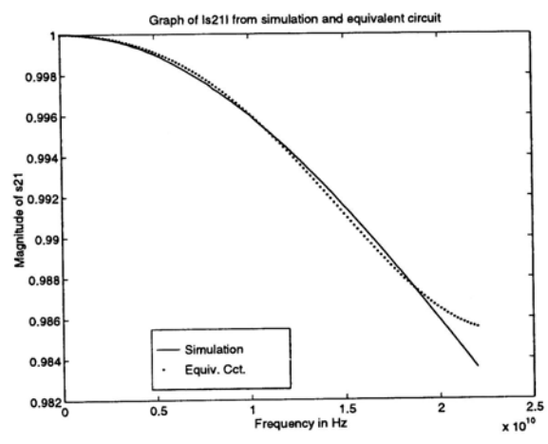

Magnitude of s_{21}

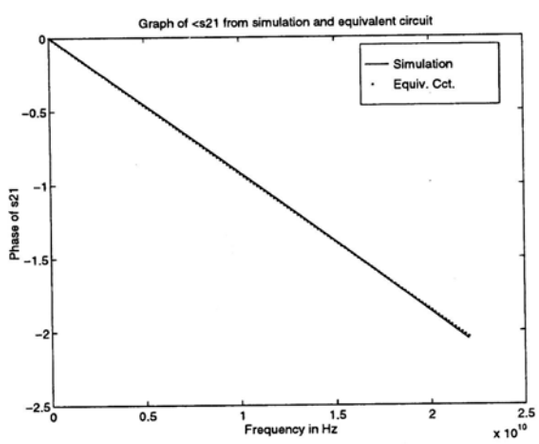

Phase of s_{21}

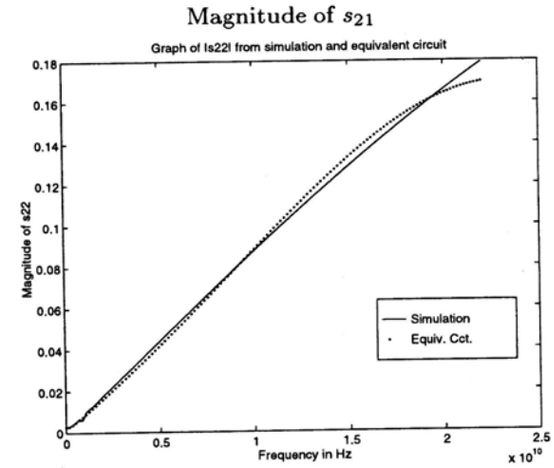

Magnitude of s_{22}

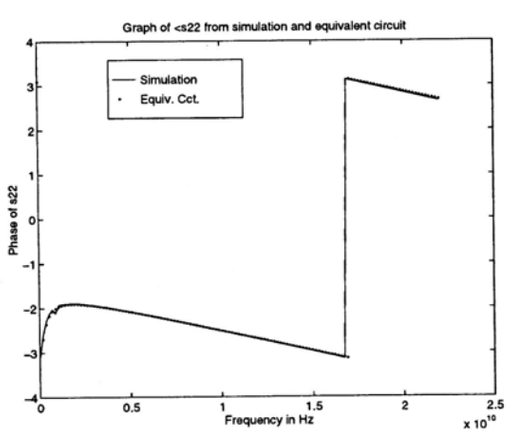

Phase of s_{22}

Figure 6.1: S parameters difference between simulation and circuit 1L (lossless metal strip), $\frac{h}{w} = 0.6$

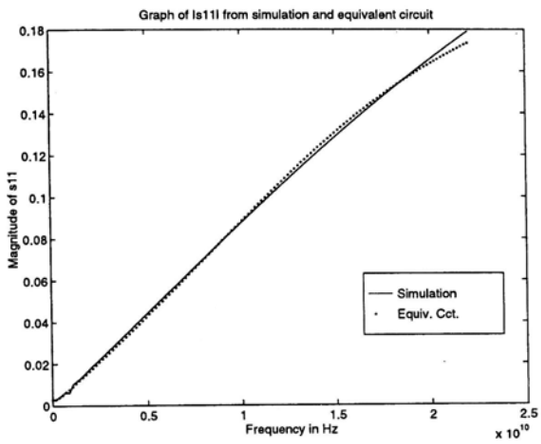

Magnitude of s_{11}

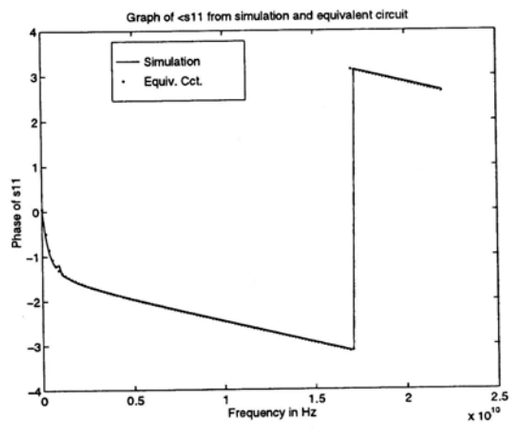

Phase of s_{11}

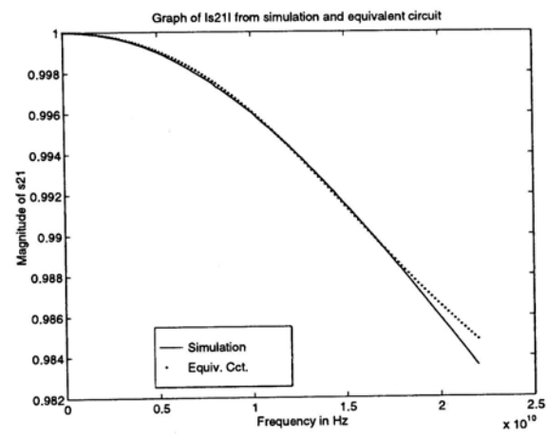

Magnitude of s_{21}

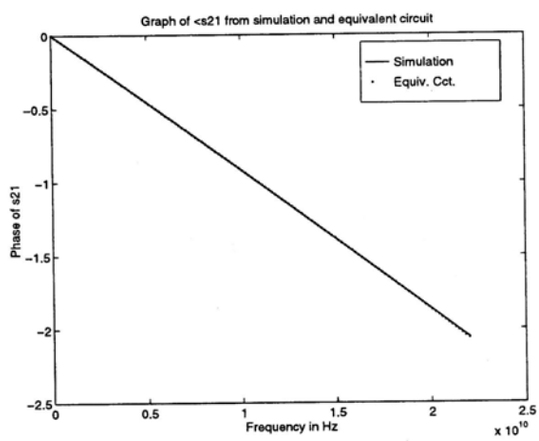

Phase of s_{21}

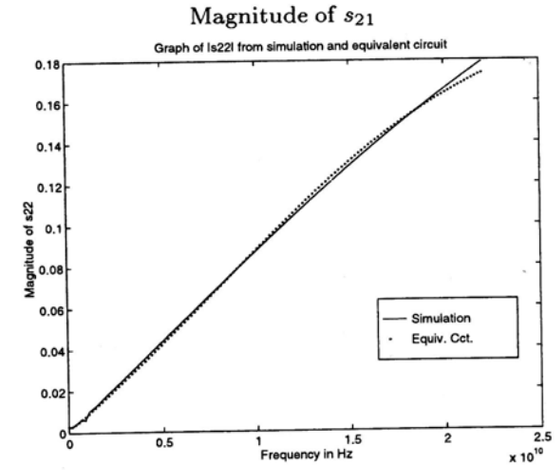

Magnitude of s_{22}

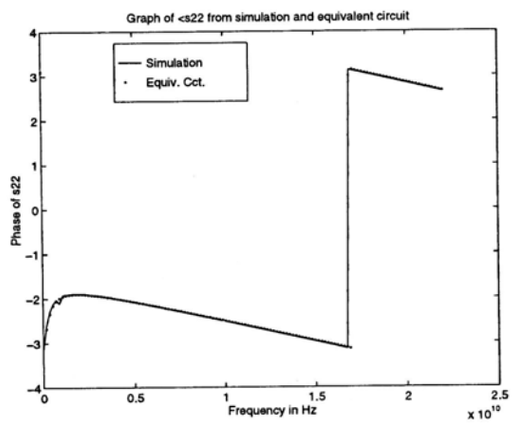

Phase of s_{22}

Figure 6.2: S parameters difference between simulation and circuit 2L (lossless metal strip), $\frac{h}{w} = 0.6$

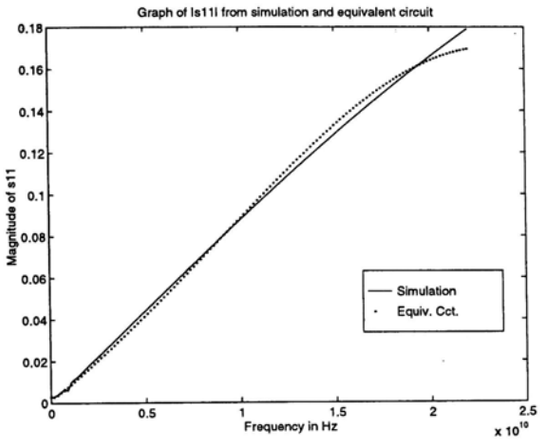

Magnitude of s_{11}

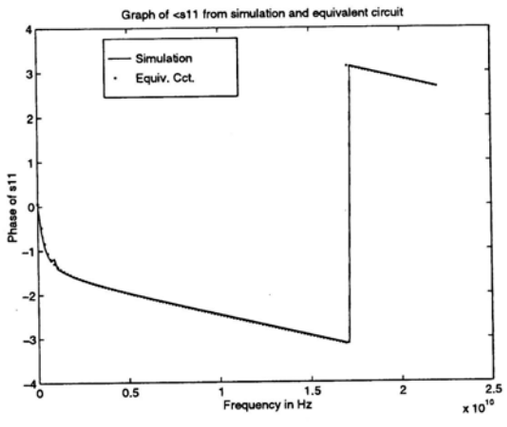

Phase of s_{11}

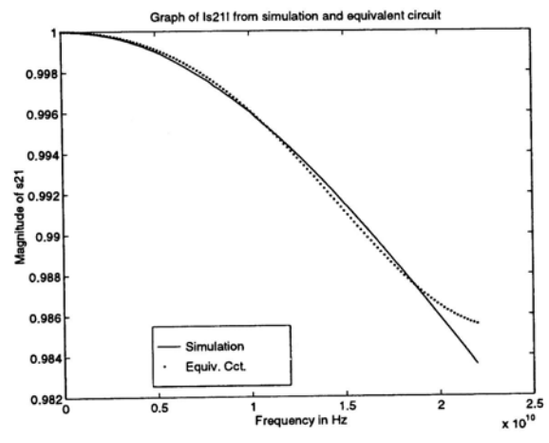

Magnitude of s_{21}

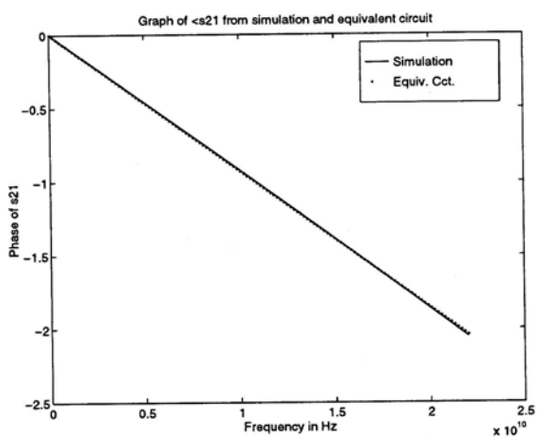

Phase of s_{21}

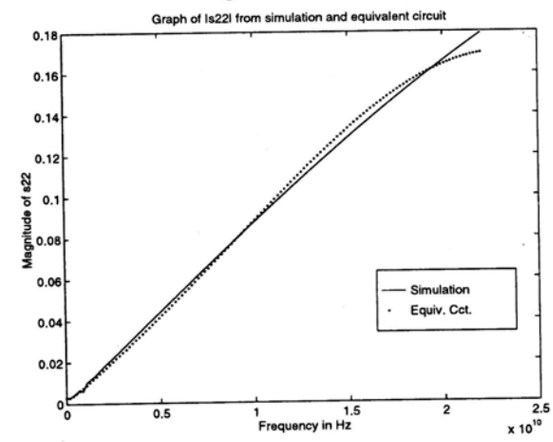

Magnitude of s_{22}

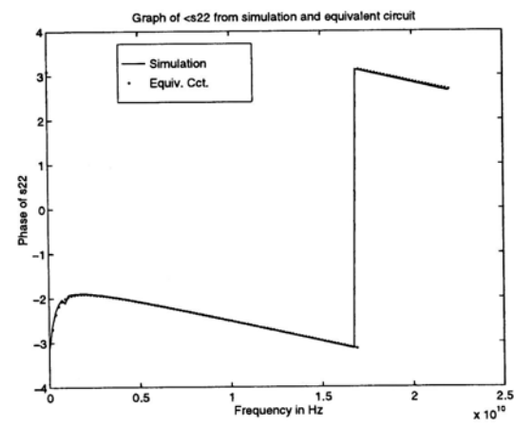

Phase of s_{22}

Figure 6.3: S parameters difference between simulation and circuit 3L (lossless metal strip), $\frac{h}{w} = 0.6$

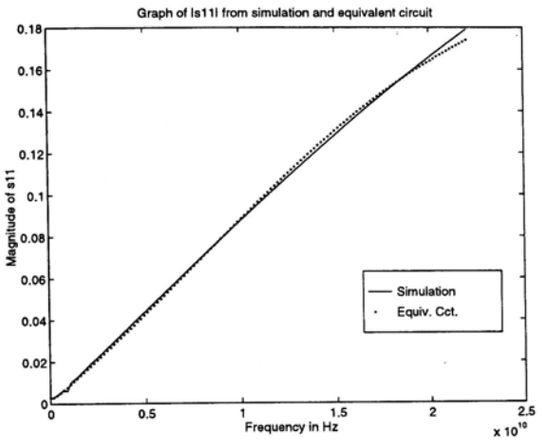

Magnitude of s_{11}

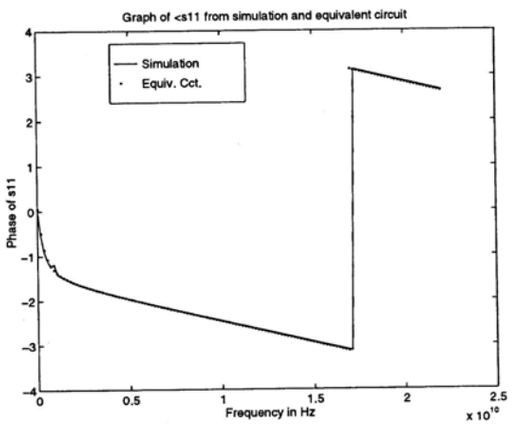

Phase of s_{11}

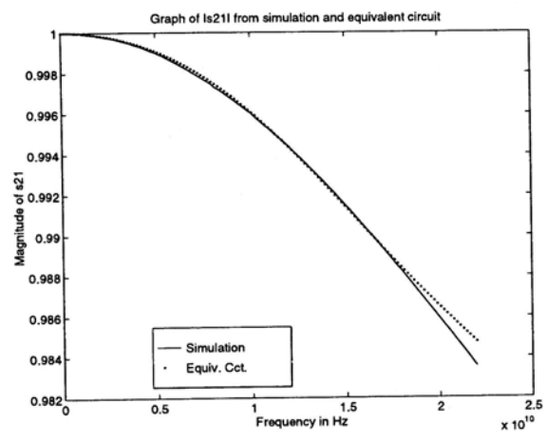

Magnitude of s_{21}

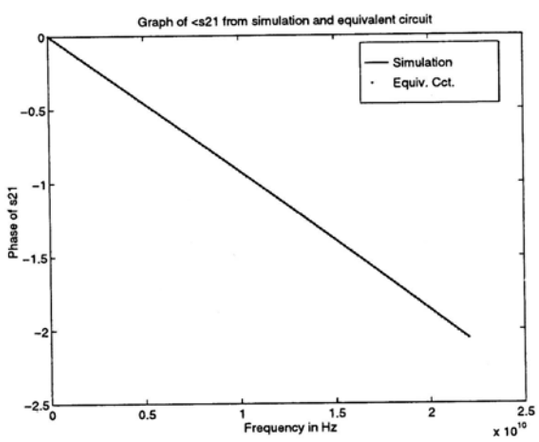

Phase of s_{21}

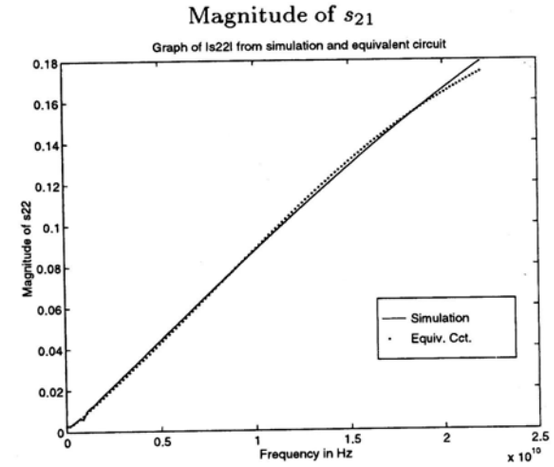

Magnitude of s_{22}

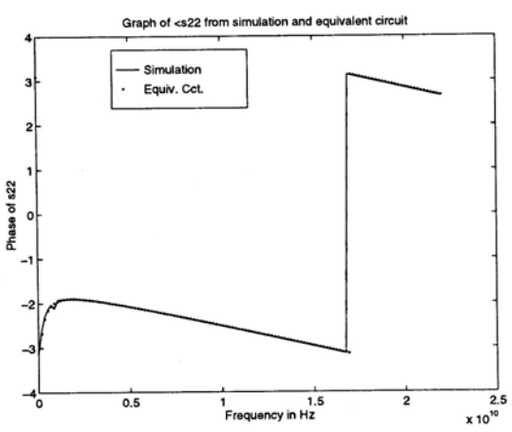

Phase of s_{22}

Figure 6.4: S parameters difference between simulation and circuit 4L (lossless metal strip), $\frac{h}{w} = 0.6$

$\frac{h}{w} = 0.8$	s_{11}	s_{21}	s_{22}
Circuit 1L: $err/\%$	5.8200	0.88885	6.0777
Circuit 2L: $err/\%$	4.9785	0.16834	4.7775
Circuit 3L: $err/\%$	5.8171	0.87117	6.0689
Circuit 4L: $err/\%$	5.0190	0.20863	4.9690

Table 6.8: Relative error between the simulated and calculated scattering parameters, $\frac{h}{w} = 0.8$ (lossless metal strip)

$\frac{h}{w} = 1.0$	s_{11}	s_{21}	s_{22}
Circuit 1L: $err/\%$	5.2211	1.1238	5.2836
Circuit 2L: $err/\%$	4.2074	0.28141	3.9977
Circuit 3L: $err/\%$	5.2027	1.1180	5.2649
Circuit 4L: $err/\%$	4.4311	0.32518	4.2961

Table 6.9: Relative error between the simulated and calculated scattering parameters, $\frac{h}{w} = 1.0$ (lossless metal strip)

6.1.2 With Conductor Loss

As stated previously, only one type of geometry of the right-angled bend has been analyzed for the lossy metal strip case. The performance results of the equivalent circuits are tabulated in Table 6.11. It is observed that increasing the number of microstrip lines in the equivalent circuit does not help much in the optimization. Circuit 3L and 4L give nearly the same relative errors in the scattering parameters, which implies that three microstrip lines are enough to model the right-angled bend if purely distributed equivalent circuit is required. On the other hand, Circuit 2L (combination of lumped and distributed circuit element) performs a little bit better than other ones. So the three proposed equivalent circuits can be used to model the right-angled bend with conductor loss being considered.

Table 6.10 records the parameter values of the equivalent circuits being found. Fig. 6.5 – 6.7 shows the degree of fitness between the simulated and calculated scattering parameters. It is seen that the matching result is not very good (compared with that from the conductor lossless case) especially at the low frequency

region. The reason is that the HFSS software does not actually simulate the EM field inside the lossy conductor. It just uses some analytical methods, not stated explicitly in the manual, to calculate the conductor loss and the field pattern on the surface of the lossy conductor. So several approaches of modelling the skin-effect are tried and finally a rather good skin-effect model (effective thickness approach) is chosen. By using this effective thickness approach, it is seen from Eq. 5.14 that the effective thickness will be equal to the physical thickness only at zero frequency. Its value is usually smaller than the physical thickness. So the conductor loss at low frequency is slightly over-estimated[3] and therefore the curves of the calculated s_{11} and s_{22} are above those of the simulated ones at low frequency.

Refer to the magnitude plots of s_{21} of the Circuit 3L and 4L (Fig. 6.6 and 6.7), the calculated curves are slightly below the simulated ones. There may be two mechanisms causing this result. The first one is due to the over-estimate of the skin-effect loss in the equivalent circuits at low frequency. The second effect is that there is a week coupling effect between the arms of the right-angled bend when frequency increases. Since the equivalent circuits (Circuit 3L and 4L) do not take care of the second effect, the estimated total loss is slightly larger at high frequency. As the difference is very small, the coupling effect can be neglected within the frequency range. Refer to Fig. 6.5, the calculated s_{21} is not totally below the simulated one. The reason is that the EM field around the junction of the right-angled bend, including the week coupling effect, has been taken into account by the inductors and capacitor.

6.2 T-Junction

As the structure of a T-junction is more complex than that of a right-angled

[3]For aluminium metal strip with $1\mu m$ in thickness, skin effect occurs when the frequency is greater than 7.2372 GHz. Below this frequency, t_{eff} should be equal to the physical thickness t.

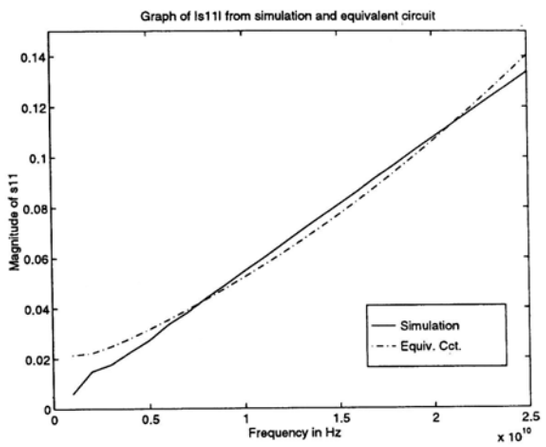

Magnitude of s_{11}

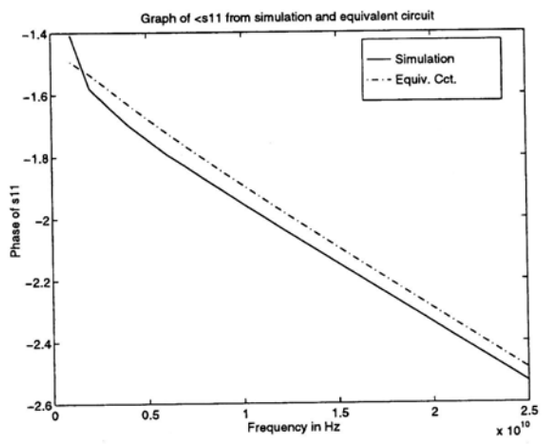

Phase of s_{11}

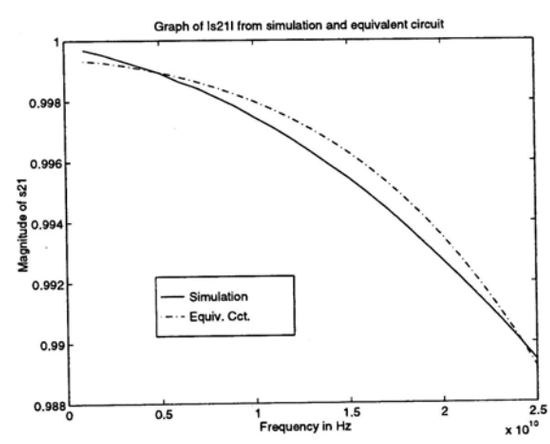

Magnitude of s_{21}

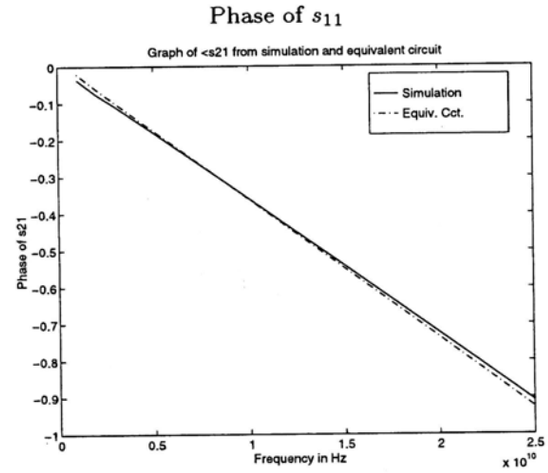

Phase of s_{21}

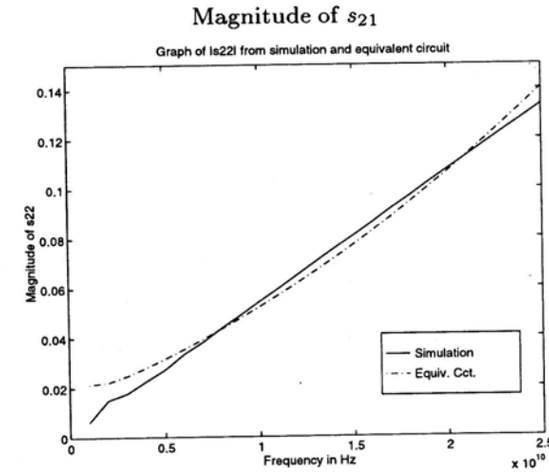

Magnitude of s_{22}

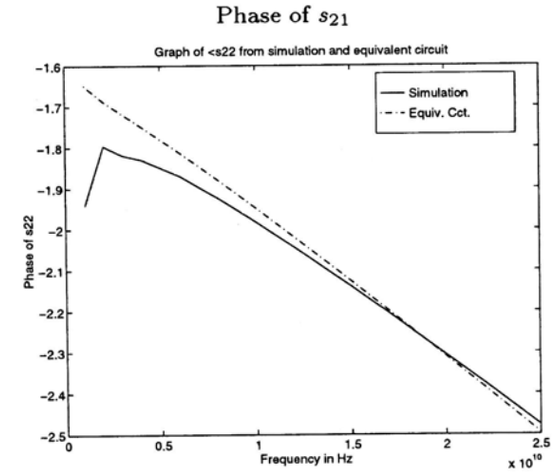

Phase of s_{22}

Figure 6.5: S parameters difference between simulation and circuit 2L (lossy metal strip), $\frac{h}{w} = 1.0$.

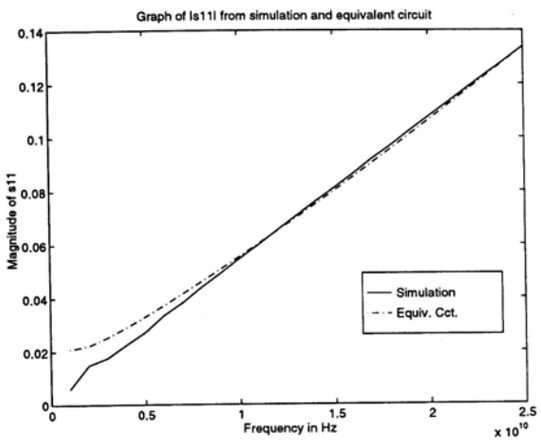

Magnitude of s_{11}

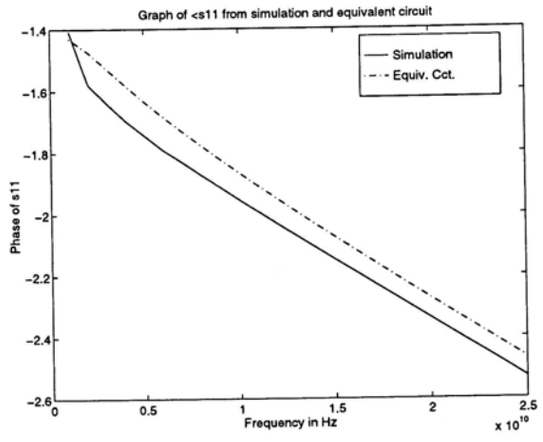

Phase of s_{11}

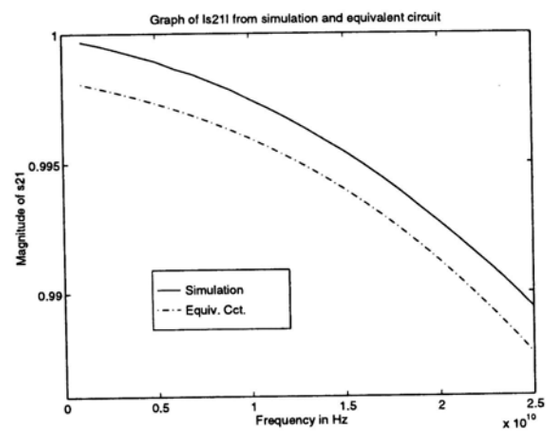

Magnitude of s_{21}

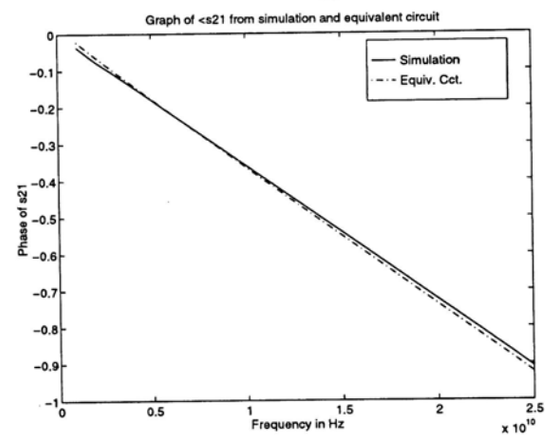

Phase of s_{21}

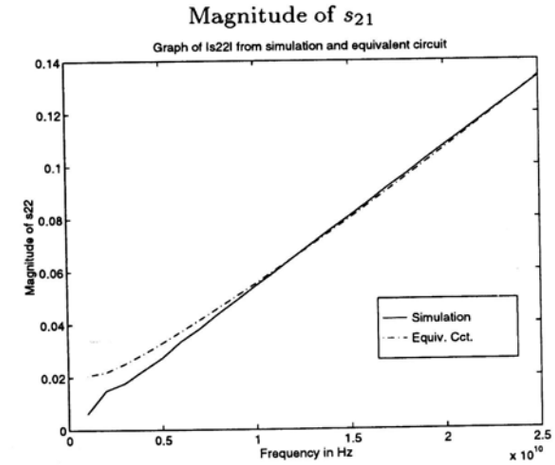

Magnitude of s_{22}

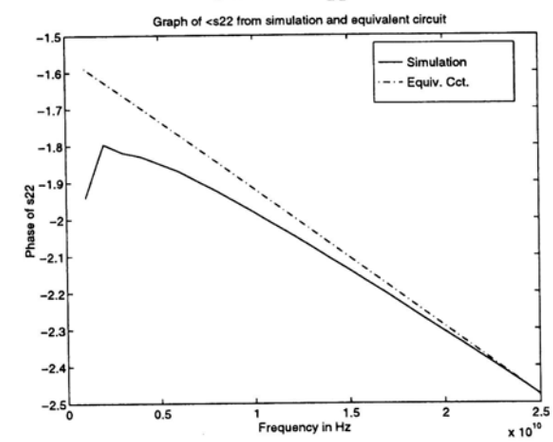

Phase of s_{22}

Figure 6.6: S parameters difference between simulation and circuit 3L (lossy metal strip), $\frac{h}{w} = 1.0$.

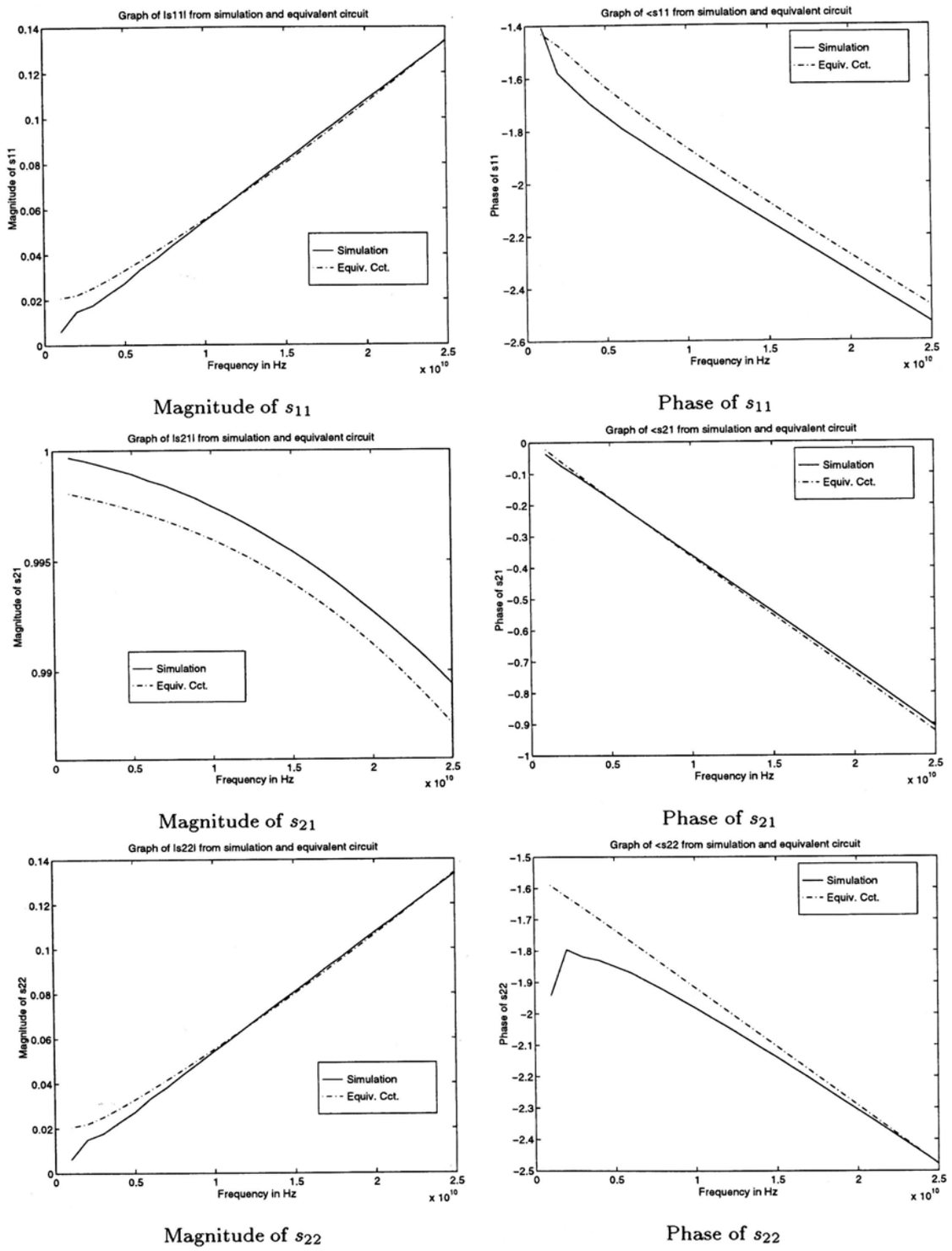

Magnitude of s_{11} Phase of s_{11}

Magnitude of s_{21} Phase of s_{21}

Magnitude of s_{22} Phase of s_{22}

Figure 6.7: S parameters difference between simulation and circuit 4L (lossy metal strip), $\frac{h}{w} = 1.0$.

$w, h/mm$	w_1/mm	l_1/mm	L/H	C/F	err
0.1	0.16474	0.10130	8.7335×10^{-11}	9.2409×10^{-14}	1.2740×10^{-2}

Parameter values of the equivalent circuit 2L

$w, h/mm$	w_1/mm	l_1/mm	w_2/mm	l_2/mm	err
0.1	0.12274	0.13121	0.15352	0.40491	1.3372×10^{-2}

Parameter values of the equivalent circuit 3L

$w, h/mm$	w_1/mm	l_1/mm	w_2/mm	l_2/mm	w_3/mm	l_3/mm	err
0.1	0.11922	0.083052	0.13660	0.094822	0.15602	0.31158	1.3372×10^{-2}

Parameter values of the equivalent circuit 4L

Table 6.10: Parameter values of the equivalent circuits for the lossy metal strip right-angled bend

$\frac{h}{w} = 1.0$	s_{11}	s_{21}	s_{22}
Circuit 2L: $err/\%$	7.7677	0.99710	6.3279
Circuit 3L: $err/\%$	8.7688	1.0313	6.2093
Circuit 4L: $err/\%$	8.7523	1.0329	6.1901

Table 6.11: Relative error between the simulated and calculated scattering parameters, $\frac{h}{w} = 1.0$ (lossy metal strip)

bend, it is expected that it is more difficult to find an equivalent circuit to model it. The performance results of the equivalent circuits (Section 5.3) to model this microstrip discontinuity are recorded in this section.

6.2.1 Without Conductor Loss

The unknown parameter values for each of the equivalent circuits that models the T-junction are tabulated for different values of $\frac{h}{w}$ ratio (Table 6.12 to 6.14). Some insights are observed.

- for those circuits with equivalent capacitor (Circuit 2T and 3T), its value decreases as the ratio $\frac{h}{w}$ increases. It is because the capacitance is inversely proportional to the substrate thickness.

- as in the case for the right-angled bend, the values of the equivalent inductance of the Circuit 3T increase when the ratio $\frac{h}{w}$ increases.

- the modelling result is worse when the value $\frac{h}{w}$ is larger because of the increasing mode-coupling effect.

The degree of fitness between the calculated scattering parameters and the simulated ones can be seen from Fig. 6.8 – 6.10, which is the result of the T-junction with $\frac{h}{w} = 0.6$. From these figures, it is seen that the phase plots match better than the magnitude plots because of the same reason for the right-angled bend. Besides, it is observed that Circuit 3T is the best among three in modelling the T-junction because the calculated scattering parameter curves from Circuit 3T show the same trend with the simulated ones within the frequency range. The results of the other two equivalent circuits show opposite trend in the high frequency region. It is seen from Fig. 6.8 and 6.10 that s_{11} decreases but both s_{12} and s_{13} increase in the high frequency region. In other words, more energy is transmitted from port 1 to port 2 and port 3 when frequency increases. Refer to the equivalent circuits 2T and 4T, the discontinuity region of the T-junction is directly modelled by connecting the three microstrip lines together, which may not be able to model the field at the junction when frequency increases. On the other hand, the electric and magnetic energy at the discontinuity region is represented by three inductors and a capacitor in Circuit 3T, which can model the EM field behaviour at the discontinuity region.

Table 6.15 – 6.19 record the performance of the equivalent circuits for other geometries of the T-junction. Again, it is observed that the values of the relative errors from Circuit 3T is much smaller than those from Circuit 2T and 4T. So Circuit 3T is the choice in modelling the T-junction when conductor loss is not considered.

As in right-angled bend, the parameters of the Circuit 3T shows a monotonic behaviour with respect to the geometry of the T-junction (Table 6.13). So some empirical formulae which relate the equivalent circuit parameters to the geometry of the T-junction can be derived.

$\frac{h}{w}$	w_1/mm	l_1/mm	w_2/mm	l_2/mm	C/F	err
0.2	0.26635	1.3538	0.26363	1.2405	1.1976×10^{-14}	6.4044×10^{-3}
0.4	0.27164	1.3561	0.26788	1.2163	1.2332×10^{-14}	7.6513×10^{-3}
0.6	0.27058	1.3581	0.26525	1.1962	5.9627×10^{-15}	1.0973×10^{-2}
0.8	0.26919	1.3636	0.25973	1.1824	2.1725×10^{-15}	1.4077×10^{-2}
1.0	0.27004	1.3675	0.25462	1.1612	2.1226×10^{-15}	1.7873×10^{-2}

Table 6.12: Parameter values for equivalent circuit 2T (lossless metal strip)

$\frac{h}{w}$	w_1/mm	l_1/mm	w_2/mm	l_2/mm	L_1/H
0.2	0.27231	1.0288	0.27439	0.88843	5.2551×10^{-11}
0.4	0.28009	1.0030	0.29044	0.79592	9.0717×10^{-11}
0.6	0.28544	0.95205	0.31342	0.68715	1.3349×10^{-10}
0.8	0.29133	0.90566	0.35571	0.58187	1.7666×10^{-10}
1.0	0.30224	0.86831	0.43308	0.47441	2.1426×10^{-10}

$\frac{h}{w}$	L_2/H	C/F	err
0.2	5.7966×10^{-11}	5.2135×10^{-13}	4.4809×10^{-3}
0.4	1.1073×10^{-10}	3.4296×10^{-13}	3.5953×10^{-3}
0.6	1.7320×10^{-10}	2.9051×10^{-13}	4.9560×10^{-3}
0.8	2.4157×10^{-10}	2.6590×10^{-13}	7.0330×10^{-3}
1.0	3.1082×10^{-10}	2.5339×10^{-13}	8.2536×10^{-3}

Table 6.13: Parameter values for equivalent circuit 3T (lossless metal strip)

$\frac{h}{w}$	w_1/mm	l_1/mm	w_2/mm	l_2/mm	w_3/mm	l_3/mm	err
0.2	0.26629	1.2164	0.27948	0.14226	0.26375	1.2405	6.3756×10^{-3}
0.4	0.27071	0.88859	0.28023	0.47572	0.26846	1.2171	7.3413×10^{-3}
0.6	0.26965	0.81179	0.27613	0.55167	0.26578	1.1966	1.0755×10^{-2}
0.8	0.26885	0.90615	0.27239	0.45987	0.25989	1.1826	1.4020×10^{-2}
1.0	0.26963	0.90306	0.27397	0.46715	0.25477	1.1613	1.7774×10^{-2}

Table 6.14: Parameter values for equivalent circuit 4T (lossless metal strip)

$\frac{h}{w} = 0.2$	s_{11}	s_{12}	s_{13}	s_{22}	s_{23}	s_{33}
Circuit 2T: $err/\%$	1.1095	0.63223	0.45339	1.4149	0.28699	1.5358
Circuit 3T: $err/\%$	0.49139	0.33948	0.36962	1.0723	0.25563	1.2309
Circuit 4T: $err/\%$	1.0972	0.62922	0.44579	1.3975	0.29079	1.5498

Table 6.15: Relative error between the simulated and calculated scattering parameters, $\frac{h}{w} = 0.2$ (lossless metal strip)

$\frac{h}{w} = 0.4$	s_{11}	s_{12}	s_{13}	s_{22}	s_{23}	s_{33}
Circuit 2T: $err/\%$	1.8749	0.60022	0.64007	1.5858	0.32464	1.6523
Circuit 3T: $err/\%$	0.85432	0.19384	0.17063	0.94474	0.23342	0.94583
Circuit 4T: $err/\%$	1.7113	0.57076	0.62306	1.5985	0.29714	1.6219

Table 6.16: Relative error between the simulated and calculated scattering parameters, $\frac{h}{w} = 0.4$ (lossless metal strip)

$\frac{h}{w} = 0.6$	s_{11}	s_{12}	s_{13}	s_{22}	s_{23}	s_{33}
Circuit 2T: $err/\%$	2.9391	0.81579	0.85291	2.2295	0.45487	2.4310
Circuit 3T: $err/\%$	1.2396	0.18546	0.21754	1.2240	0.36062	1.3733
Circuit 4T: $err/\%$	2.8377	0.79597	0.83166	2.2372	0.42927	2.4369

Table 6.17: Relative error between the simulated and calculated scattering parameters, $\frac{h}{w} = 0.6$ (lossless metal strip)

$\frac{h}{w} = 0.8$	s_{11}	s_{12}	s_{13}	s_{22}	s_{23}	s_{33}
Circuit 2T: $err/\%$	3.6395	1.1289	1.1299	2.9682	0.42346	3.0684
Circuit 3T: $err/\%$	1.6115	0.36585	0.37036	1.7819	0.48285	1.8898
Circuit 4T: $err/\%$	3.6161	1.1252	1.1190	2.9682	0.41073	3.0851

Table 6.18: Relative error between the simulated and calculated scattering parameters, $\frac{h}{w} = 0.8$ (lossless metal strip)

$\frac{h}{w} = 1.0$	s_{11}	s_{12}	s_{13}	s_{22}	s_{23}	s_{33}
Circuit 2T: $err/\%$	4.8192	1.4764	1.4541	3.6460	0.54480	3.4801
Circuit 3T: $err/\%$	2.0936	0.31384	0.36186	2.1311	0.64917	2.0341
Circuit 4T: $err/\%$	4.7950	1.4640	1.4394	3.6524	0.51999	3.4966

Table 6.19: Relative error between the simulated and calculated scattering parameters, $\frac{h}{w} = 1.0$ (lossless metal strip)

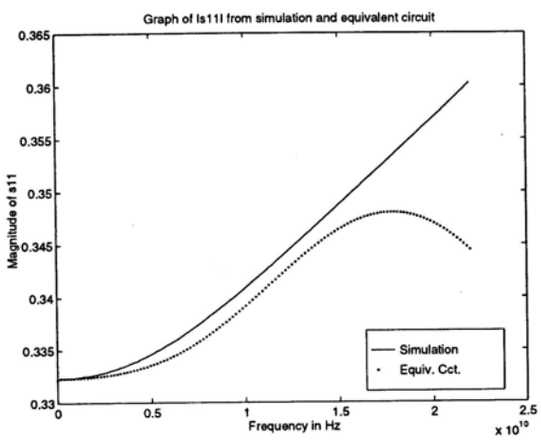

Magnitude of s_{11}

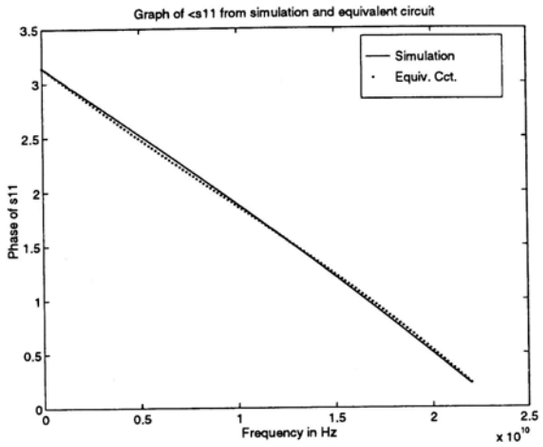

Phase of s_{11}

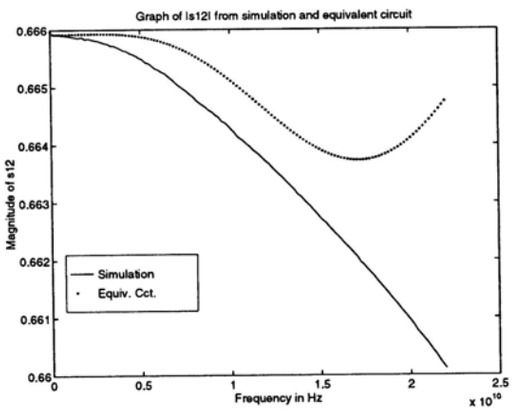

Magnitude of s_{12}

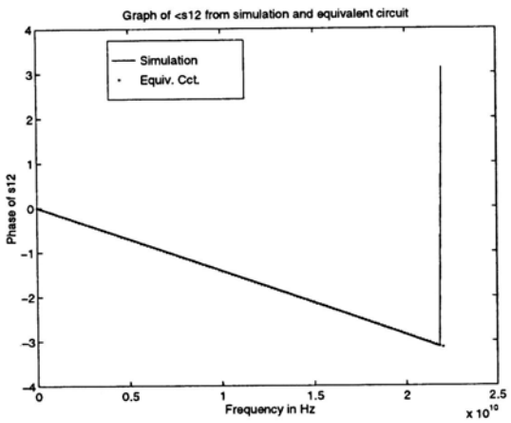

Phase of s_{12}

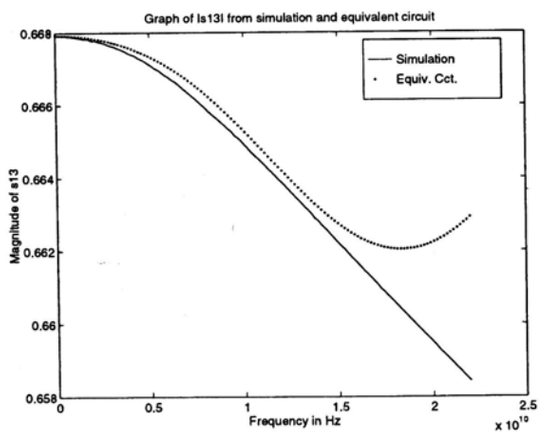

Magnitude of s_{13}

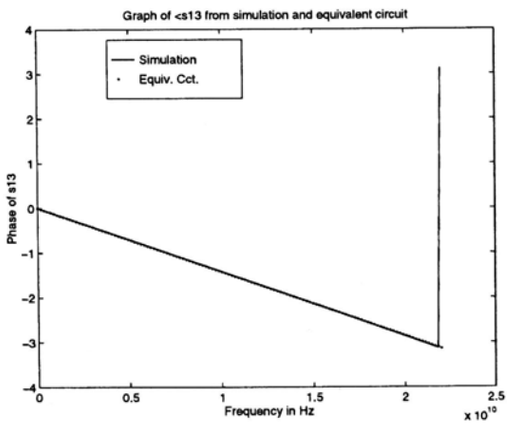

Phase of s_{13}

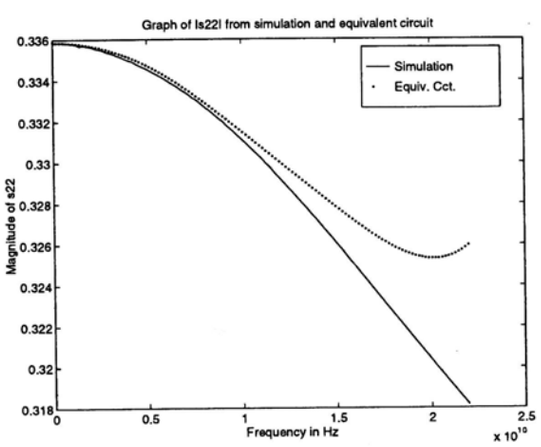

Magnitude of s_{22}

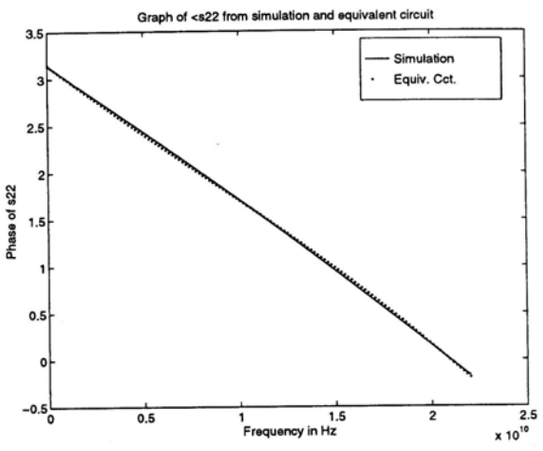

Phase of s_{22}

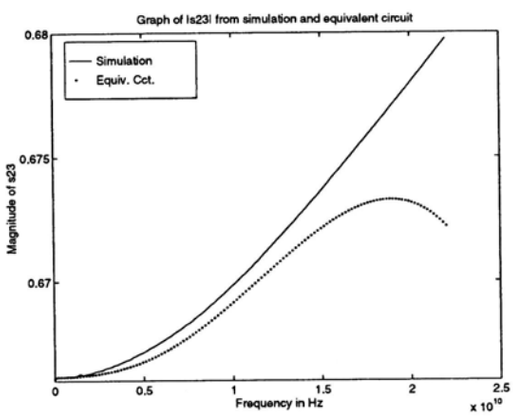

Magnitude of s_{23}

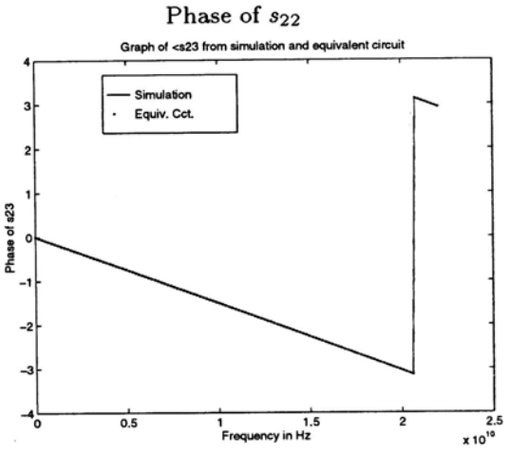

Phase of s_{23}

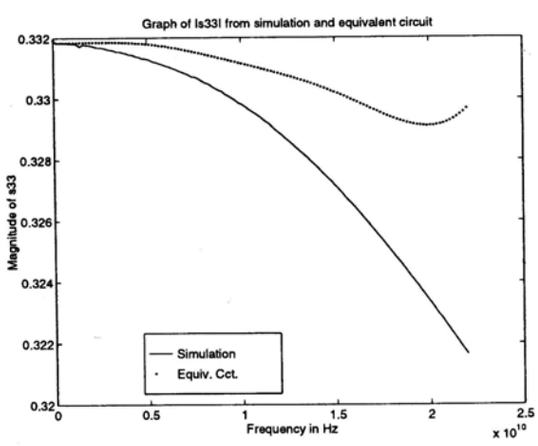

Magnitude of s_{33}

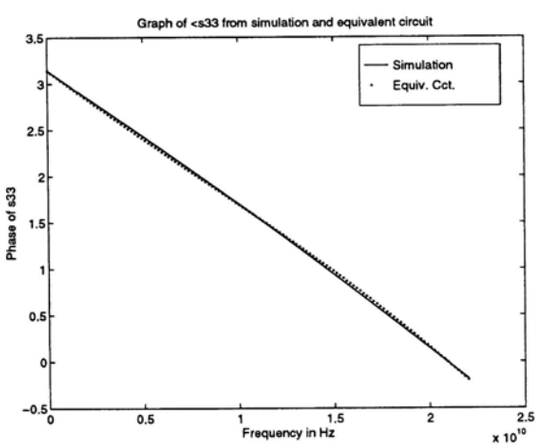

Phase of s_{33}

Figure 6.8: S parameters difference between simulation and circuit 2T (lossless metal strip), $\frac{h}{w} = 0.6$

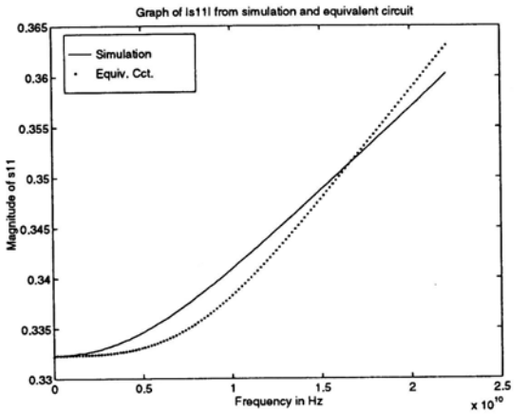

Magnitude of s_{11}

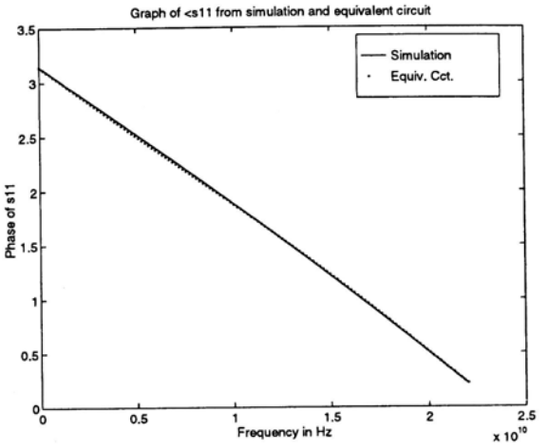

Phase of s_{11}

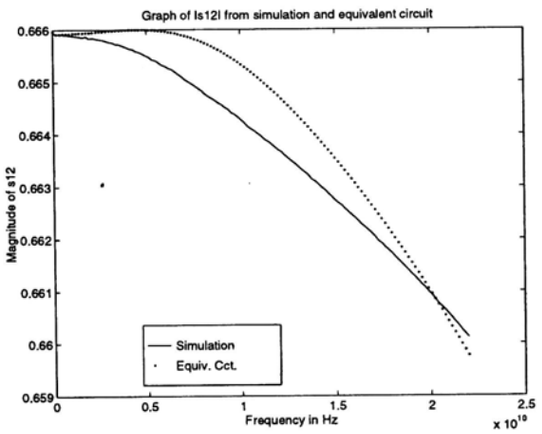

Magnitude of s_{12}

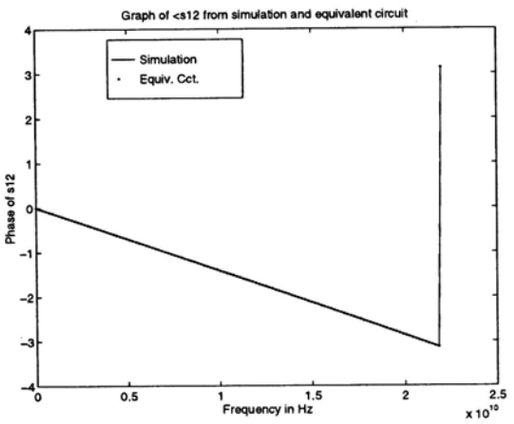

Phase of s_{12}

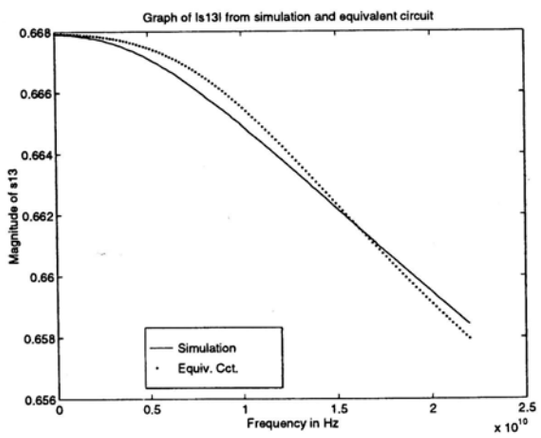

Magnitude of s_{13}

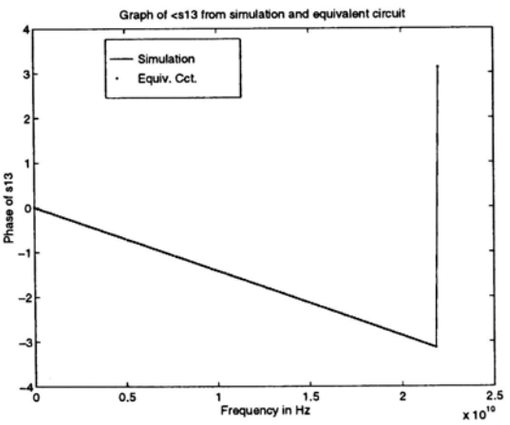

Phase of s_{13}

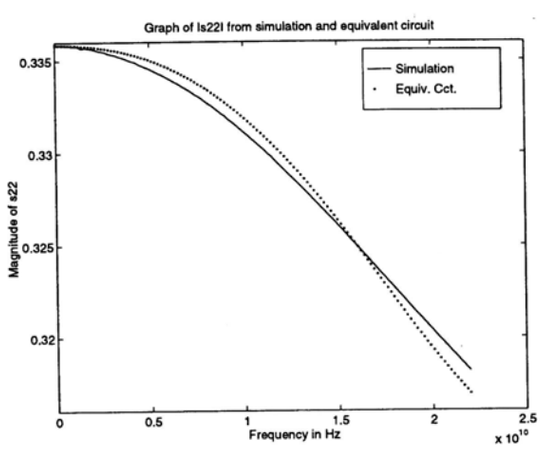

Magnitude of s_{22}

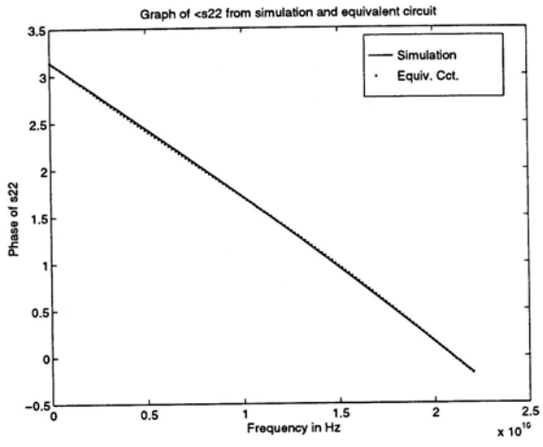

Phase of s_{22}

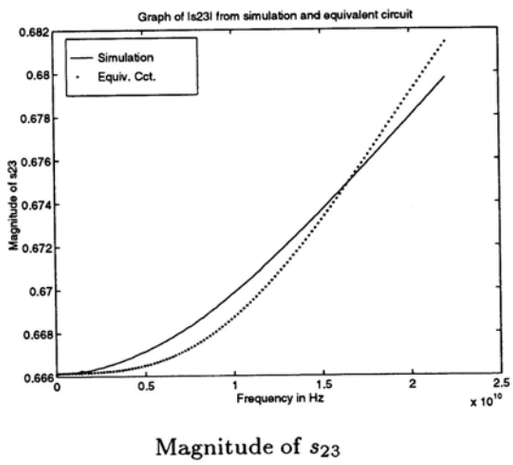

Magnitude of s_{23}

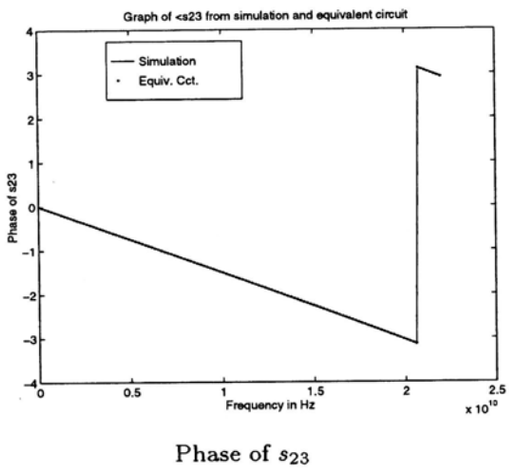

Phase of s_{23}

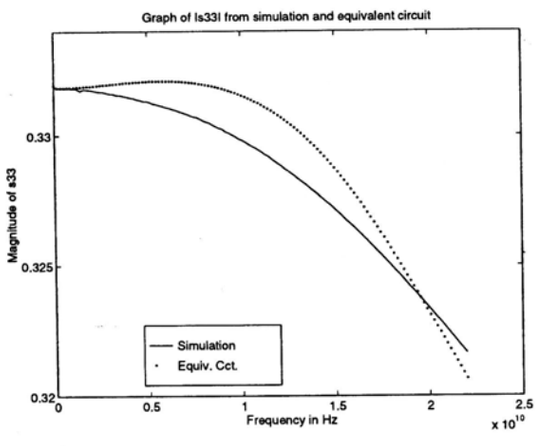

Magnitude of s_{33}

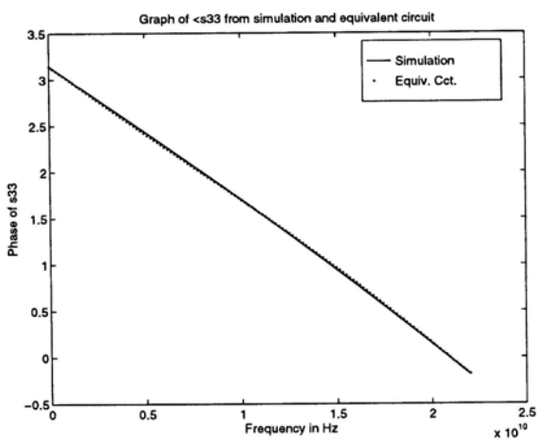

Phase of s_{33}

Figure 6.9: S parameters difference between simulation and circuit 3T (lossless metal strip), $\frac{h}{w} = 0.6$

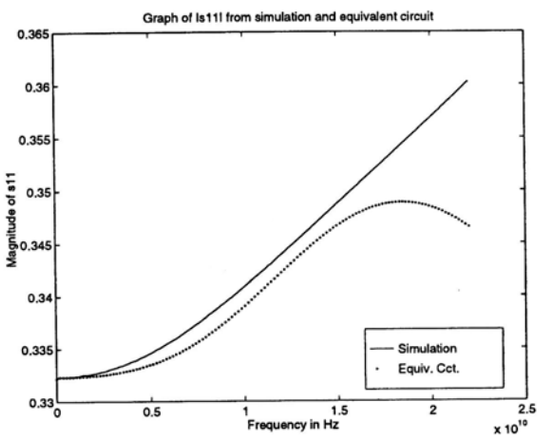

Magnitude of s_{11}

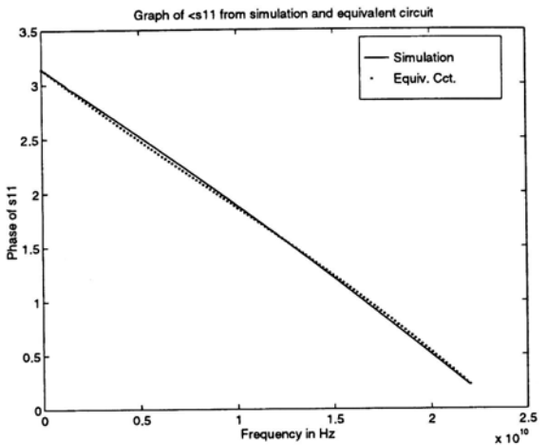

Phase of s_{11}

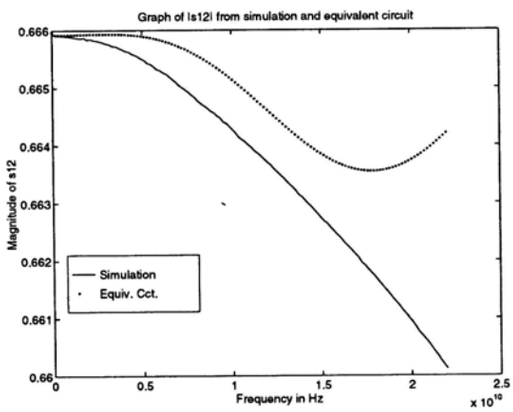

Magnitude of s_{12}

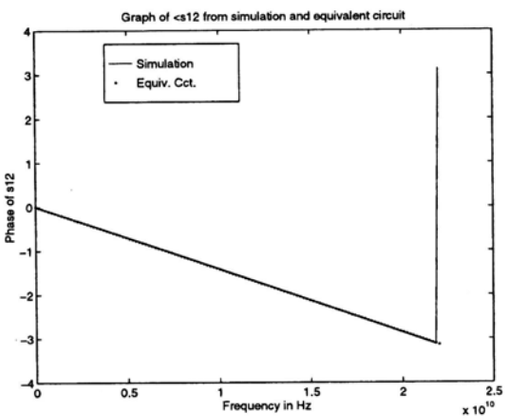

Phase of s_{12}

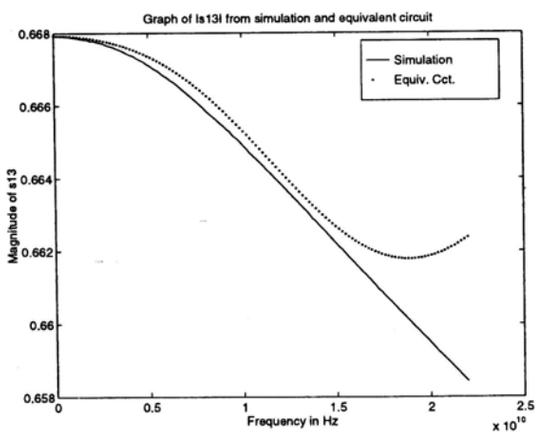

Magnitude of s_{13}

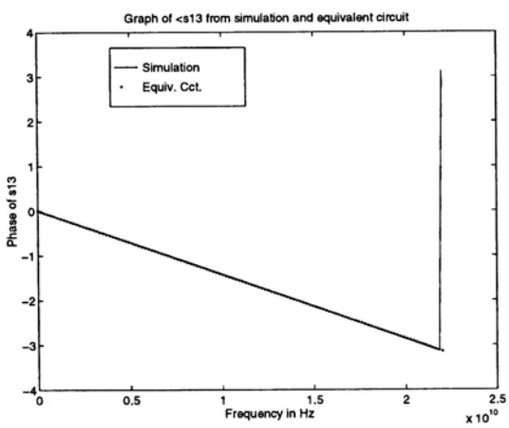

Phase of s_{13}

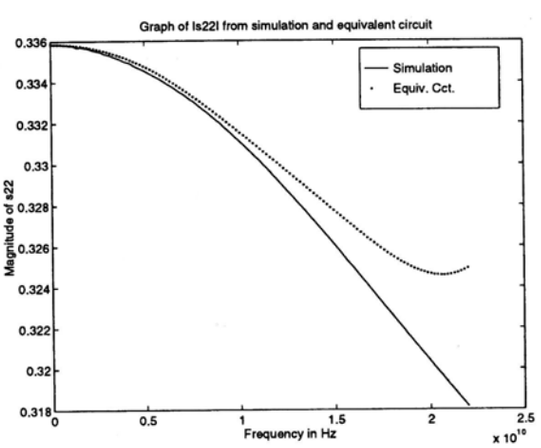

Magnitude of s_{22}

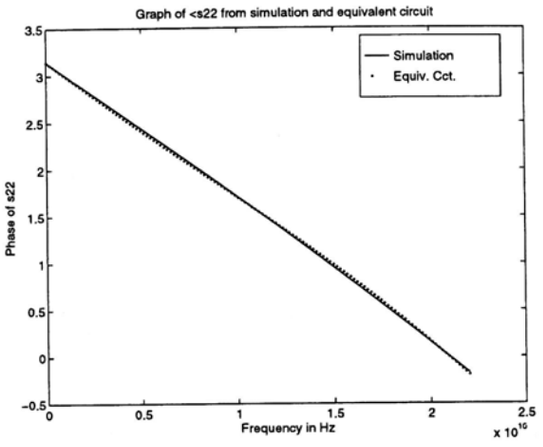

Phase of s_{22}

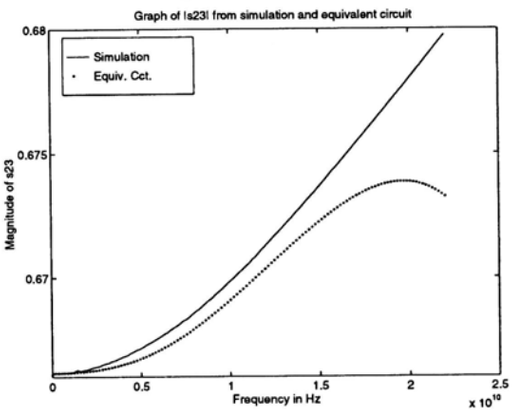

Magnitude of s_{23}

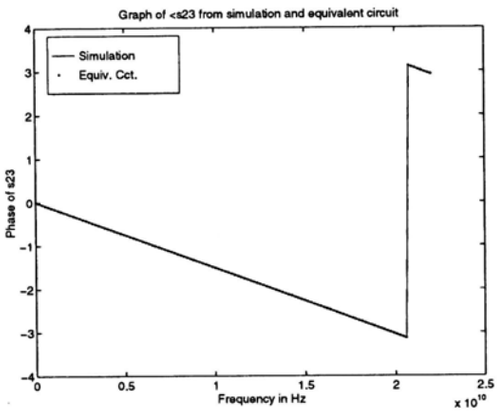

Phase of s_{23}

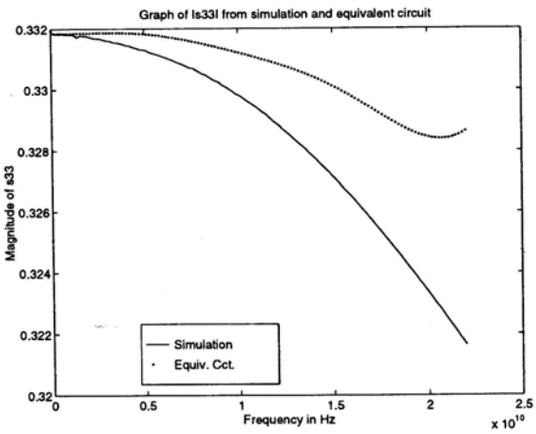

Magnitude of s_{33}

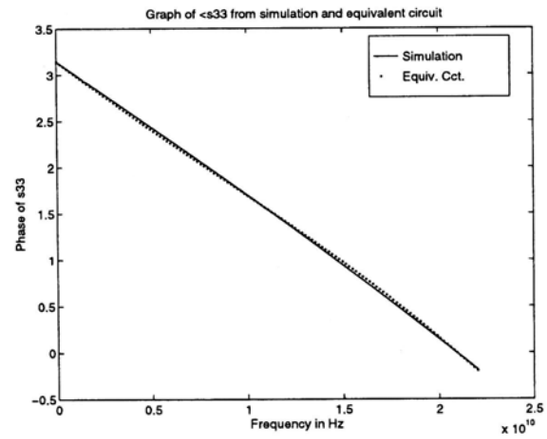

Phase of s_{33}

Figure 6.10: S parameters difference between simulation and circuit 4T (lossless metal strip), $\frac{h}{w} = 0.6$

6.2.2 With Conductor Loss

By considering the conductor loss effect, it is found that Circuit 3T cannot be used to model the T-junction because the values of some of the circuit elements become negative after the optimization no matter how the initial guess is tried. As for Circuit 4T, Table 6.21 records its values of the circuit elements being found. It is seen that the value of w_2 is about 9mm; however, the width of the arms of the T-junction is $100\mu m$ only. So Circuit 4T is not realistic to model the T-junction.

Table 6.21 also records the parameter values of the equivalent circuits Circuit 1T and 2T used to model the lossy metal strip T-junction. Fig. 6.11 – 6.12 shows the corresponding degree of fitness between the simulated scattering parameters and calculated ones. From the figures, it is once again observed that the optimization matches the phases better than the magnitudes. Morever, it is observed that all the calculated scattering parameter curves in the magnitude plots are below the corresponding simulated ones. By examining the relationship among the magnitudes of the scattering parameters,

$$|s_{11}|^2 + |s_{21}|^2 + |s_{31}|^2 \leq 1 \tag{6.1}$$

$$|s_{12}|^2 + |s_{22}|^2 + |s_{32}|^2 \leq 1 \tag{6.2}$$

$$|s_{13}|^2 + |s_{23}|^2 + |s_{33}|^2 \leq 1 \tag{6.3}$$

it is found that the values from the simulated scattering parameters are greater than those from the calculated ones. In other words, the equivalent circuits overestimate the loss in the T-junction being analyzed; nevertheless, the relative errors of the scattering parameters (Table 6.20) are less than 5%.

Refer to Table 6.20, it summarizes the performance of the equivalent circuits used in modelling the lossy metal strip T-junction. It is seen that the simplier the structure of the equivalent circuit, the better is the optimization (modelling) result. So Circuit 1T is the choice of modelling the T-junction if conductor loss

is considered.

$\frac{h}{w} = 1.0$	s_{11}	s_{12}	s_{13}	s_{22}	s_{23}	s_{33}
Circuit 2T: $err/\%$	4.4616	0.86934	0.78471	4.5378	0.80955	4.5942
Circuit 1T: $err/\%$	3.8771	0.83869	0.76584	3.6341	0.81331	3.7318

Table 6.20: Relative error between the simulated and calculated scattering parameters, $\frac{h}{w} = 1.0$ (lossy metal strip)

$w, h/mm$	w_1/mm	l_1/mm	w_2/mm	$l_2/\mu m$	w_3/mm	l_3/mm	err
0.1	0.093922	0.51680	9.5635	2.7315	0.079616	0.40738	1.7126×10^{-2}

Parameter values for equivalent circuit 4T

$w, h/mm$	w_1/mm	l_1/mm	w_2/mm	l_2/mm	C/F	err
0.1	0.093846	0.51675	0.079516	0.40723	4.7440×10^{-14}	1.7111×10^{-2}

Parameter values for equivalent circuit 2T

$w, h/mm$	w_1/mm	l_1/mm	w_2/mm	l_2/mm	err
0.1	0.11354	0.55233	0.10876	0.46071	1.4735×10^{-2}

Parameter values for equivalent circuit 1T

Table 6.21: Parameter values of equivalent circuit for the lossy metal strip T-junction

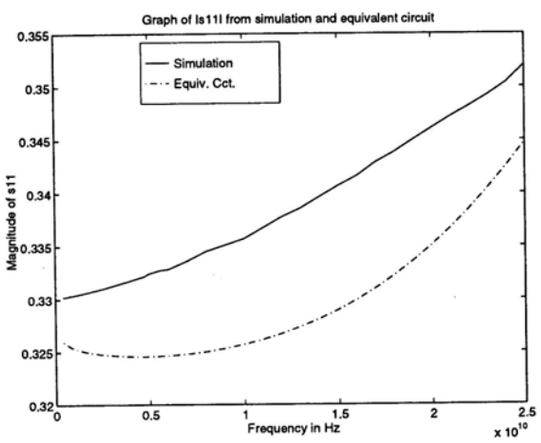

Magnitude of s_{11}

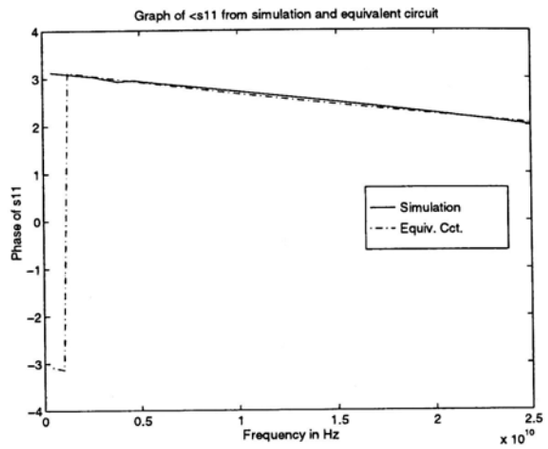

Phase of s_{11}

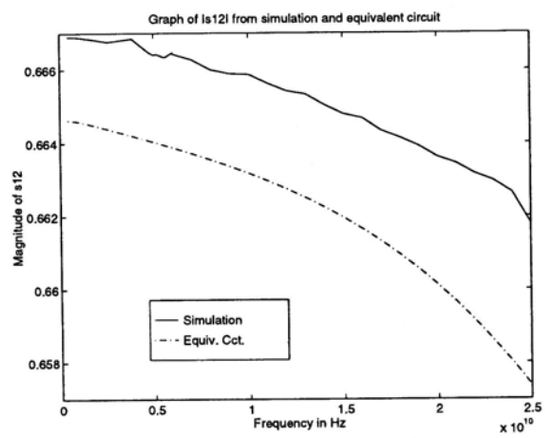

Magnitude of s_{12}

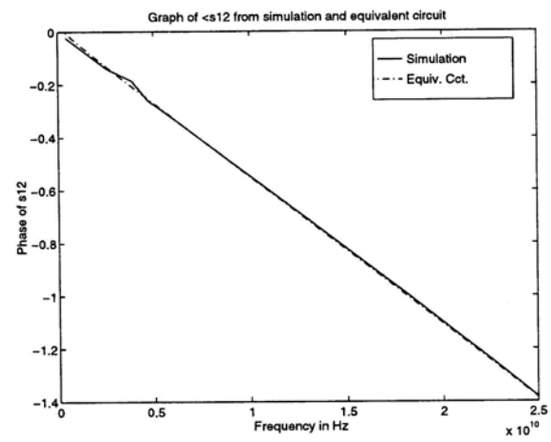

Phase of s_{12}

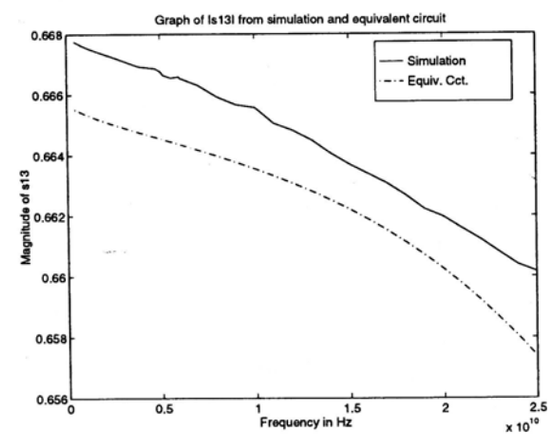

Magnitude of s_{13}

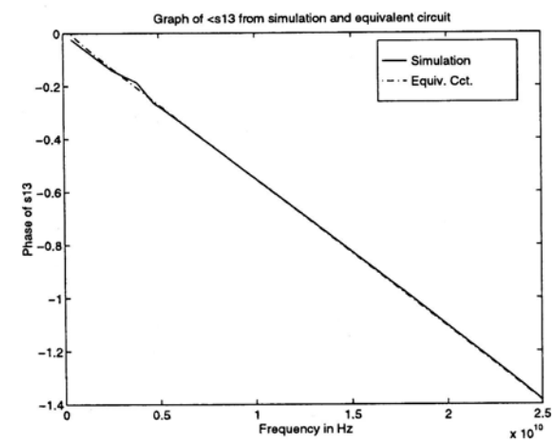

Phase of s_{13}

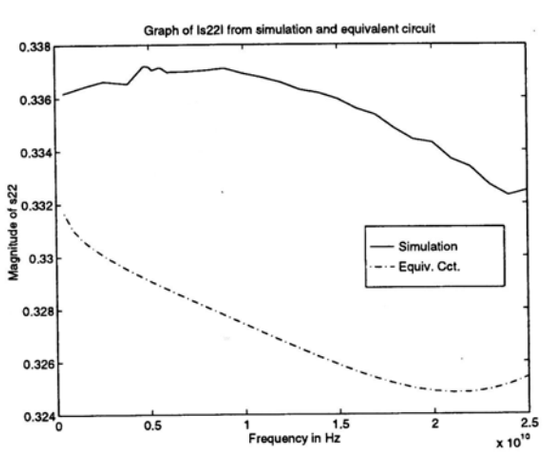

Magnitude of s_{22}

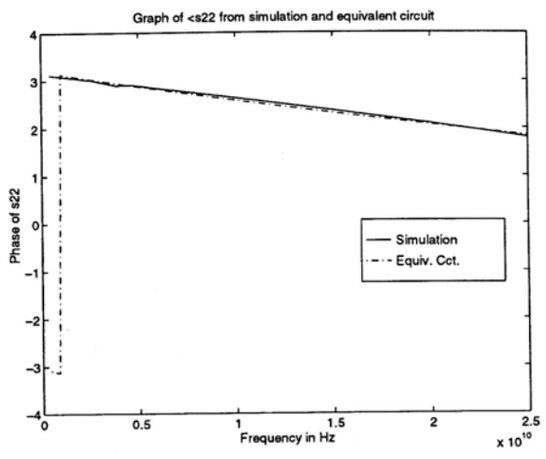

Phase of s_{22}

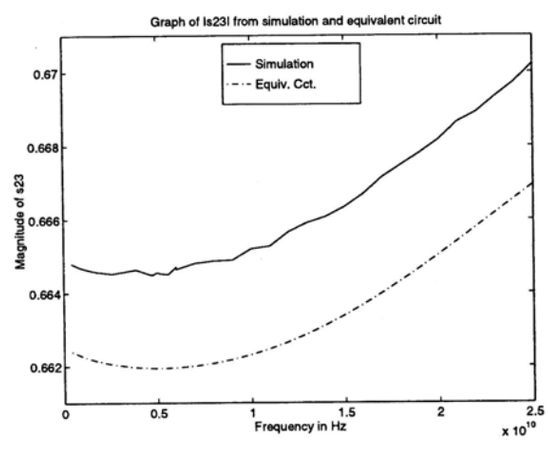

Magnitude of s_{23}

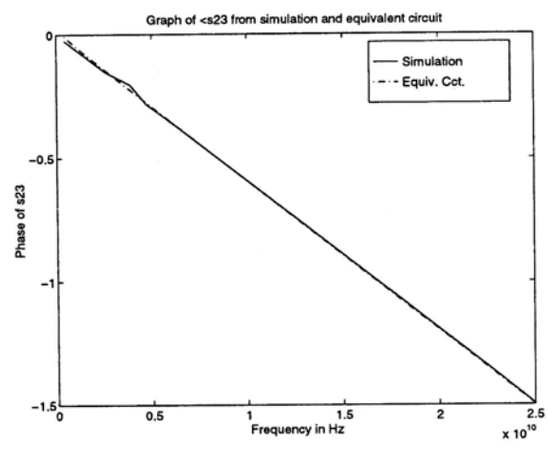

Phase of s_{23}

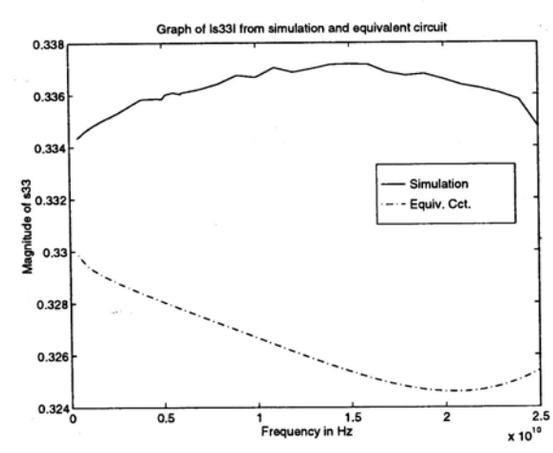

Magnitude of s_{33}

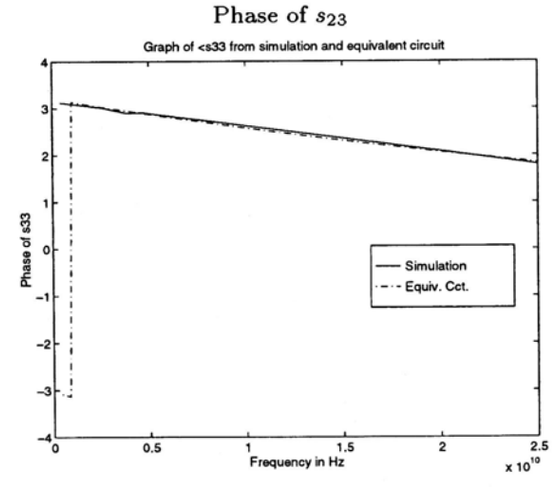

Phase of s_{33}

Figure 6.11: S parameters difference between simulation and circuit 2T (lossy metal strip), $\frac{h}{w} = 1.0$

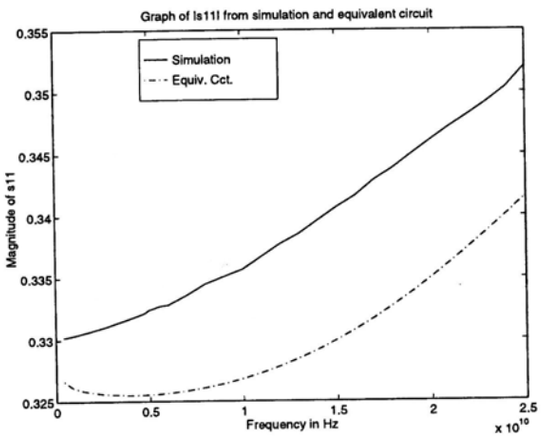

Magnitude of s_{11}

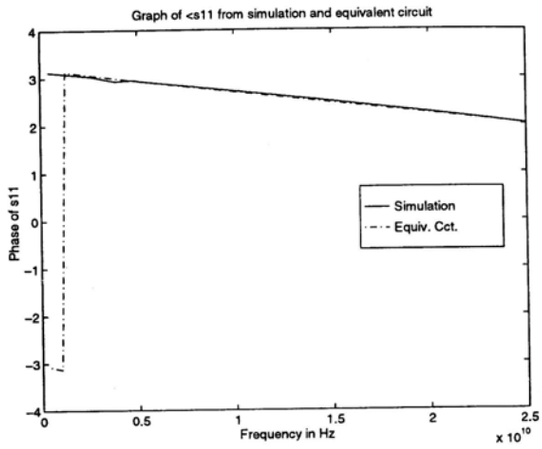

Phase of s_{11}

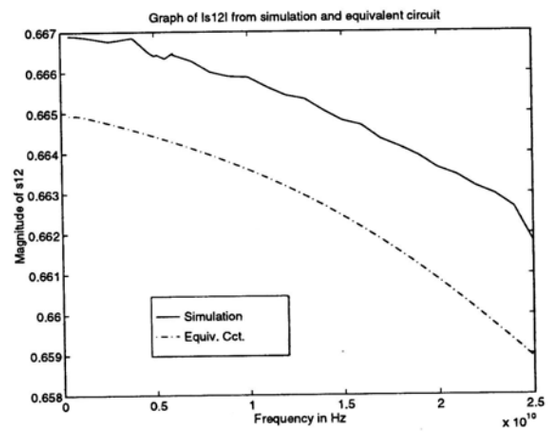

Magnitude of s_{12}

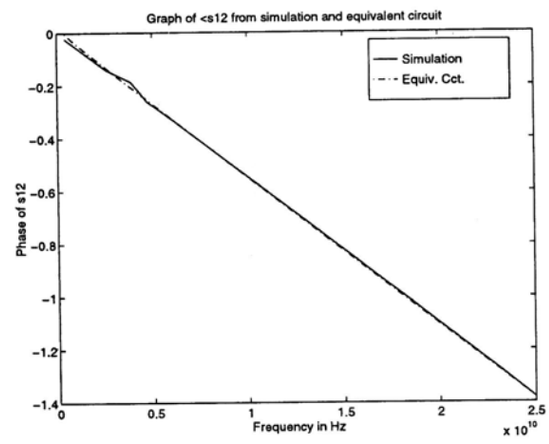

Phase of s_{12}

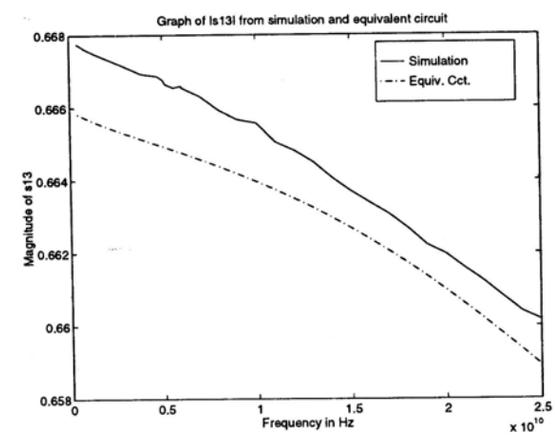

Magnitude of s_{13}

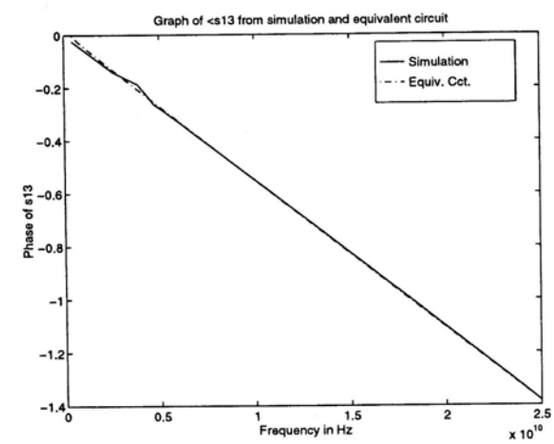

Phase of s_{13}

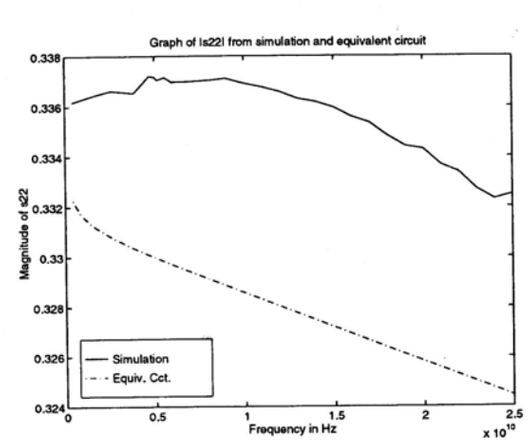

Magnitude of s_{22}

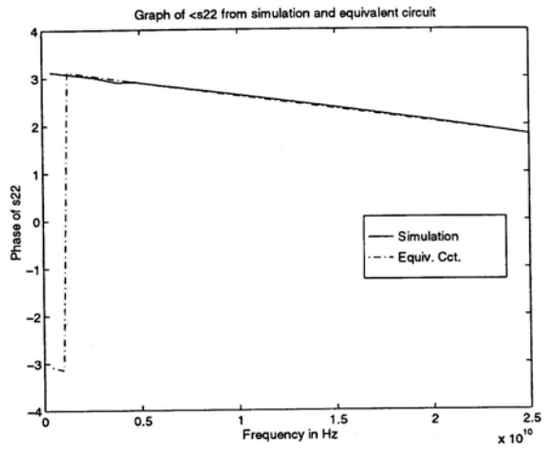

Phase of s_{22}

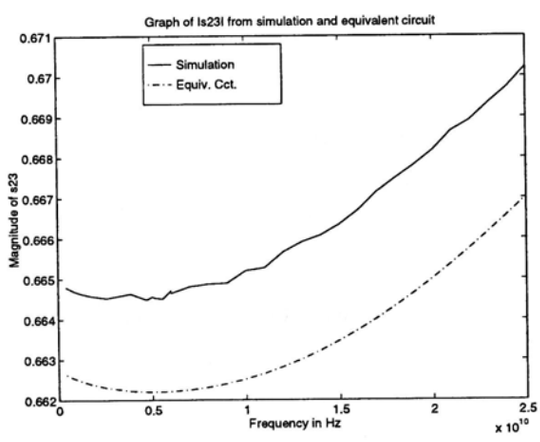

Magnitude of s_{23}

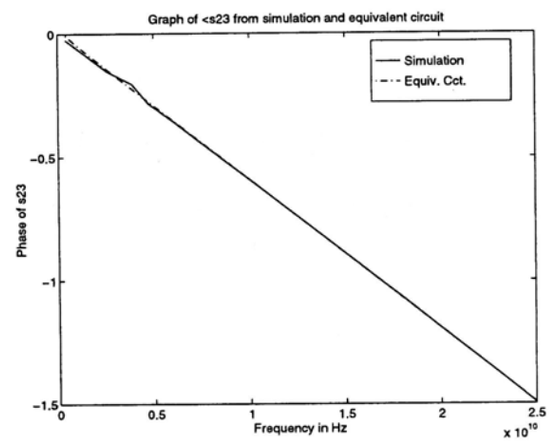

Phase of s_{23}

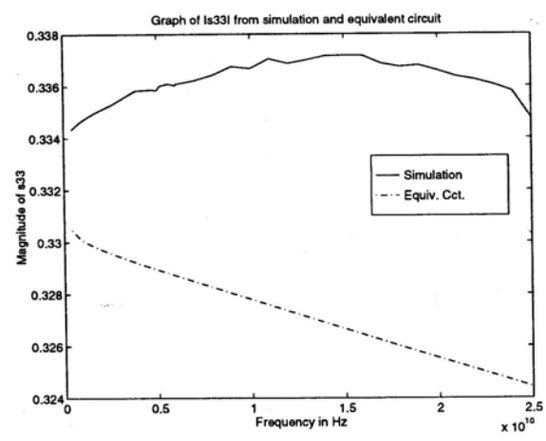

Magnitude of s_{33}

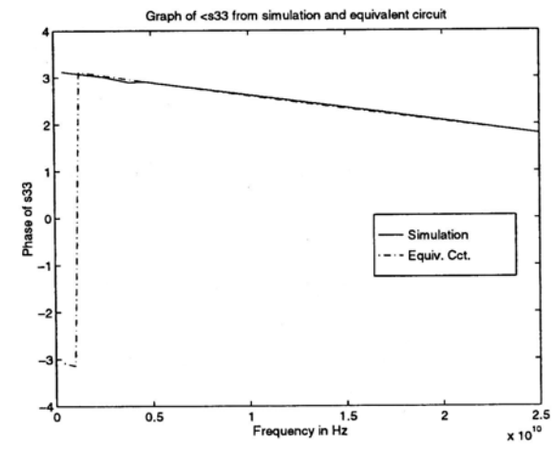

Phase of s_{33}

Figure 6.12: S parameters difference between simulation and circuit 1T (lossy metal strip), $\frac{h}{w} = 1.0$

6.3 Tapered Line

The only tapered line being analyzed is the 20% one. The metal strip is treated both as a perfect metal and aluminium. It is found that when the metal strip is a perfect metal, three microstrip transmission lines are enough to model the tapered line. On the other hand, when the metal strip is aluminium, five microstrip lines are required. The equivalent circuits consisting of more number of microstrip lines[4] have been tried but the results are not satisfactory. One thing is that the values of the width of the microstrip lines do not get larger and larger gradually. The middle sections are usually very narrow compared with the end sections so that they are not realistic in modelling the tapered line. Another thing is that the optimization may result in the negative values of the parameters (e.g. the width of the microstrip lines). The reason for these phenomena is that the cost function may be easily trapped into a local minimum.

6.3.1 Without Conductor Loss

Table 6.22 shows the parameter values of the equivalent Circuit 1t being found and Table 6.23 shows the relative error between the simulated and calculated scattering parameters. From Table 6.23, it is seen that the relative errors of the scattering parameters is about 1% only. Therefore, it can be concluded that the equivalent circuit consisting of three consecutive transmission lines is good in modelling the 20% lossless metal strip tapered line. It is also seen that the values of the width of the microstrip lines become larger and larger gradually.

The degree of fitness of the simulated and calculated scattering parameters can be visualized in Fig. 6.13. It is again seen that the matching result of the phase plots are better than that of the magnitude plots. It is because the effective length of the tapered line and that of the equivalent circuit must be

[4]Four, five, seven, ten, and twenty sections of microstrip lines have been used to model the tapered line (with and without conductor loss).

comparable in the physical point of view after the optimization. The effective length of the Circuit 1t is found to be 0.44952mm and that of the tapered line is about 0.359mm.

Refer to the magnitude plots of the scattering parameters (Fig. 6.13), the rate of change of the calculated curves are smaller than that of the simulated ones. It is because a tapered line can be regarded as a combination of infinite microstrip lines with gradually increasing cross-section and there are only three microstrip lines in Circuit 1t. The rate of change of the characteristic impedance values (and the input impedances seeing from one of the ports) of the tapered line is therefore greater than that of the equivalent circuit.

$h/\mu m$	$w_1/\mu m$	$l_1/\mu m$	$w_2/\mu m$	$l_2/\mu m$	$w_3/\mu m$	$l_3/\mu m$	err
100	19.75	97.729	84.519	220.16	100	131.64	5.4851×10^{-3}

Table 6.22: Parameter values of the equivalent circuit 1t (lossless metal strip), $\frac{w_2-w_1}{l} = 0.2$

$\frac{w_2-w_1}{l} = 0.2$	s_{11}	s_{21}	s_{22}
Circuit 1t: $err/\%$	1.0286	0.20098	1.1154

Table 6.23: Relative error between the simulated and calculated scattering parameters (lossless metal strip)

Since the optimization fails in finding the parameter values of the equivalent circuits with more number of microstrip lines, we try to analyze the effect of using more number of microstrip lines by the following method. The basic idea is that the length of each microstrip line in the equivalent circuit is kept the same. Let l be the length of each microstrip line and N be the number of microstrip lines in the equivalent circuit. We start to calculate the width of the first microstrip line from the wider side of the tapered line[5] (width w_2, Fig.3.3).

[5]The case with the width of the microstrip lines calculated from the narrower side has been tried. It is found that the relative errors of the scattering parameters are very large.

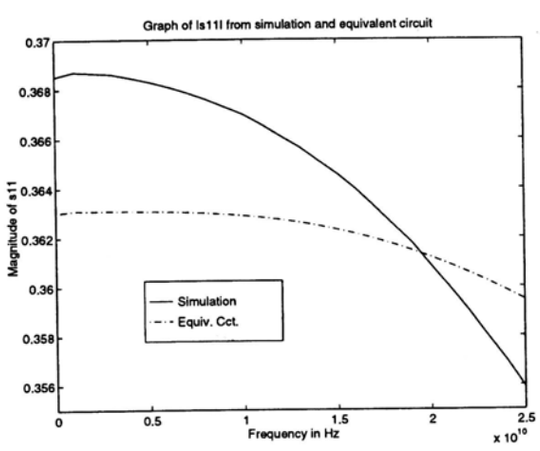

Magnitude of s_{11}

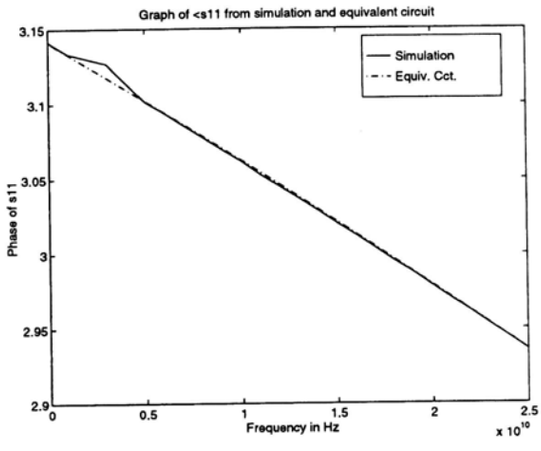

Phase of s_{11}

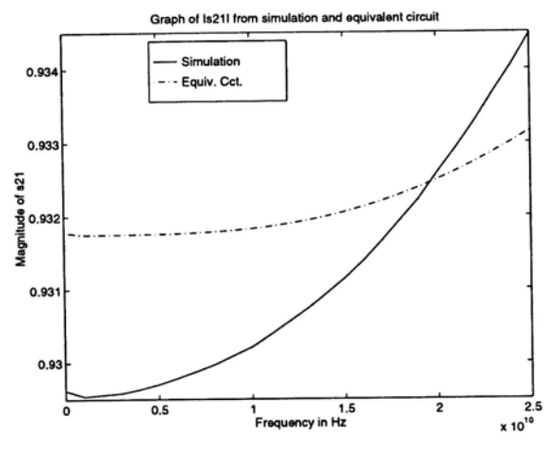

Magnitude of s_{21}

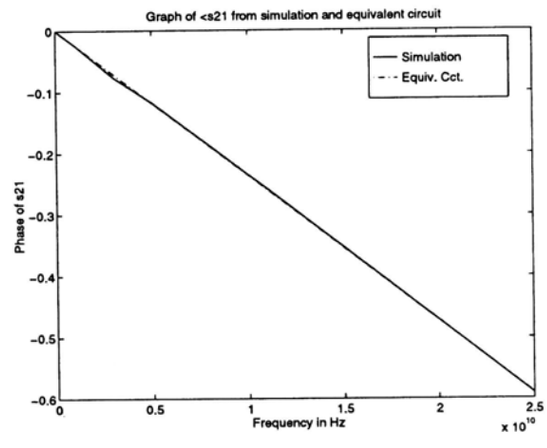

Phase of s_{21}

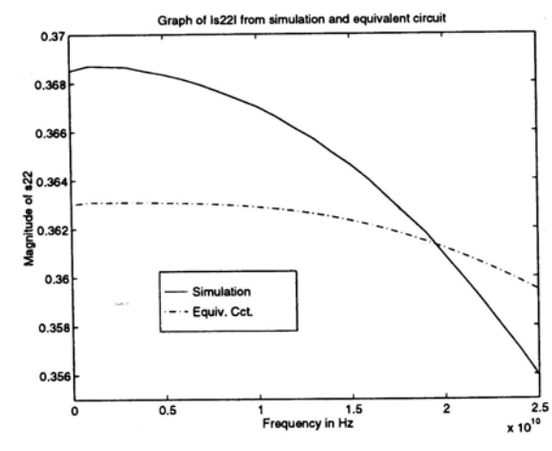

Magnitude of s_{22}

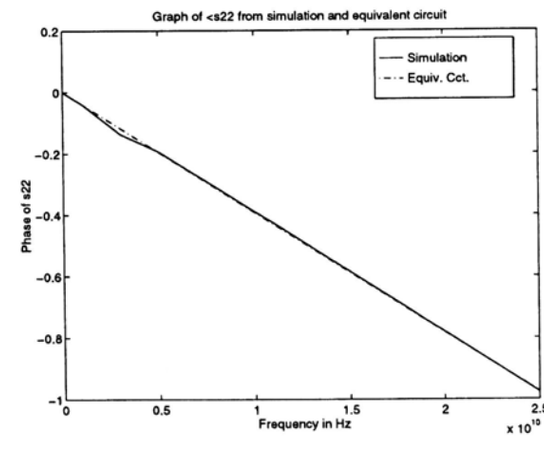

Phase of s_{22}

Figure 6.13: S parameters difference between simulation and circuit 1t (lossless metal strip)

The width of the remaining lines are then calculated by the formula:

$$w_i = w_{i+1} - 0.2l, \quad i = N-1, N-2, ..., 1 \tag{6.4}$$

After that, the scattering parameters of the equivalent circuit is found by using the formulae developed in Chapter 5. The relative errors of the scattering parameters when more number of microstrip lines are used are tabulated in Table 6.24.

N	s_{11}	s_{21}	s_{22}
3	1.6029	0.56761	2.2855
4	3.3433	0.74810	4.6091
5	4.6363	0.84990	6.1362
7	6.2139	0.95829	7.9450
10	7.4546	1.0331	9.3401
20	8.9636	1.1124	11.010

Table 6.24: Relative error of the scattering parameters with different number of microstrip lines used. (lossless metal strip)

It is observed from Table 6.23 and 6.24 that the optimization result is the best, i.e., three microstrip lines are enough to model the 20% tapered line. Moreover, for the lossless metal strip case, it is seen that the more number of microstrip lines are used, the worse the matching result of the scattering parameters (for the above stated method in the analysis).

6.3.2 With Conductor Loss

In this lossy case, optimization leads to a 3-section structure with the width of the middle section being narrower than the two end sections. This is physically unreasonable and it points to the pitfall of any optimization technique used to determine an equivalent circuit. Besides, since the same geometry of the lossless metal strip tapered line is adopted in the lossy metal strip case, we use the parameter values of the equivalent circuit (Circuit 1t) for the lossless case to calculate the scattering parameters for the lossy tapered line. The result is

then compared with the simulated scattering parameters. Fig. 6.14 shows the matching result. The matching result is worse and the phase is even not matched well. By using this set of parameter values, the loss is under-estimated in the low frequency region and over-estimated in the high frequency region.

Table 6.25 tabulates the relative error of the scattering parameters. It is seen that the same equivalent circuit (with the same parameter values) can also be used to model the lossy metal strip tapered line with about 10% in error, which can be tolerated in the engineering point of view.

By using the similar approach as in the lossless metal strip case to find the performance of the equivalent circuits with more number of microstrip lines, the results are tabulated in Table 6.26. It is seen that the analysis result of using three microstrip lines is better than the performance by using the parameter values of the perfect metal strip case to the lossy case. Besides, it is observed that five microstrip lines are required to model the 20% lossy metal strip tapered line with an relative error less than 10%. When more number of microstrip lines are used, the matching result is worse. So, it can be concluded that no optimization is necessary to find the model parameters of the equivalent circuits and the analysis method is sufficient to find an equivalent circuit for the lossy tapered line. Fig. 6.15 shows the matching result of the equivalent circuit consisting of five microstrip lines.

$\frac{w_2-w_1}{l} = 0.2$	s_{11}	s_{21}	s_{22}
Circuit 1t: $err/\%$	10.448	0.96977	6.0167

Table 6.25: Relative error between the simulated and calculated scattering parameters (lossless metal strip)

6.4 Summary

The performance results of the proposed equivalent circuits has been shown. It

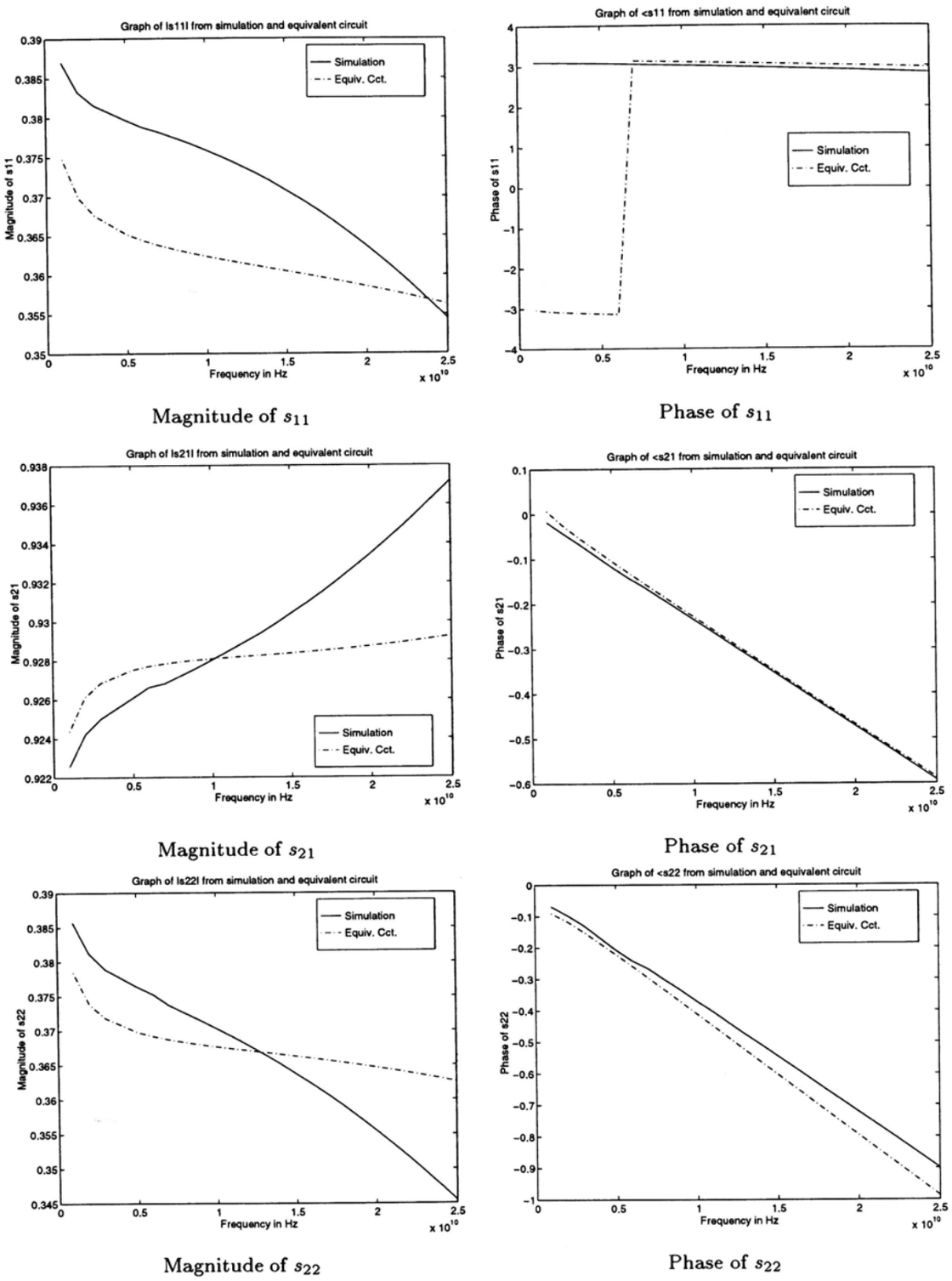

Magnitude of s_{11} Phase of s_{11}

Magnitude of s_{21} Phase of s_{21}

Magnitude of s_{22} Phase of s_{22}

Figure 6.14: S parameters difference between simulation and circuit 1t (lossy metal strip)

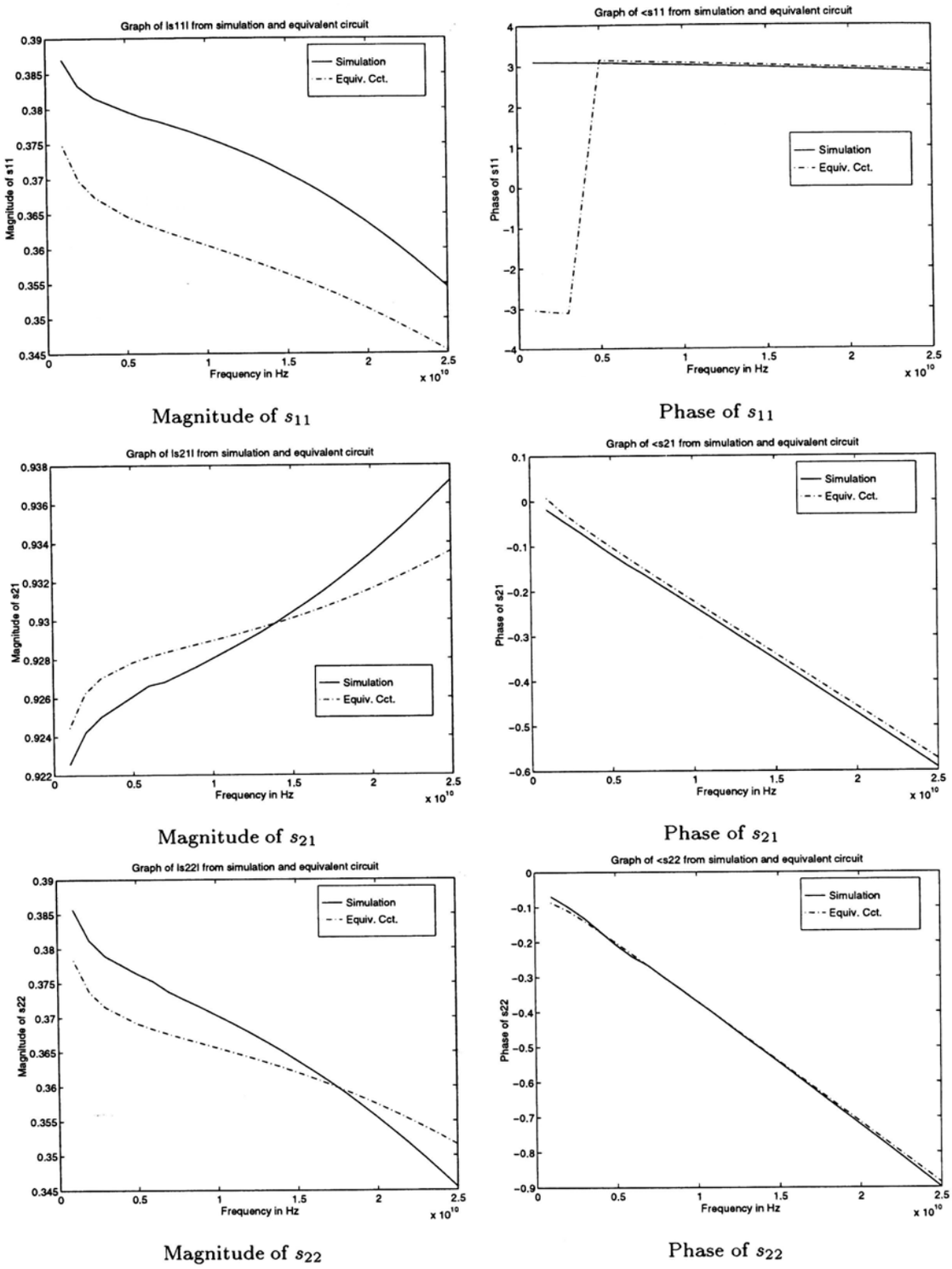

Magnitude of s_{11} Phase of s_{11}

Magnitude of s_{21} Phase of s_{21}

Magnitude of s_{22} Phase of s_{22}

Figure 6.15: S parameters difference between simulation and circuit 2t (lossy metal strip)

N	s_{11}	s_{21}	s_{22}
3	10.053	1.3274	4.0611
4	8.3323	1.4664	1.8439
5	7.4142	1.5442	1.5106
7	6.5729	1.6253	2.7711
10	6.1742	1.6790	4.0897
20	6.0663	1.7321	5.7562

Table 6.26: Relative error of the scattering parameters with different number of microstrip lines used. (lossy metal strip)

is seen that they are able to model the corresponding microstrip discontinuities. Since the frequency range employed in the analysis is up to 22GHz for perfect conductor metal strip and 25GHz for aluminium metal strip, the proposed equivalent circuits are valid within this frequency range.

Chapter 7

Modelling Performance Using TEM Approximation

In Chapter 5, several wideband equivalent circuits are proposed to model the three types of microstrip discontinuities. Their modelling performance which is shown to be acceptable in the engineering point of view is recorded in Chapter 6. In this chapter, we try to use TEM equivalent transmission line to model the microstrip discontinuities. This is called low frequency approximation because non-TEM mode waves will be generated inside the microstrip lines when frequency is increased. The equivalent circuits are still the same but TEM line is used instead of the line modelled in section 5.1. The basic idea of using TEM line approximation is that the dispersive effect of the microstrip lines in the equivalent circuits is modelled by the lumped circuit element(s). The equivalent lines are only used to model the dielectric loss and/or conductor loss. However, it is found that all the dispersive and lossy effect can be modelled by the lumped element(s) and the TEM lines are used as lossless microstrip transmission lines.

7.1 Right-Angled Bend

The optimization is firstly performed without considering the conductor loss, i.e., the metal strip is assumed to be a perfect conductor. After that, the conductor loss is introduced in order to test whether the TEM line approximation

is possible to model the right-angled bend.

7.1.1 Without Conductor Loss

Since conductor loss is not considered in this case, only three transmission line parameters, L_i, G_i, and C_i, are used in modelling a TEM line, where i is the ith transmission line. When modelling the microstrip lines, two cases are considered: the TEM lines have low dielectric loss (G_i is taken into account) and lossless TEM lines (G_i is not considered). In the former case, it is obtained that the value of G_i is found to be very large which is not reasonable with respect to the low loss dielectric. So this approach cannot be used to model the right-angled bend practically. Since alumina substrate is a low loss dielectric, it leads to the latter case. For the latter case with the equivalent circuits having lumped element(s), the values of L_i and C_i are found comparable to those calculated by using the model in section 5.1.

Circuit 1L

$\frac{h}{w}$	L_1/Hm^{-1}	G_1/Sm^{-1}	C_1/Fm^{-1}
0.2	1.5517×10^{-7}	6.3079×10^{-14}	5.6293×10^{-10}
0.4	2.4284×10^{-7}	3.7152×10^{-14}	3.3514×10^{-10}
0.6	3.0231×10^{-7}	2.8553×10^{-14}	2.5916×10^{-10}
0.8	3.4299×10^{-7}	2.4499×10^{-14}	2.2322×10^{-10}
1.0	3.7374×10^{-7}	2.2062×10^{-14}	2.0158×10^{-10}

Table 7.1: LGC values of the equivalent circuit 1L by using the non-TEM microstrip line model

The parameter values of the equivalent circuit when G_1 is considered is recorded in Table 7.2. From the table, it is seen that the values of the conductance per unit length G_1 are found in the order of -11. Since the electrical conductivity of the alumina substrate is $10^{-14} Sm^{-1}$ and from Eq. 5.11, the value of G_1 should be in the order of -14 (Table 7.1). So Table 7.2 implies that the

$\frac{h}{w}$	L_1/Hm^{-1}	G_1/Sm^{-1}	C_1/Fm^{-1}	l_1/mm	C/F	err
0.2	1.5495×10^{-7}	7.2963×10^{-11}	5.5877×10^{-10}	0.80170	9.8946×10^{-14}	5.2386×10^{-3}
0.4	2.4288×10^{-7}	4.9062×10^{-11}	3.3008×10^{-10}	0.79919	6.6376×10^{-14}	8.9799×10^{-3}
0.6	3.0227×10^{-7}	7.7661×10^{-11}	2.5505×10^{-10}	0.79146	5.0177×10^{-14}	1.3207×10^{-2}
0.8	3.4827×10^{-7}	6.0904×10^{-11}	2.2053×10^{-10}	0.78642	3.4586×10^{-14}	1.9726×10^{-2}
1.0	3.7394×10^{-7}	6.6101×10^{-11}	1.9720×10^{-10}	0.79880	2.9074×10^{-14}	2.4750×10^{-2}

Table 7.2: Parameter values of the equivalent circuit 1L (lossless metal strip and G being considered)

substrate is much lossy and therefore the equivalent circuit with G_1 being taken into account cannot be used to model the right-angled bend practically.

The reason why the values of G is found too large is due to Eq. 5.16. It is obtained from the result of Chapter 6 that the capacitance per unit length of a microstrip line is frequency dependent (increases with increasing frequency). Now, its value is kept constant in the TEM approximation; so its frequency dependent effect is compensated by G during the optimization process (Eq. 5.16).

$\frac{h}{w}$	L_1/Hm^{-1}	C_1/Fm^{-1}	l_1/mm	C/F	err
0.2	1.5607×10^{-7}	5.5070×10^{-10}	0.79777	1.1259×10^{-13}	3.5438×10^{-3}
0.4	2.4283×10^{-7}	3.1612×10^{-10}	0.80239	8.2759×10^{-14}	5.4676×10^{-3}
0.6	3.0670×10^{-7}	2.4122×10^{-10}	0.78514	7.0176×10^{-14}	8.0536×10^{-3}
0.8	3.6530×10^{-7}	2.0648×10^{-10}	0.75805	6.2200×10^{-14}	1.1366×10^{-2}
1.0	4.2448×10^{-7}	1.9263×10^{-10}	0.71324	6.1999×10^{-14}	1.3475×10^{-2}

Table 7.3: Parameter values of the equivalent circuit 1L (lossless metal strip and G not being considered)

As the electric loss tangent of the alumina substrate is about 0.0003 at 10GHz, the dielectric loss can be neglected from modelling the microstrip line. The effect of the low loss dielectric is modelled by the lumped capacitance. Table 7.3 records the parameter values of the equivalent circuit when G_1 is not taken into account. By comparing Table 7.1 and 7.3, it is seen that the parameter values by assuming the TEM lines are lossless is reasonable because the corresponding parameter values are in the same order of magnitude. Refer to Table 6.1 and 7.3, it is observed that the lumped capacitor value in Table 6.1 is

smaller than that in Table 7.3. It may be accounted that the effect of dielectric loss is also modelled by the lumped capacitor other than the discontinuity field effect.

$\frac{h}{w}$	s_{11}	s_{21}	s_{22}
0.2	1.2450	0.33611	0.85334
0.4	1.1010	0.53877	0.63465
0.6	1.5962	0.75956	0.22034
0.8	3.7227	1.0092	4.3637
1.0	2.0458	1.3110	2.7563

Table 7.4: Percentage error between the simulated and calculated scattering parameters from circuit 1L, (lossless metal strip)

Table 7.4 records the percentage errors between the simulated and calculated scattering parameters. It is seen that the lossless TEM line approximation (for Circuit 1L) can also be used to model the right-angled bend with frequency beyond 20GHz.

Fig. 7.1 shows the plots of the scattering parameters of the right-angled bend and Circuit 1L when the $\frac{h}{w}$ ratio is equal to 0.6. By comparing the figure with Fig. 6.1, it is seen that the matching result of the equivalent circuit with TEM lines is better than that with non-TEM lines. This can also be observed from the corresponding relative errors (Table 6.1 and 7.3). So it can be concluded that Circuit 1L with lossless TEM lines is the choice to model the right-angled bend with perfect conductor or very large conductivity metal strip.

Circuit 2L

As in the case of Circuit 1L, the values of the conductance per unit length is too large to represent the dielectric loss of the alumina substrate (Table 7.6). So Circuit 2L with G being considered in modelling the microstrip line is not suitable to model the right-angled bend.

When G is neglected, the result of the parameter values is recorded in Table 7.7.

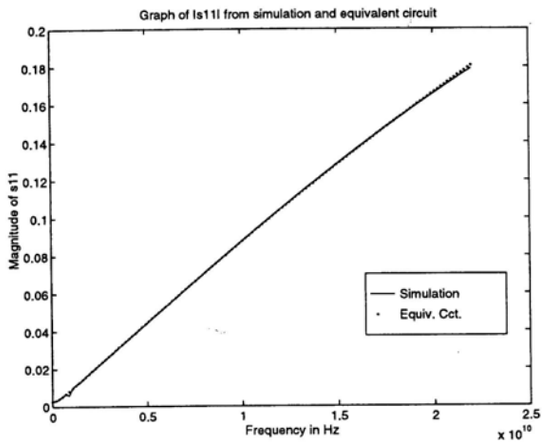

Magnitude of s_{11}

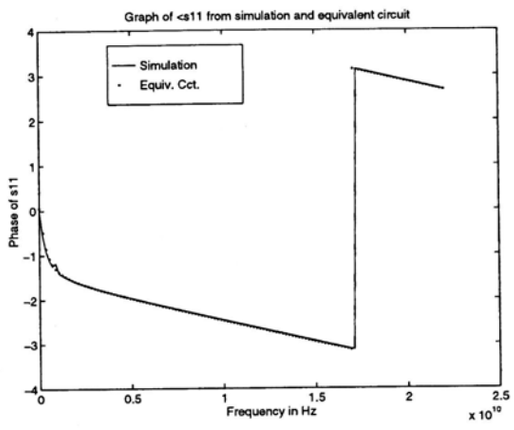

Phase of s_{11}

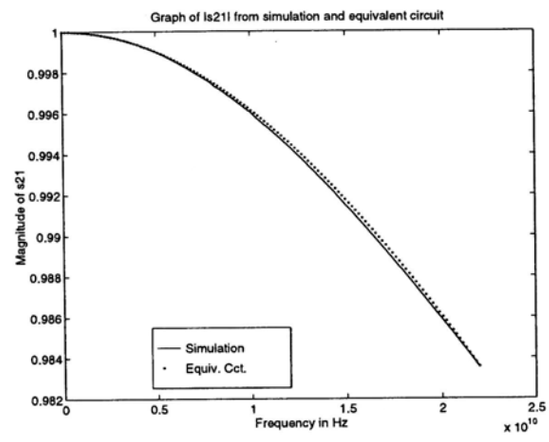

Magnitude of s_{21}

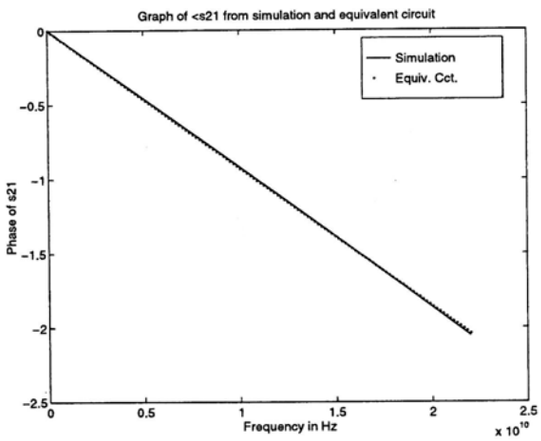

Phase of s_{21}

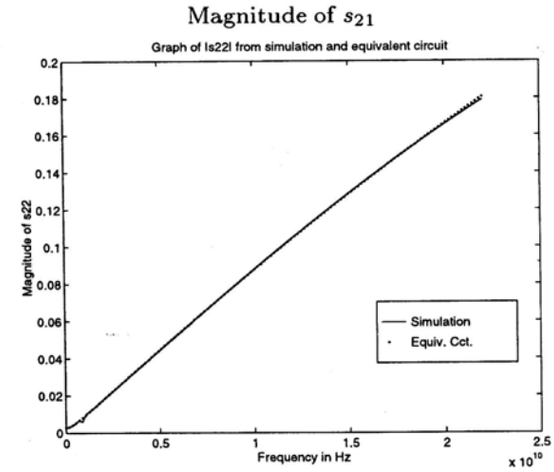

Magnitude of s_{22}

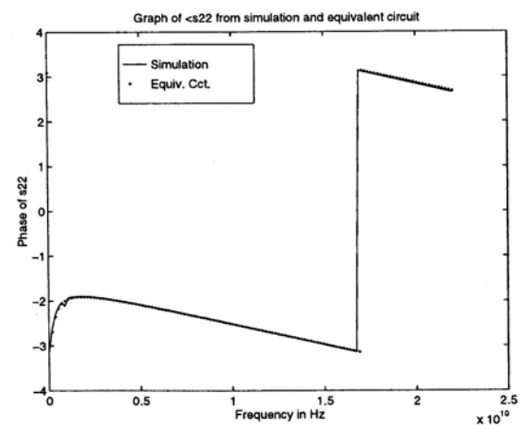

Phase of s_{22}

Figure 7.1: S parameters difference between simulation and circuit 1L (lossless metal strip)

$\frac{h}{w}$	L_1/Hm^{-1}	G_1/Sm^{-1}	C_1/Fm^{-1}
0.2	1.4202×10^{-7}	6.9937×10^{-14}	6.2298×10^{-10}
0.4	2.0562×10^{-7}	4.5290×10^{-14}	4.0681×10^{-10}
0.6	2.3547×10^{-7}	3.8545×10^{-14}	3.4742×10^{-10}
0.8	2.4003×10^{-7}	3.7674×10^{-14}	3.3973×10^{-10}
1.0	2.3910×10^{-7}	3.7848×10^{-14}	3.4127×10^{-10}

Table 7.5: LGC values of the equivalent circuit 2L by using the non-TEM microstrip line model

$\frac{h}{w}$	L_1/Hm^{-1}	G_1/Sm^{-1}	C_1/Fm^{-1}
0.2	1.4427×10^{-7}	6.4747×10^{-11}	6.1702×10^{-10}
0.4	2.1283×10^{-7}	2.9812×10^{-11}	3.9911×10^{-10}
0.6	2.4879×10^{-7}	1.0818×10^{-10}	3.4365×10^{-10}
0.8	2.6015×10^{-7}	4.9591×10^{-11}	3.2622×10^{-10}
1.0	2.6042×10^{-7}	6.7491×10^{-11}	3.3262×10^{-10}

$\frac{h}{w}$	l_1/mm	L/H	C/F	err
0.2	0.45366	5.7654×10^{-11}	4.2706×10^{-13}	3.4093×10^{-3}
0.4	0.36884	1.1298×10^{-10}	2.9145×10^{-13}	4.4611×10^{-3}
0.6	0.29988	1.6075×10^{-10}	2.3915×10^{-13}	5.5783×10^{-3}
0.8	0.24916	2.0479×10^{-10}	2.0902×10^{-13}	9.0812×10^{-3}
1.0	0.21044	2.3858×10^{-10}	1.9392×10^{-13}	9.9095×10^{-3}

Table 7.6: Parameter values of the equivalent circuit 2L (lossless metal strip and G being considered)

$\frac{h}{w}$	L_1/Hm^{-1}	C_1/Fm^{-1}	l_1/mm	L/H	C/F	err
0.2	1.6969×10^{-7}	6.3304×10^{-10}	0.51367	3.6828×10^{-11}	3.3854×10^{-13}	1.8393×10^{-3}
0.4	2.6558×10^{-7}	3.8814×10^{-10}	0.44353	7.5608×10^{-11}	2.4321×10^{-13}	2.4499×10^{-3}
0.6	3.4385×10^{-7}	3.4222×10^{-10}	0.33940	1.2109×10^{-10}	2.1364×10^{-13}	3.9889×10^{-3}
0.8	4.4544×10^{-7}	3.3305×10^{-10}	0.27970	1.4853×10^{-10}	1.8590×10^{-13}	7.2352×10^{-3}
1.0	4.6267×10^{-7}	3.6623×10^{-10}	0.20060	2.0354×10^{-10}	1.8607×10^{-13}	6.6111×10^{-3}

Table 7.7: Parameter values of the equivalent circuit 2L (lossless metal strip and G not being considered)

By comparing Table 7.5 and 7.7, it is seen that the corresponding transmission line parameters are in the same order of magnitude. Moreover, the values of the corresponding lumped inductors and capacitors are comparable in magnitude with the equivalent circuit using non-TEM lines (Table 6.2 and 7.7). So Circuit 2L with lossless TEM lines can be used to model the right-angled bend. Table 7.8 records the percentage errors of the scattering parameters.

$\frac{h}{w}$	s_{11}	s_{21}	s_{22}
0.2	1.2111	0.13194	1.1138
0.4	1.1039	0.20461	1.0154
0.6	1.9934	0.25748	2.0619
0.8	4.1661	0.45408	4.3441
1.0	2.6771	0.52768	2.6496

Table 7.8: Percentage error between the simulated and calculated scattering parameters from circuit 2L, (lossless metal strip)

The matching result between the scattering parameters of the right-angled bend and Circuit 2L is plotted in Fig. 7.2. It is again seen that the matching performance of Circuit 2L with lossless TEM lines is better than that with non-TEM lines (Fig. 6.2). It can also be seen from the result of the relative errors (Table 6.2 and 7.7). So the same conclusion from Circuit 1L can be drawn, i.e., Circuit 2L with lossless TEM lines is the choice in modelling the right-angled bend where its metal strip is a perfect conductor or with very large conductivity.

Circuit 3L

Besides applying TEM approximation on Circuit 1L and Circuit 2L, we also try to apply this method to the equivalent circuits with purely distributed element. However, it is found that this method does not work in modelling the right-angled bend no matter G is considered or not. Table 7.9 records the parameter values of Circuit 3L when G is considered and Table 7.10 for G being

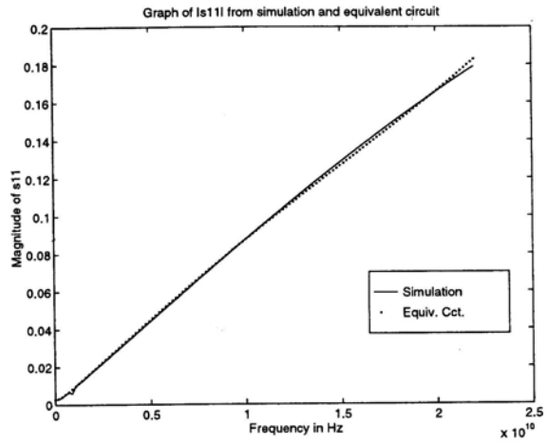

Magnitude of s_{11}

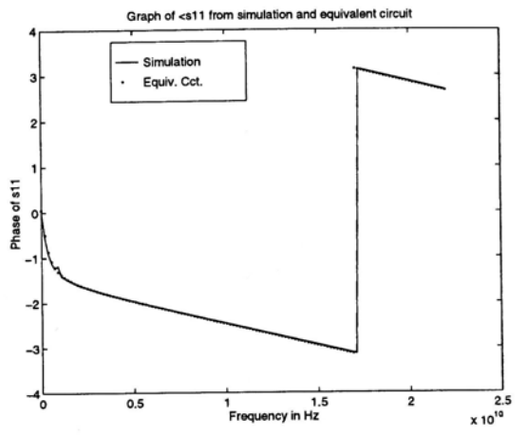

Phase of s_{11}

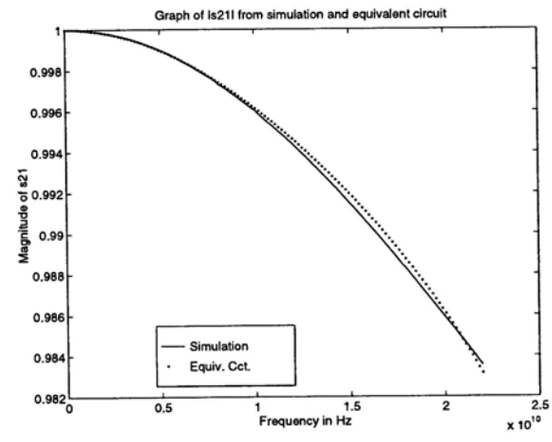

Magnitude of s_{21}

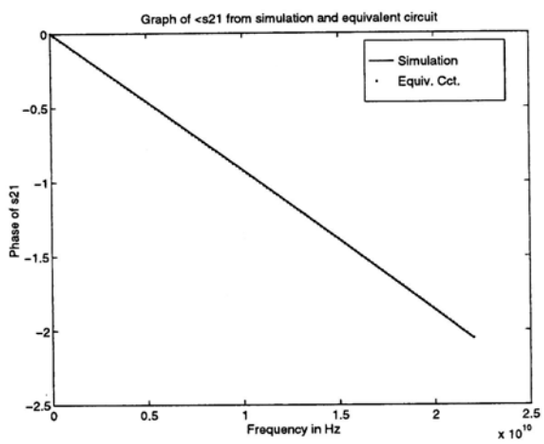

Phase of s_{21}

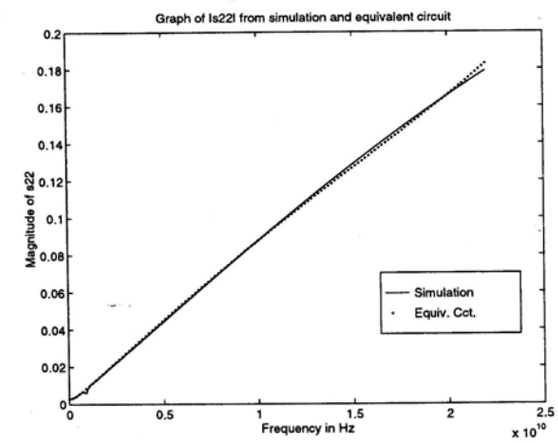

Magnitude of s_{22}

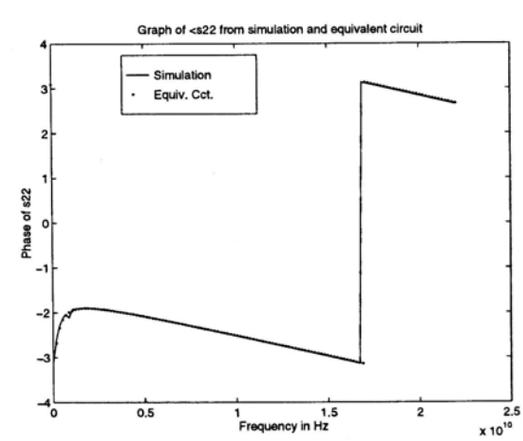

Phase of s_{22}

Figure 7.2: S parameters difference between simulation and circuit 2L (lossless metal strip)

$\frac{h}{w}$	L_1/Hm^{-1}	G_1/Sm^{-1}	C_1/Fm^{-1}	l_1/mm
0.2	9.8129×10^{-7}	1.1957×10^{-4}	1.2392×10^{-9}	0.014254
0.4	2.3888×10^{-7}	1.7020×10^{-12}	3.0532×10^{-10}	0.73043
0.6	3.0592×10^{-7}	6.8910×10^{-6}	2.3432×10^{-10}	0.59400
0.8	3.6124×10^{-7}	5.4977×10^{-11}	2.0974×10^{-10}	0.68441
1.0	4.2188×10^{-7}	7.5733×10^{-11}	2.0298×10^{-10}	0.70906

$\frac{h}{w}$	L_2/Hm^{-1}	G_2/Sm^{-1}	C_2/Fm^{-1}	l_2/mm	err
0.2	7.4199×10^{-7}	1.0564×10^{-2}	3.1965×10^{-9}	0.29881	4.4234×10^{-3}
0.4	2.2050×10^{-7}	2.0106×10^{-7}	7.6127×10^{-10}	0.18780	6.0341×10^{-3}
0.6	4.7069×10^{-7}	5.2567×10^{-3}	6.7500×10^{-10}	0.25265	8.4735×10^{-3}
0.8	2.0981×10^{-7}	5.8253×10^{-7}	3.2593×10^{-10}	0.27614	1.2529×10^{-2}
1.0	3.8645×10^{-8}	1.2580×10^{-4}	5.2253×10^{-10}	0.099568	1.5680×10^{-2}

Table 7.9: Parameter values of the equivalent circuit 3L (lossless metal strip and G being considered)

$\frac{h}{w}$	L_1/Hm^{-1}	C_1/Fm^{-1}	l_1/mm	L_2/Hm^{-1}	C_2/Fm^{-1}	l_2/mm	err
0.2	1.8495×10^{-7}	6.5262×10^{-10}	0.67319	2.5788×10^{-14}	9.9376×10^{-10}	0.11329	3.5437×10^{-3}
0.4	2.6544×10^{-7}	3.4556×10^{-10}	0.73407	1.8266×10^{-13}	6.4145×10^{-10}	0.12899	5.4672×10^{-3}
0.6	3.4909×10^{-7}	2.7457×10^{-10}	0.68981	5.8632×10^{-13}	4.5656×10^{-10}	0.15368	8.0546×10^{-3}
0.8	3.8729×10^{-7}	2.1893×10^{-10}	0.71501	1.0219×10^{-13}	2.8418×10^{-10}	0.21877	1.1369×10^{-2}
1.0	4.2451×10^{-7}	2.0237×10^{-10}	0.70987	1.7667×10^{-14}	5.4143×10^{-10}	0.096098	1.5117×10^{-2}

Table 7.10: Parameter values of the equivalent circuit 3L (lossless metal strip and G not being considered)

neglected. It is found that when G is included in the model, its values are found very large. However, when G is neglected in the model, the inductance per unit length of the middle line, L_2, is found to be very small. As the junction of the right-angled bend is a discontinuity centre, part of the signal wave is reflected at the junction and therefore the propagation is reduced. From Eq. 5.16, the value of the inductance per unit length of the TEM line should be small in order to satisfy this condition.

Circuit 4L

$\frac{h}{w}$	L_1/Hm^{-1}	G_1/Sm^{-1}	C_1/Fm^{-1}	l_1/mm	L_2/Hm^{-1}	G_2/Sm^{-1}
0.2	9.6528×10^{-8}	3.3380×10^{-10}	1.2311×10^{-9}	0.079634	2.2083×10^{-7}	5.2232×10^{-6}
0.4	1.6638×10^{-7}	1.5758×10^{-4}	6.6782×10^{-10}	0.10795	3.7987×10^{-7}	1.0820×10^{-4}
0.6	2.1253×10^{-7}	7.6331×10^{-4}	4.8437×10^{-10}	0.12783	5.1713×10^{-7}	5.0836×10^{-4}
0.8	2.6199×10^{-7}	9.8787×10^{-11}	3.8581×10^{-10}	0.14193	6.2127×10^{-7}	3.6383×10^{-8}
1.0	2.2811×10^{-7}	9.0110×10^{-11}	3.1559×10^{-10}	0.16457	8.1869×10^{-7}	5.2207×10^{-14}

$\frac{h}{w}$	C_2/Fm^{-1}	l_2/mm	L_3/Hm^{-1}	G_3/Sm^{-1}	C_3/Fm^{-1}	l_3/mm	err
0.2	3.7831×10^{-10}	0.35035	1.1452×10^{-7}	1.2355×10^{-4}	7.8647×10^{-10}	0.67401	2.9964×10^{-3}
0.4	2.0416×10^{-10}	0.36060	1.4629×10^{-7}	1.1699×10^{-5}	5.7518×10^{-10}	0.51760	3.3862×10^{-3}
0.6	1.4201×10^{-10}	0.33420	1.6165×10^{-7}	2.5348×10^{-5}	4.9713×10^{-10}	0.46268	5.3948×10^{-3}
0.8	1.1547×10^{-10}	0.31474	1.7768×10^{-7}	4.3579×10^{-3}	4.3009×10^{-10}	0.44951	8.6889×10^{-3}
1.0	9.3933×10^{-11}	0.26404	2.1475×10^{-7}	4.5637×10^{-4}	4.3168×10^{-10}	0.42083	1.7229×10^{-2}

Table 7.11: Parameter values of the equivalent circuit 4L (lossless metal strip and G being considered)

$\frac{h}{w}$	L_1/Hm^{-1}	C_1/Fm^{-1}	l_1/mm	L_2/Hm^{-1}	C_2/Fm^{-1}
0.2	4.8602×10^{-7}	1.8214×10^{-9}	0.16360	1.8351×10^{-7}	2.0387×10^{-10}
0.4	5.4812×10^{-7}	8.4178×10^{-10}	0.16358	3.3095×10^{-7}	1.6676×10^{-10}
0.6	5.6370×10^{-7}	6.1583×10^{-10}	0.15516	4.8597×10^{-7}	9.8811×10^{-11}
0.8	6.4282×10^{-7}	4.9563×10^{-10}	0.17838	5.8241×10^{-7}	2.5177×10^{-11}
1.0	5.0952×10^{-7}	3.8357×10^{-10}	0.19344	7.9587×10^{-7}	4.0436×10^{-12}

$\frac{h}{w}$	l_2/mm	L_3/Hm^{-1}	C_3/Fm^{-1}	l_3/mm	err
0.2	0.24266	2.3143×10^{-14}	6.4165×10^{-10}	0.45882	2.0254×10^{-3}
0.4	0.31365	8.1828×10^{-16}	4.9977×10^{-10}	0.41592	2.7353×10^{-3}
0.6	0.30933	5.8747×10^{-14}	4.6710×10^{-10}	0.41528	4.1643×10^{-3}
0.8	0.27201	2.3260×10^{-13}	4.5856×10^{-10}	0.39625	7.2478×10^{-3}
1.0	0.24901	1.5069×10^{-13}	5.0129×10^{-10}	0.36473	6.9111×10^{-3}

Table 7.12: Parameter values of the equivalent circuit 4L (lossless metal strip and G not being considered)

The optimization results are similar to those of Circuit 3L. When G is included in the transmssion line model, its values are found too large to represent the substrate dielectric loss. On the other hand, when G is not considered, the inductance per unit length of the middle line, L_3, of the equivalent circuit is too small for the same reason given for Circuit 3L. Table 7.11 and 7.12 record the results of the parameter values.

7.1.2 With Conductor Loss

With conductor loss being considered, there are now four transmission line parameters to describe a microstrip line. Three cases have been analyzed to model the right-angled bend. The first case is that the microstrip line model includes both the conductor and dielectric loss, i.e. $RLGC$ are included in the line model. The second case is that the line model considers only the conductor loss and the dielectric loss is neglected (or modelled by the lumped element). Finally the line model is assumed to be lossless. It will be seen that for the equivalent circuits with lumped element(s), they can model the right-angled bend only when the TEM lines are assumed lossless. The conductor and dielectric loss seem to be modelled by the lumped element(s).

Circuit 1L

R	L	G	C	$R_1/\Omega m^{-1}$	L_1/Hm^{-1}	G_1/Sm^{-1}	C_1/Fm^{-1}
√	√	√	√	342.35	5.8162×10^{-7}	2.0654×10^{-1}	9.5522×10^{-11}
√	√		√	7.3067×10^{-7}	3.2354×10^{-7}	–	1.8063×10^{-10}
	√		√	–	6.5435×10^{-7}	–	1.1358×10^{-10}

R	L	G	C	l_1/mm	C/F	err
√	√	√	√	0.22015	9.3907×10^{-14}	1.4965×10^{-2}
√	√		√	0.39388	1.4884×10^{-15}	2.3670×10^{-2}
	√		√	0.19598	9.1828×10^{-14}	1.5233×10^{-2}

Table 7.13: Parameter values of the equivalent circuit 1L (lossy metal strip)

Table 7.13 records the optimization results of the three cases. It is seen

that when all the transmission line parameters are considered, the value of the conductance per unit length is too large to represent the dielectric loss. On the other hand, when the conductor loss is considered only, the value of the resistance per unit length is too small to represent the conductor loss. The reason is that part of the signal wave is reflected at the junction of the right-angled bend and consequently the propagation is reduced. Therefore, from Eq. 5.16, either G is increased or R is reduced so as to satisfy this condition.

When the TEM lines are assumed lossless, the values of the transmission line parameters (L_1 and C_1) are found reasonable. It seems that all the loss and dispersive effect is modelled by the lumped capacitor. Table 7.14 records the corresponding percentage error of the scattering parameters and Fig. 7.3 shows the matching result. From the magnitude plots of s_{21}, it is seen that the curve of the equivalent circuit is above that of the right-angled bend, which means that the equivalent circuit lower-estimates the loss in the right-angled bend. However, Circuit 1L can be used to model the 90° bend when 10% error is tolerable (Table 7.14).

$\frac{h}{w} = 1.0$	s_{11}	s_{21}	s_{22}
err	8.3391	1.2405	7.4766

Table 7.14: Percentage error between the simulated and calculated scattering parameters from circuit 1L, (lossy metal strip)

There is no modelling result for the non-TEM approximation because the value of the lumped capacitor is found to be negative no matter how the initial guess is changed during the optimization. So, if Circuit 1L is needed to model the lossy metal strip right-angled bend, the TEM model is only the choice.

Circuit 2L

For the optimization results of Circuit 2L, there are similar phenomena as in

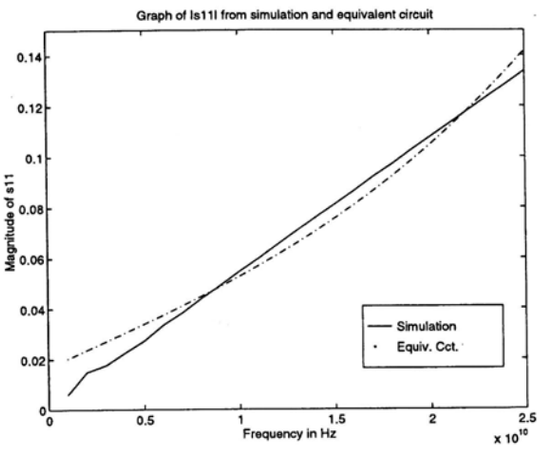

Magnitude of s_{11}

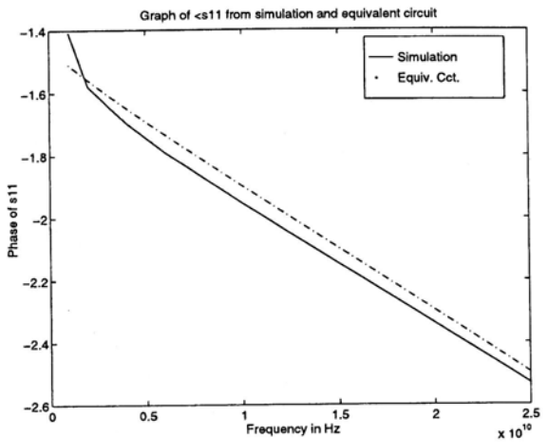

Phase of s_{11}

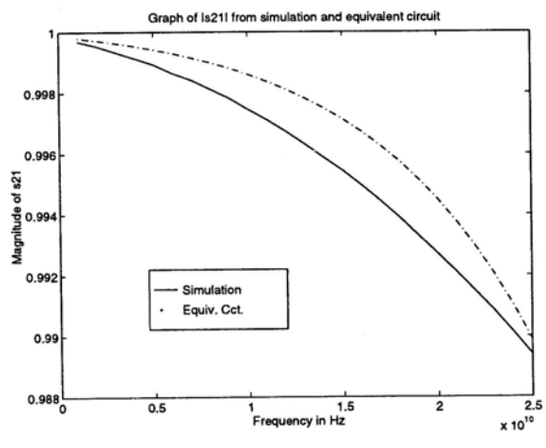

Magnitude of s_{21}

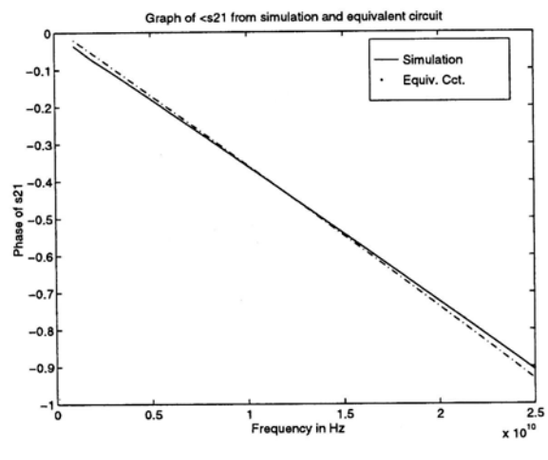

Phase of s_{21}

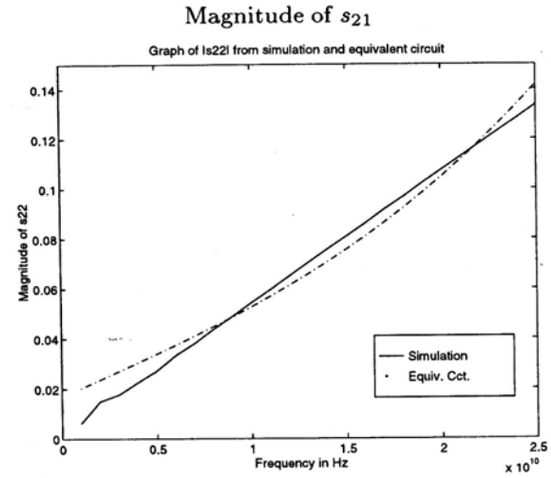

Magnitude of s_{22}

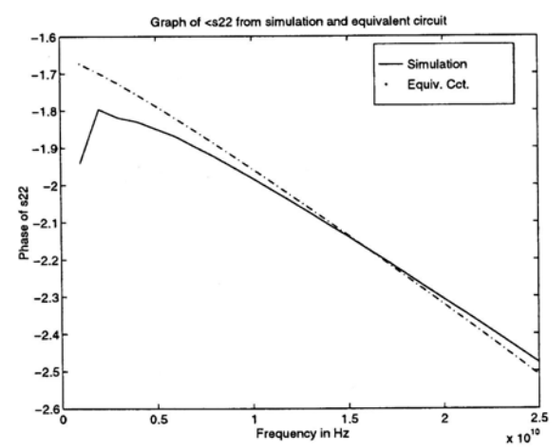

Phase of s_{22}

Figure 7.3: S parameters difference between simulation and circuit 1L (lossy metal strip), $\frac{h}{w} = 1.0$.

R	L	G	C	$R_1/\Omega m^{-1}$	L_1/Hm^{-1}	G_1/Sm^{-1}	C_1/Fm^{-1}
√	√	√	√	403.72	7.1063×10^{-7}	2.4354×10^{-1}	1.1682×10^{-10}
√	√		√	2.4725×10^{-6}	3.6141×10^{-7}	-	2.2522×10^{-10}
	√		√	-	8.9982×10^{-7}	-	1.5561×10^{-10}

R	L	G	C	l_1/mm	L/H	C/F	err
√	√	√	√	0.18668	-4.6213×10^{-12}	9.2349×10^{-14}	1.4964×10^{-2}
√	√		√	0.10066	8.7483×10^{-11}	9.2906×10^{-14}	1.3312×10^{-2}
	√		√	0.13843	3.6782×10^{-12}	9.3244×10^{-14}	1.5242×10^{-2}

Table 7.15: Parameter values of the equivalent circuit 2L (lossy metal strip)

Circuit 1L. When the conductor and dielectric loss are considered in modelling the microstrip lines, negative value of the lumped inductor is even obtained. From Table 7.15, it is seen that Circuit 2L can only model the right-angled bend reasonably and practically when the TEM lines are treated as lossless lines and the loss as well as dispersive effect are modelled by the lumped inductors and capacitor. Table 7.16 shows the percentage error of the scattering parameters and Fig. 7.4 the matching result. It is seen that both the performance of Circuit 1L and 2L are nearly the same (lower-estimating the loss of the right-angled bend). So either Circuit 1L and 2L can be used to model the right-angled bend when 10% error is allowed.

$\frac{h}{w} = 1.0$	s_{11}	s_{21}	s_{22}
err	8.3466	1.2409	7.4851

Table 7.16: Percentage error between the simulated and calculated scattering parameters from circuit 2L, (lossy metal strip)

By comparing the performance with the equivalent circuit using non-TEM lines, it is seen that the non-TEM line model is better in modelling than the TEM approximation. This can be observed from the percentage error of the scattering parameters (Table 6.11 and 7.16). So, when the metal strip has a finite conductivity and Circuit 2L is chosen, the non-TEM model is the choice.

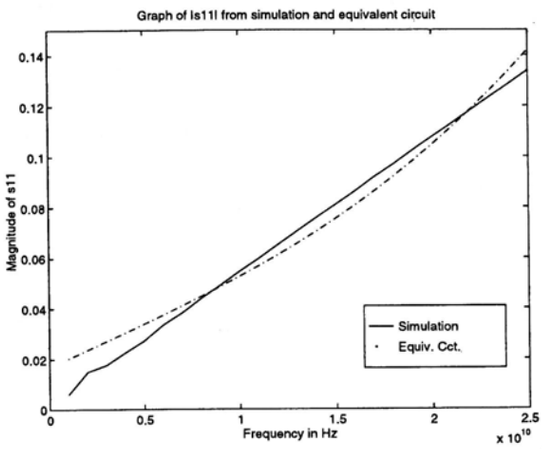

Magnitude of s_{11}

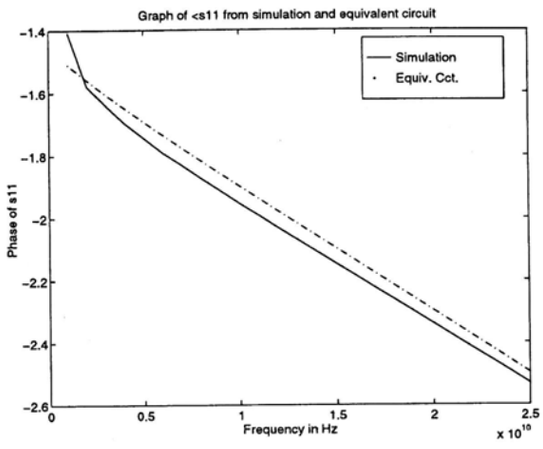

Phase of s_{11}

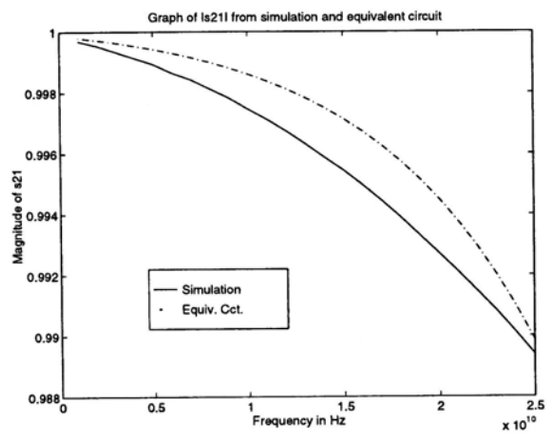

Magnitude of s_{21}

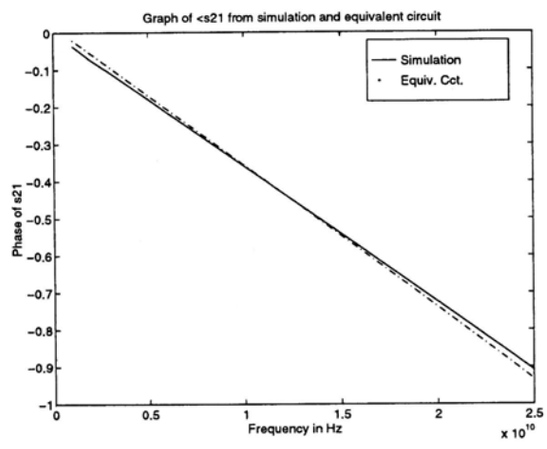

Phase of s_{21}

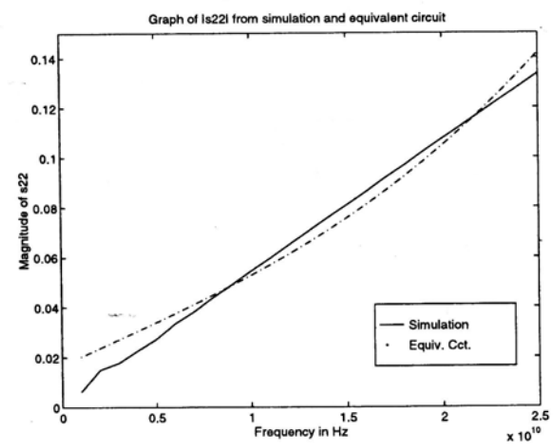

Magnitude of s_{22}

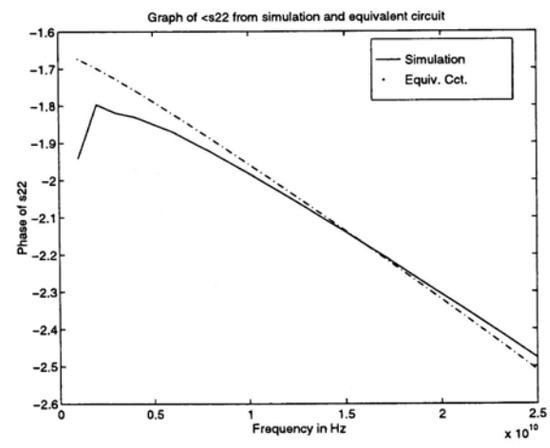

Phase of s_{22}

Figure 7.4: S parameters difference between simulation and circuit 2L (lossy metal strip), $\frac{h}{w} = 1.0$.

Circuit 3L and 4L

It is found that the equivalent circuits with purely distributed element are not able to model the right-angled bend. The optimization results either negative parameter values (no matter trying different initial guesses) or the values which cannot represent the loss (either too large or too small in values of R or L). Table 7.17 and 7.18 record the optimization results of Circuit 3L and 4L respectively.

R	L	G	C	$R_1/\Omega m^{-1}$	L_1/Hm^{-1}	G_1/Sm^{-1}	C_1/Fm^{-1}	l_1/mm
√	√	√	√	556.96	5.0326×10^{-7}	-1.1649×10^{-1}	1.0526×10^{-10}	0.10014
√	√		√	93.515	4.1301×10^{-7}	–	1.8157×10^{-10}	0.12629
	√		√	–	4.8024×10^{-13}	–	-3.0360×10^{-10}	0.10036

R	L	G	C	$R_2/\Omega m^{-1}$	L_2/Hm^{-1}	G_2/Sm^{-1}	C_2/Fm^{-1}	l_2/mm
√	√	√	√	−229.98	3.14327×10^{-7}	1.7189×10^{-1}	2.4465×10^{-10}	0.48584
√	√		√	6.7924×10^{-7}	3.4143×10^{-7}	–	2.2693×10^{-10}	0.41851
	√		√	–	4.5777×10^{-7}	–	3.5025×10^{-10}	0.5646

R	L	G	C	err
√	√	√	√	1.4732×10^{-2}
√	√		√	1.5354×10^{-2}
	√		√	1.4337×10^{-2}

Table 7.17: Parameter values of the equivalent circuit 3L (lossy metal strip)

7.2 T-Junction

Same equivalent circuits (Fig. 5.4) are used to test whether TEM lines can be used to model the T-junction with frequency beyond 20GHz. As in the case of the right-angled bend, the circuit can model the T-junction only when the TEM lines are lossless.

7.2.1 Without Conductor Loss

This section records the optimization results when the metal strip is a perfect metal. So there are only three transmission line parameters (L, G, and C) in the model of the TEM lines. Firstly, we try to the LGC TEM lines to model

R	L	G	C	$R_1/\Omega m^{-1}$	L_1/Hm^{-1}	G_1/Sm^{-1}	C_1/Fm^{-1}	l_1/mm
√	√	√	√	672.11	5.6561×10^{-7}	-1.2576×10^{-1}	1.0583×10^{-10}	0.080960
√	√		√	133.96	4.2649×10^{-7}	–	1.7612×10^{-10}	0.084309
	√		√	–	2.3433×10^{-12}	–	-4.9797×10^{-10}	0.093967

R	L	G	C	$R_2/\Omega m^{-1}$	L_2/Hm^{-1}	G_2/Sm^{-1}	C_2/Fm^{-1}	l_2/mm
√	√	√	√	−36.394	2.8930×10^{-7}	2.2552×10^{-1}	2.3398×10^{-10}	0.099127
√	√		√	4.4891×10^{-8}	3.5895×10^{-7}	–	2.1117×10^{-10}	0.095144
	√		√	–	2.3433×10^{-12}	–	2.3590×10^{-7}	0.10853

R	L	G	C	$R_3/\Omega m^{-1}$	L_3/Hm^{-1}	G_3/Sm^{-1}	C_3/Fm^{-1}	l_3/mm
√	√	√	√	−24.393	3.1964×10^{-7}	1.0018×10^{-1}	2.3458×10^{-10}	0.32604
√	√		√	42.998	3.4009×10^{-7}	–	2.2668×10^{-10}	0.31288
	√		√	–	5.0842×10^{-7}	–	3.6654×10^{-10}	0.40789

R	L	G	C	err
√	√	√	√	1.4724×10^{-2}
√	√		√	1.5264×10^{-2}
	√		√	1.4455×10^{-2}

Table 7.18: Parameter values of the equivalent circuit 4L (lossy metal strip)

the T-junction. However, it is found that the values of the conductance per unit length is too large to represent the substrate dielectric loss. As the alumina substrate is a low loss material, so we neglect G in the TEM line model. It is found that the parameter values of these equivalent circuits are reasonable and comparable to those calculated from the equivalent circuits with non-TEM lines.

Circuit 2T

$\frac{h}{w}$	L_1/Hm^{-1}	G_1/Sm^{-1}	C_1/Fm^{-1}	L_2/Hm^{-1}	G_2/Sm^{-1}	C_2/Fm^{-1}
0.2	1.5716×10^{-7}	6.2147×10^{-14}	5.5476×10^{-10}	1.5835×10^{-7}	6.1602×10^{-14}	5.4999×10^{-10}
0.4	2.4833×10^{-7}	3.6172×10^{-14}	3.2649×10^{-10}	2.5049×10^{-7}	3.5799×10^{-14}	3.2320×10^{-10}
0.6	3.1553×10^{-7}	2.7111×10^{-14}	2.4639×10^{-10}	3.1896×10^{-7}	2.6758×10^{-14}	2.4326×10^{-10}
0.8	3.6708×10^{-7}	2.2552×10^{-14}	2.0593×10^{-10}	3.7349×10^{-7}	2.2080×10^{-14}	2.0174×10^{-10}
1.0	4.0658×10^{-7}	1.9895×10^{-14}	1.8229×10^{-10}	4.1714×10^{-7}	1.9276×10^{-14}	1.7678×10^{-10}

Table 7.19: LGC values of the equivalent circuit 2T by using the non-TEM microstrip line model

Refer to Table 7.20, it is again seen that the values of the conductance per unit length (G_1 and G_2) is too large to represent the substrate dielectric loss.

$\frac{h}{w}$	L_1/Hm^{-1}	G_1/Sm^{-1}	C_1/Fm^{-1}	l_1/mm	L_2/Hm^{-1}
0.2	1.5548×10^{-7}	2.3692×10^{-2}	5.6163×10^{-10}	1.3552	1.5450×10^{-7}
0.4	2.4434×10^{-7}	6.8579×10^{-11}	3.3231×10^{-10}	1.3607	2.4843×10^{-7}
0.6	3.0143×10^{-7}	5.8667×10^{-2}	2.4672×10^{-10}	1.3970	3.1324×10^{-7}
0.8	3.5518×10^{-7}	7.0855×10^{-9}	2.1171×10^{-10}	1.3767	4.0378×10^{-7}
1.0	3.9712×10^{-7}	2.8435×10^{-2}	1.9051×10^{-10}	1.3671	4.1717×10^{-7}

$\frac{h}{w}$	G_2/Sm^{-1}	C_2/Fm^{-1}	l_2/mm	C/F	err
0.2	2.2717×10^{-5}	5.5087×10^{-10}	1.2578	1.1384×10^{-14}	6.7812×10^{-3}
0.4	1.058×10^{-3}	3.3093×10^{-10}	1.2059	1.4917×10^{-14}	7.9285×10^{-3}
0.6	3.1901×10^{-3}	2.5071×10^{-10}	1.1889	7.4792×10^{-15}	1.1330×10^{-2}
0.8	1.2334×10^{-1}	2.3044×10^{-10}	1.0624	4.7121×10^{-15}	1.3631×10^{-2}
1.0	3.9158×10^{-2}	1.8796×10^{-10}	1.1156	6.7778×10^{-15}	1.8682×10^{-2}

Table 7.20: Parameter values of the equivalent circuit 2T (lossless metal strip and G being considered)

The reason is the same as given for the equivalent circuits modelling the right-angled bend. So Circuit 2T is not suitable to model the T-junction when G is taken into account in the TEM line model.

$\frac{h}{w}$	L_1/Hm^{-1}	C_1/Fm^{-1}	l_1/mm	L_2/Hm^{-1}
0.2	1.5487×10^{-7}	5.5949×10^{-10}	1.3603	1.5432×10^{-7}
0.4	2.3799×10^{-7}	3.2459×10^{-10}	1.3947	2.4856×10^{-7}
0.6	3.0461×10^{-7}	2.4937×10^{-10}	1.3821	3.0728×10^{-7}
0.8	3.4797×10^{-7}	2.0741×10^{-10}	1.4058	4.0984×10^{-7}
1.0	3.9787×10^{-7}	1.9085×10^{-10}	1.3647	4.8565×10^{-7}

$\frac{h}{w}$	C_2/Fm^{-1}	l_2/mm	C/F	err
0.2	5.5022×10^{-10}	1.2594	1.1387×10^{-14}	6.7849×10^{-3}
0.4	3.3299×10^{-10}	1.2042	1.2914×10^{-14}	7.9464×10^{-3}
0.6	2.4555×10^{-10}	1.2129	7.6522×10^{-15}	1.0989×10^{-2}
0.8	2.3351×10^{-10}	1.0456	4.8776×10^{-15}	1.3472×10^{-2}
1.0	2.1881×10^{-10}	0.95829	6.7464×10^{-15}	1.8599×10^{-2}

Table 7.21: Parameter values of the equivalent circuit 2T (lossless metal strip and G not being considered)

When the TEM lines in Circuit 2T are assumed lossless, the transmission line parameters are found comparable to those from non-TEM lines (Table 7.19 and 7.21). Besides, from Table 6.12 and 7.21, it is seen that the values of the lumped capacitors of the TEM model is greater than those of the non-TEM model. The reason may be that the dielectric loss and the dispersive effect is

compensated by the lumped capacitor in the TEM model. So it is concluded that Circuit 2T with lossless TEM lines can model the T-junction with frequency beyond 20GHz. Table 7.22 records its percentage error of scattering parameters.

$\frac{h}{w}$	s_{11}	s_{12}	s_{23}	s_{22}	s_{23}	s_{33}
0.2	0.54338	0.73366	0.54467	1.1910	0.43911	1.0535
0.4	1.1871	0.79127	0.82035	0.63627	0.61837	0.95352
0.6	1.8845	1.0972	1.1356	0.82869	0.82717	1.0156
0.8	1.9231	1.4992	1.5455	1.1608	0.87901	0.68299
1.0	3.0956	2.1068	1.9746	1.8550	1.0407	0.85841

Table 7.22: Percentage error between the simulated and calculated scattering parameters from circuit 2T, (lossless metal strip)

Unlike the performance result of the right-angled bend, the performance of Circuit 2T with non-TEM lines is better than that with TEM lines. It can be verified from the relative error of the scattering parameters (Table 6.12 and 7.21). Fig. 7.5 shows the matching performance of the equivalent circuit. It is seen that the matching performance is similar to that of the non-TEM model (Fig. 6.8). Therefore, it can be concluded that Circuit 2T with non-TEM lines is better in modelling the T-junction with perfect conductor metal strip. Note that the matching performance becomes worse when frequency increases. It is because the dispersive and mode-coupling effect increase when frequency increases and the single lumped capacitor is not able to model these effects.

Circuit 3T

$\frac{h}{w}$	L_1/Hm^{-1}	G_1/Sm^{-1}	C_1/Fm^{-1}	L_2/Hm^{-1}	G_2/Sm^{-1}	C_2/Fm^{-1}
0.2	1.5463×10^{-7}	6.3335×10^{-14}	5.6517×10^{-10}	1.5377×10^{-7}	6.3750×10^{-14}	5.6881×10^{-10}
0.4	2.4362×10^{-7}	3.7011×10^{-14}	3.3389×10^{-10}	2.3810×10^{-7}	3.8038×10^{-14}	3.4294×10^{-10}
0.6	3.0637×10^{-7}	2.8096×10^{-14}	2.5511×10^{-10}	2.9059×10^{-7}	2.9949×10^{-14}	2.7151×10^{-10}
0.8	3.5663×10^{-7}	2.3362×10^{-14}	2.1313×10^{-10}	3.4006×10^{-7}	2.4756×10^{-14}	2.2551×10^{-10}
1.0	3.8633×10^{-7}	2.1184×10^{-10}	1.9377×10^{-10}	3.2253×10^{-7}	2.6400×10^{-14}	2.4008×10^{-10}

Table 7.23: LGC values of the equivalent circuit 3T by using the non-TEM microstrip line model

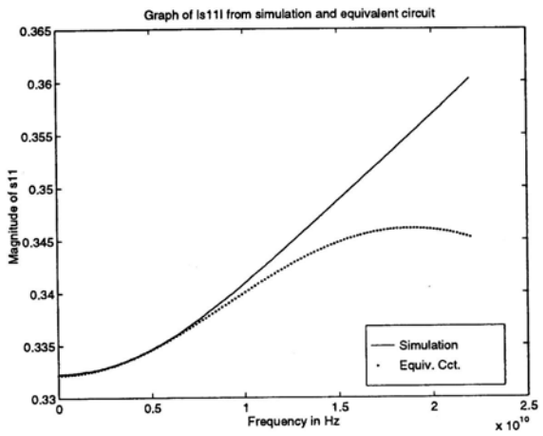

Magnitude of s_{11}

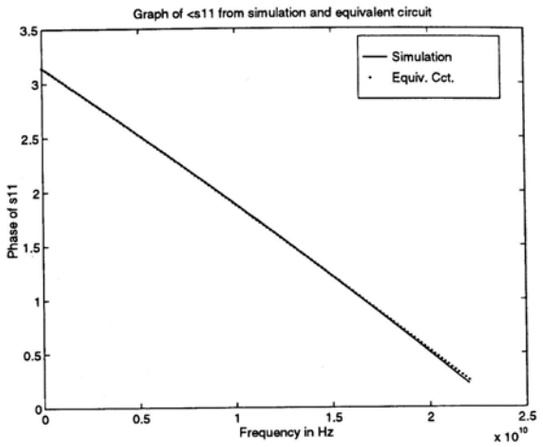

Phase of s_{11}

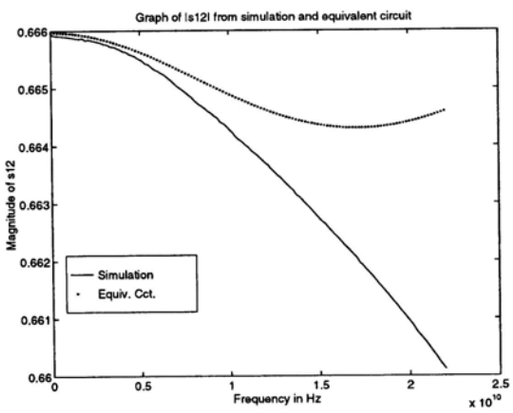

Magnitude of s_{12}

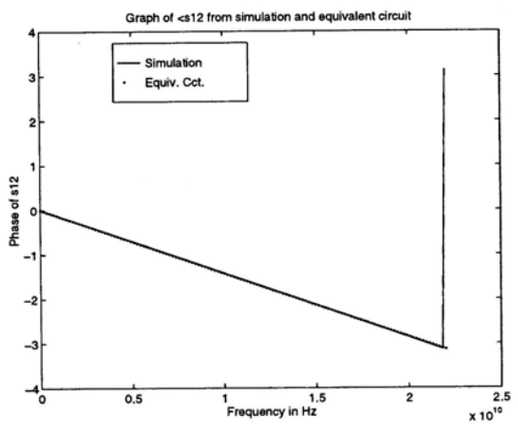

Phase of s_{12}

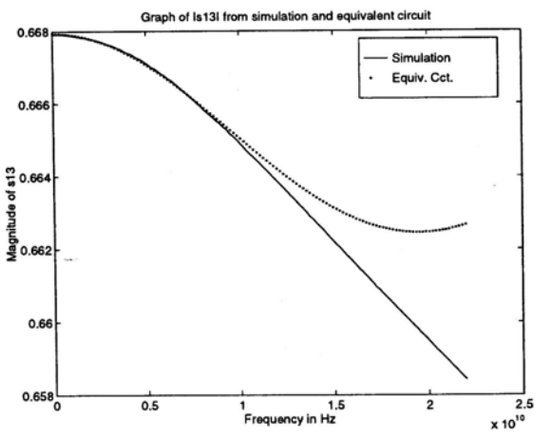

Magnitude of s_{13}

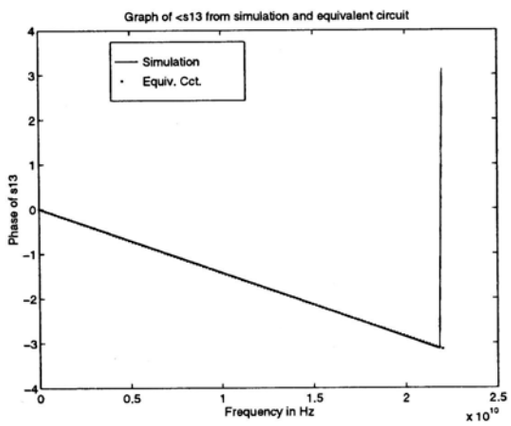

Phase of s_{13}

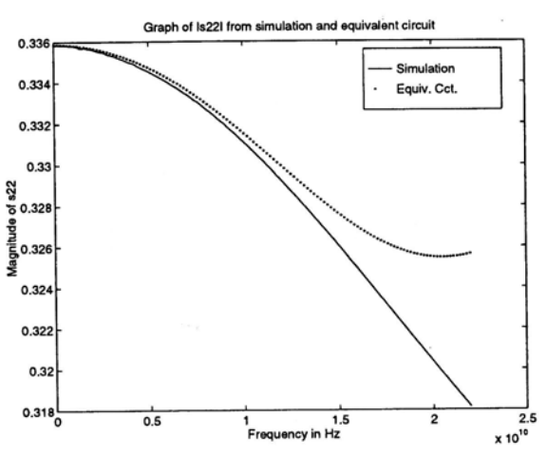

Magnitude of s_{22}

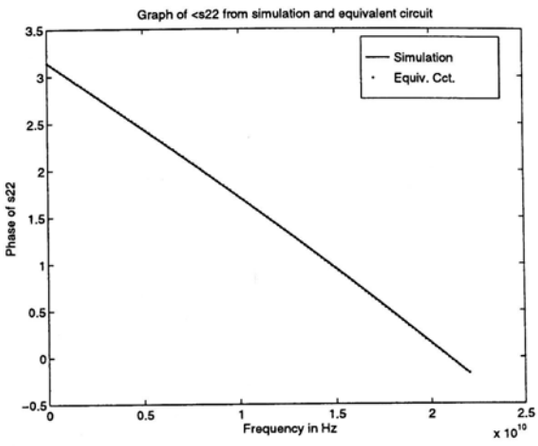

Phase of s_{22}

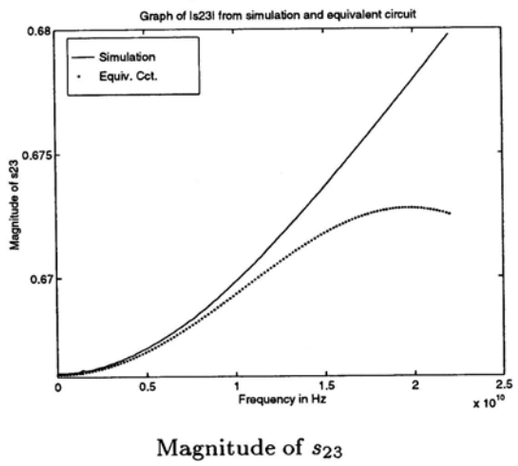

Magnitude of s_{23}

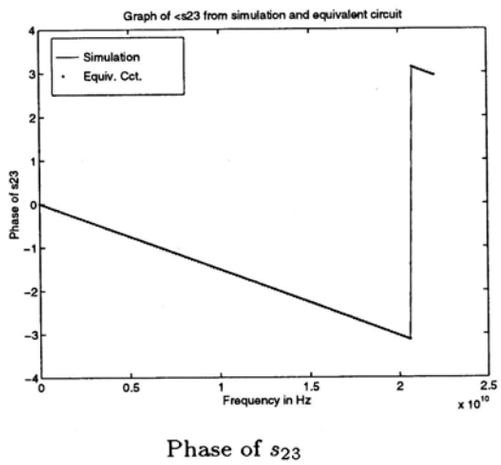

Phase of s_{23}

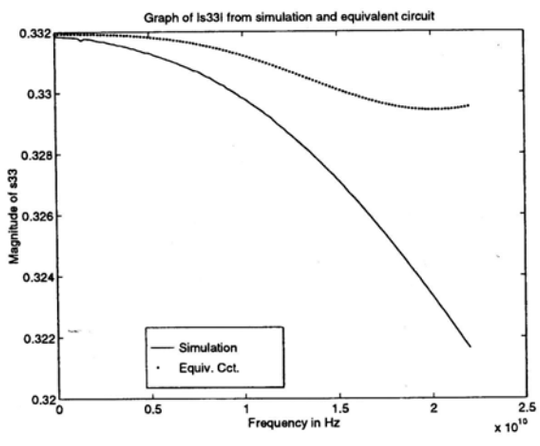

Magnitude of s_{33}

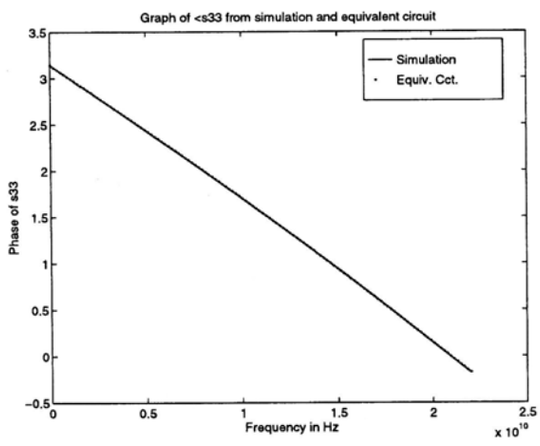

Phase of s_{33}

Figure 7.5: S parameters difference between simulation and circuit 2T (lossless metal strip), $\frac{h}{w} = 0.6$

$\frac{h}{w}$	L_1/Hm^{-1}	G_1/Sm^{-1}	C_1/Fm^{-1}	l_1/mm	L_2/Hm^{-1}	G_2/Sm^{-1}
0.2	1.5371×10^{-7}	5.5897×10^{-3}	5.6952×10^{-10}	1.0284	1.5288×10^{-7}	3.9323×10^{-12}
0.4	2.3831×10^{-7}	6.5999×10^{-11}	3.3998×10^{-10}	1.0101	2.3530×10^{-7}	9.0287×10^{-3}
0.6	2.9667×10^{-7}	1.1011×10^{-11}	2.6058×10^{-10}	0.95978	2.8383×10^{-7}	3.3841×10^{-2}
0.8	3.4047×10^{-7}	2.8123×10^{-5}	2.2207×10^{-10}	0.91335	3.0966×10^{-7}	1.2110×10^{-3}
1.0	3.7767×10^{-7}	1.0099×10^{-11}	2.0413×10^{-10}	0.86388	3.1252×10^{-7}	1.3444×10^{-2}

$\frac{h}{w}$	C_2/Fm^{-1}	l_2/mm	L_{eq1}/H	L_{eq2}/H	C_{eq}/F	err
0.2	5.9056×10^{-10}	0.88183	5.2126×10^{-11}	5.6944×10^{-11}	5.2476×10^{-13}	1.0731×10^{-2}
0.4	3.4468×10^{-10}	0.79004	8.9540×10^{-11}	1.0949×10^{-10}	3.4881×10^{-13}	8.9518×10^{-3}
0.6	2.7919×10^{-10}	0.68698	1.3219×10^{-10}	1.6902×10^{-10}	2.9803×10^{-13}	6.5273×10^{-3}
0.8	2.5296×10^{-10}	0.57883	1.7353×10^{-10}	2.3388×10^{-10}	2.7314×10^{-13}	9.5813×10^{-3}
1.0	2.5435×10^{-10}	0.46618	2.0894×10^{-10}	2.9817×10^{-10}	2.6155×10^{-13}	1.3358×10^{-2}

Table 7.24: Parameter values of the equivalent circuit 3T (lossless metal strip and G being considered)

From Table 7.24, it is seen that Circuit 3T cannot reasonably model the T-junction when the dielectric loss is included in the TEM line model. The conductance per unit length of the TEM lines are found too large to actually describe the substrate dielectric loss. When G is neglected in the TEM line model, the optimization results are recorded in Table 7.25. It is as expected that the parameter values are practical and reasonable (compared with Table 7.23) when the TEM lines are assumed lossless and the loss as well as the dispersive effect are modelled by the lumped inductors and capacitor. The percentage error of the scattering parameters are recorded in Table 7.26.

Refer to Table 6.13 and 7.25, it is observed that the relative errors of the scattering parameters of the equivalent circuit with non-TEM lines are smaller than those with TEM lines. So the non-TEM model is better to model the T-junction when Circuil 3T is selected.

Fig. 7.6 shows the matching result of the TEM model. It is seen that the scattering parameters of Circuit 3T with TEM lines shows the same trend with those of the T-junction in the investigated frequency range. Besides, the matching performance does not become worse when frequency increases, which shows

$\frac{h}{w}$	L_1/Hm^{-1}	C_1/Fm^{-1}	l_1/mm	L_2/Hm^{-1}	C_2/Fm^{-1}
0.2	1.5752×10^{-7}	5.8288×10^{-10}	1.0409	1.3164×10^{-7}	4.9471×10^{-10}
0.4	1.9700×10^{-7}	2.8160×10^{-10}	1.2105	2.4131×10^{-7}	3.6330×10^{-10}
0.6	2.8881×10^{-7}	2.5358×10^{-10}	0.98774	2.9247×10^{-7}	2.8795×10^{-10}
0.8	3.2374×10^{-7}	2.1069×10^{-10}	0.97462	3.6862×10^{-7}	2.8617×10^{-10}
1.0	3.1396×10^{-7}	1.6478×10^{-10}	1.1104	4.9607×10^{-7}	3.5112×10^{-10}

$\frac{h}{w}$	l_2/mm	L_{eq1}/H	L_{eq2}/H	C_{eq}/F	err
0.2	1.0643	4.5956×10^{-11}	5.2535×10^{-11}	4.8105×10^{-13}	5.7494×10^{-3}
0.4	0.76381	9.1370×10^{-11}	1.1026×10^{-10}	3.5345×10^{-13}	5.2274×10^{-3}
0.6	0.66580	1.3166×10^{-10}	1.6918×10^{-10}	2.9760×10^{-13}	6.4628×10^{-3}
0.8	0.52234	1.6859×10^{-10}	2.2244×10^{-10}	2.6758×10^{-13}	8.6463×10^{-3}
1.0	0.34970	1.8856×10^{-10}	2.7429×10^{-10}	2.4613×10^{-13}	1.1734×10^{-2}

Table 7.25: Parameter values of the equivalent circuit 3T (lossless metal strip and G not being considered)

$\frac{h}{w}$	s_{11}	s_{12}	s_{23}	s_{22}	s_{23}	s_{33}
0.2	0.72918	0.44378	0.33155	1.1868	0.28782	1.2160
0.4	1.0151	0.27455	0.20857	0.99605	0.22110	1.1849
0.6	1.2792	0.27330	0.33799	1.3610	0.30763	1.2780
0.8	1.4755	0.43842	0.65762	1.9439	0.40577	1.4718
1.0	1.9090	0.83092	0.78266	2.3783	0.63900	2.1518

Table 7.26: Percentage error between the simulated and calculated scattering parameters from circuit 3T, (lossless metal strip)

that the lumped inductor-capacitor network is able to model the increasing dispersive and mode-coupling effect within the investigated frequency range.

Circuit 4T

$\frac{h}{w}$	L_1/Hm^{-1}	G_1/Sm^{-1}	C_1/Fm^{-1}	L_2/Hm^{-1}	G_2/Sm^{-1}
0.2	1.5719×10^{-7}	6.2134×10^{-14}	5.5465×10^{-10}	1.5170×10^{-7}	6.4767×10^{-14}
0.4	2.4887×10^{-7}	3.6079×10^{-14}	3.2567×10^{-10}	2.4354×10^{-7}	3.7024×10^{-14}
0.6	3.1612×10^{-7}	2.7050×10^{-14}	2.4584×10^{-10}	3.1204×10^{-7}	2.7479×10^{-14}
0.8	3.6731×10^{-7}	2.2535×10^{-14}	2.0578×10^{-10}	3.6497×10^{-7}	2.2712×10^{-14}
1.0	4.0685×10^{-7}	1.9878×10^{-14}	1.8215×10^{-10}	4.0399×10^{-7}	2.0052×10^{-14}

$\frac{h}{w}$	C_2/Fm^{-1}	L_3/Hm^{-1}	G_3/Sm^{-1}	C_3/Fm^{-1}
0.2	5.7771×10^{-10}	1.5829×10^{-7}	6.1627×10^{-14}	5.5021×10^{-10}
0.4	3.3401×10^{-10}	2.5016×10^{-7}	3.5856×10^{-14}	3.2371×10^{-10}
0.6	2.4965×10^{-10}	3.1862×10^{-7}	2.6794×10^{-14}	2.4357×10^{-10}
0.8	2.0735×10^{-10}	3.7338×10^{-7}	2.2088×10^{-14}	2.0181×10^{-10}
1.0	1.8369×10^{-10}	4.1703×10^{-7}	1.9282×10^{-14}	1.7684×10^{-10}

Table 7.27: LGC values of the equivalent circuit 4T by using the non-TEM microstrip line model

$\frac{h}{w}$	L_1/Hm^{-1}	G_1/Sm^{-1}	C_1/Fm^{-1}	l_1/mm
0.2	1.5646×10^{-7}	3.4975×10^{-3}	5.6025×10^{-10}	1.2161
0.4	2.4284×10^{-7}	7.100×10^{-9}	3.2900×10^{-10}	0.88861
0.6	3.0582×10^{-7}	7.5170×10^{-2}	2.4878×10^{-10}	0.80593
0.8	4.3034×10^{-7}	2.0903×10^{-5}	2.5636×10^{-10}	0.82562
1.0	3.3886×10^{-7}	1.4827×10^{-5}	1.6005×10^{-10}	0.63642

$\frac{h}{w}$	L_2/Hm^{-2}	G_2/Sm^{-2}	C_2/Fm^{-2}	l_2/mm
0.2	1.4862×10^{-7}	4.9257×10^{-8}	5.5788×10^{-10}	1.4062
0.4	2.3871×10^{-7}	4.5837×10^{-3}	3.3874×10^{-10}	0.48813
0.6	3.0994×10^{-7}	7.7264×10^{-7}	2.6108×10^{-10}	0.56481
0.8	3.2665×10^{-7}	2.4175×10^{-7}	2.0103×10^{-10}	0.40889
1.0	4.3649×10^{-7}	6.5620×10^{-2}	2.1480×10^{-10}	0.75147

$\frac{h}{w}$	L_3/Hm^{-3}	G_3/Sm^{-3}	C_3/Fm^{-3}	l_3/mm	err
0.2	1.5708×10^{-7}	5.5821×10^{-7}	5.6702×10^{-10}	1.2345	1.0050×10^{-2}
0.4	2.4992×10^{-7}	6.6022×10^{-2}	3.3644×10^{-10}	1.1969	7.7706×10^{-3}
0.6	3.1240×10^{-7}	6.0081×10^{-3}	2.5061×10^{-10}	1.1914	1.0773×10^{-2}
0.8	3.8092×10^{-7}	1.2735×10^{-1}	2.1747×10^{-10}	1.1264	1.3365×10^{-2}
1.0	3.6952×10^{-7}	1.8149×10^{-2}	1.6742×10^{-10}	1.2578	1.8153×10^{-2}

Table 7.28: Parameter values of the equivalent circuit 4T (lossless metal strip and G being considered)

As in other equivalent circuits to model the T-junction, the values of the conductance per unit length of the TEM lines in Circuit 4T are too large to

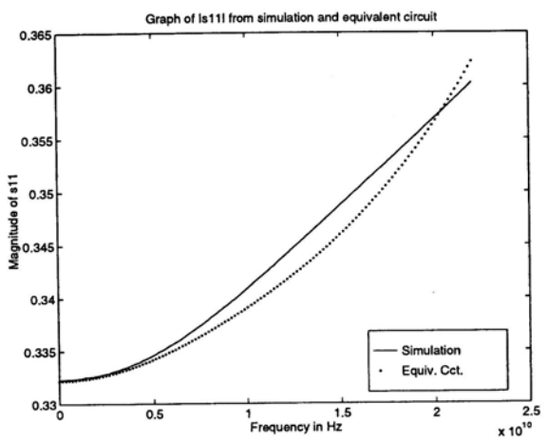

Magnitude of s_{11}

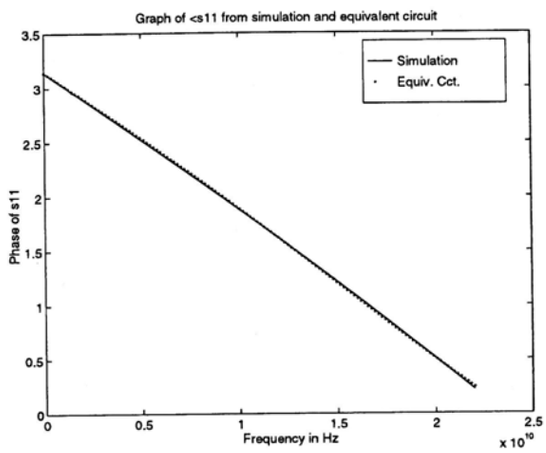

Phase of s_{11}

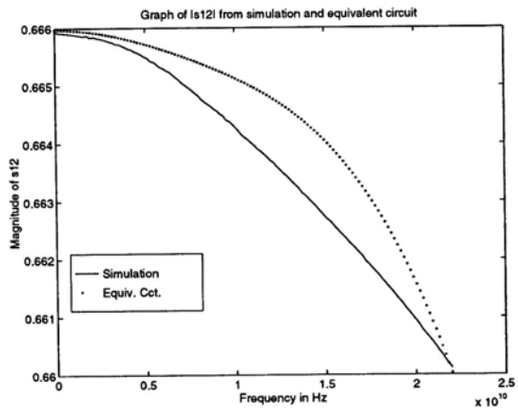

Magnitude of s_{12}

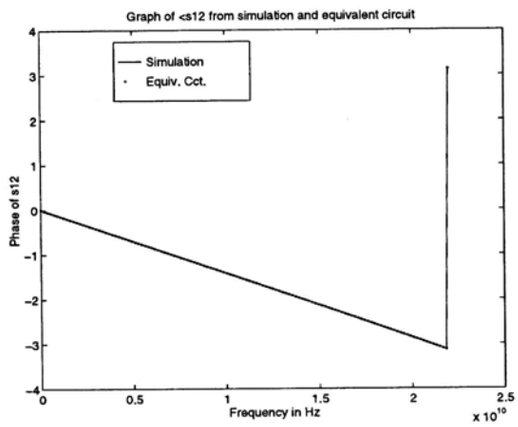

Phase of s_{12}

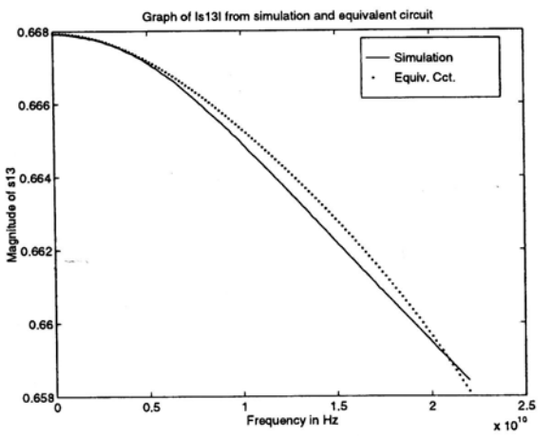

Magnitude of s_{13}

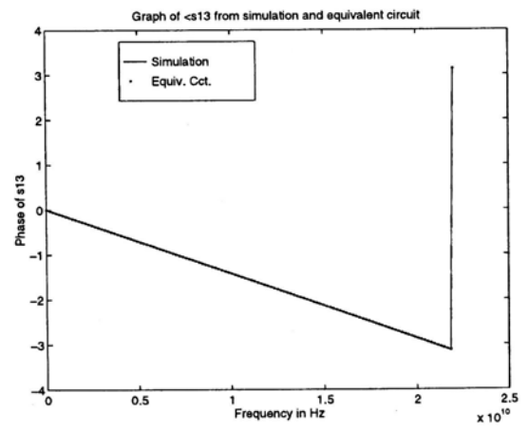

Phase of s_{13}

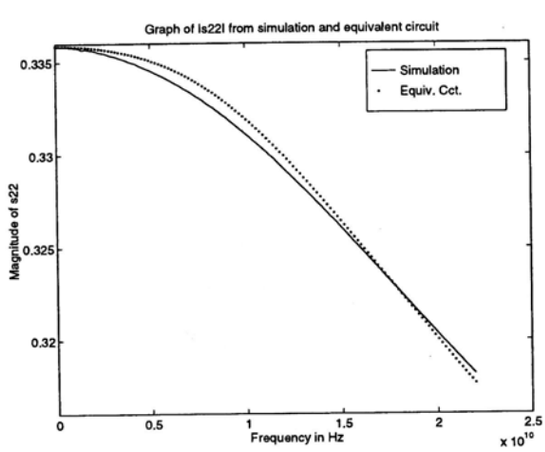

Magnitude of s_{22}

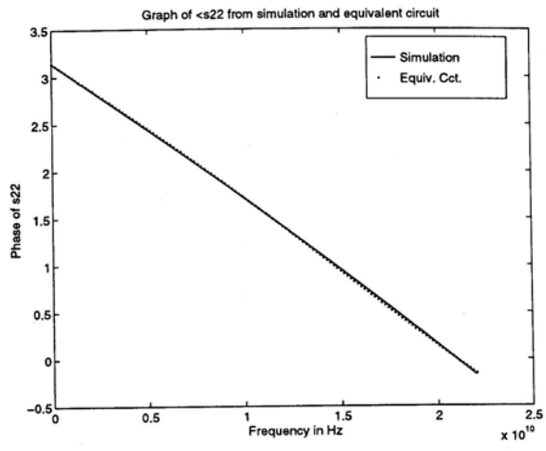

Phase of s_{22}

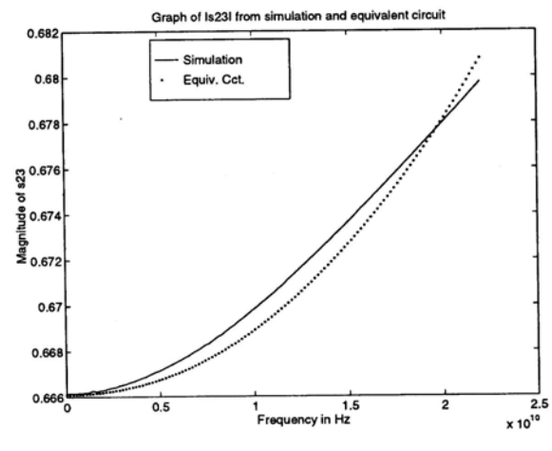

Magnitude of s_{23}

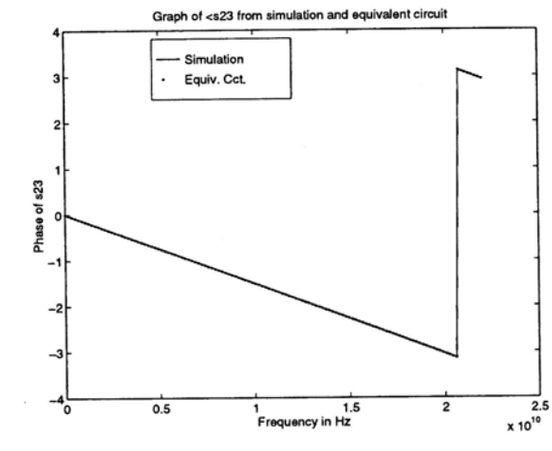

Phase of s_{23}

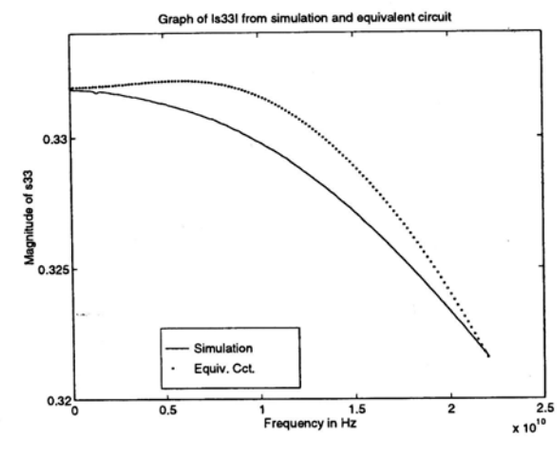

Magnitude of s_{33}

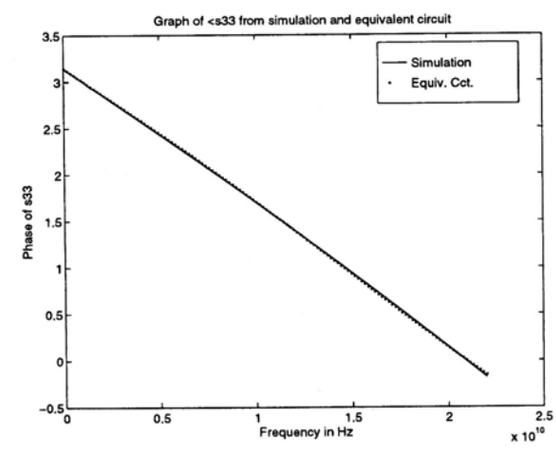

Phase of s_{33}

Figure 7.6: S parameters difference between simulation and circuit 3T (lossless metal strip), $\frac{h}{w} = 0.6$

describe the dielectric loss in the substrate (Table 7.28). On the other hand, Circuit 4T with lossless TEM lines can model the T-junction because the parameter values are in the same order of magnitude of the equivalent circuit with non-TEM lines (see Table 7.27 and Table 7.29).

$\frac{h}{w}$	L_1/Hm^{-1}	C_1/Fm^{-1}	l_1/mm	L_2/Hm^{-1}	C_2/Fm^{-1}
0.2	2.1608×10^{-7}	7.6844×10^{-10}	0.29091	8.4235×10^{-8}	3.0851×10^{-10}
0.4	2.3015×10^{-7}	3.1165×10^{-10}	0.84287	2.3408×10^{-7}	3.3138×10^{-10}
0.6	5.4215×10^{-7}	4.2138×10^{-10}	0.13017	1.4228×10^{-7}	1.1850×10^{-10}
0.8	3.3549×10^{-7}	1.9856×10^{-10}	0.69418	3.8407×10^{-7}	2.3319×10^{-10}
1.0	4.0062×10^{-7}	1.9086×10^{-10}	0.89271	3.9819×10^{-7}	1.9678×10^{-10}

$\frac{h}{w}$	l_2/mm	L_3/Hm^{-1}	C_3/Fm^{-1}	l_3/mm	err
0.2	1.7577	7.2443×10^{-8}	2.5898×10^{-10}	2.6796	6.5664×10^{-3}
0.4	0.59059	2.5208×10^{-7}	3.3884×10^{-10}	1.1865	7.2602×10^{-3}
0.6	2.4695	1.5412×10^{-7}	1.2371×10^{-10}	2.4153	1.0221×10^{-2}
0.8	0.66830	3.5868×10^{-7}	2.0494×10^{-10}	1.1940	1.3165×10^{-2}
1.0	0.46609	4.0313×10^{-7}	1.8360×10^{-10}	1.1520	1.9046×10^{-2}

Table 7.29: Parameter values of the equivalent circuit 4T (lossless metal strip and G not being considered)

It is a little bit surprised that the equivalent circuit with purely TEM lines can model the T-junction. The reason may be that the discontinuity effect at the joint of the T-junction is modelled by connecting one end of the three TEM lines together, which is contrary to the right-angled bend that the bend is modelled by a TEM line. Table 7.30 records the percentage error of the scattering parameters.

$\frac{h}{w}$	s_{11}	s_{12}	s_{23}	s_{22}	s_{23}	s_{33}
0.2	0.30820	0.72579	0.51377	1.0488	0.45952	1.1353
0.4	0.81069	0.76265	0.80271	0.50300	0.61262	0.76998
0.6	1.5364	1.0652	1.1006	0.59005	0.83156	0.85441
0.8	1.7704	1.4850	1.5214	1.0553	0.89174	0.65769
1.0	3.0755	2.1063	2.0255	2.1395	1.1405	0.79408

Table 7.30: Percentage error between the simulated and calculated scattering parameters from circuit 4T, (lossless metal strip)

By comparing the relative errors of the scattering parameters with those from the non-TEM model again (Table 6.14 and 7.29), it is seen that their values are

comparable. Therefore, if Circuit 4T is selected to model the T-junction, both TEM and non-TEM model can be used.

Fig. 7.7 shows the plots of the scattering parameters of the equivalent circuit. It is seen that the scattering parameters mismatch when frequency increases because the dispersive and mode-coupling effect increase and the TEM lines cannot model these effects.

7.2.2 With Conductor Loss

As similar as the analysis of the right-angled bend, the same three cases are adopted to analyze the T-junction. The first case is that the microstrip line model includes both the conductor and dielectric loss. The second case is that the line model considers only the conductor loss and the dielectric loss is neglected (or modelled by the lumped element). The last case is to assume the line model to be lossless.

Circuit 1T

R	L	G	C	$R_1/\Omega m^{-1}$	L_1/Hm^{-1}	G_1/Sm^{-1}	C_1/Fm^{-1}	l_1/mm
√	√	√	√	-247.28	3.8338×10^{-7}	4.7422×10^{-1}	1.7334×10^{-10}	0.59512
√	√		√	9.8208×10^{-8}	3.9686×10^{-7}	–	1.9106×10^{-10}	0.55765
	√		√	–	3.7892×10^{-7}	–	1.6986×10^{-10}	0.60269

R	L	G	C	$R_2/\Omega m^{-1}$	L_2/Hm^{-1}	G_2/Sm^{-1}	C_2/Fm^{-1}	l_2/mm	err
√	√	√	√	-64.639	3.8956×10^{-7}	2.7952×10^{-2}	1.6845×10^{-10}	0.50443	2.9459×10^{-2}
√	√		√	346.99	4.0409×10^{-7}	–	1.1665×10^{-10}	0.46960	5.5666×10^{-2}
	√		√	–	4.5572×10^{-7}	–	2.0003×10^{-10}	0.43320	2.8217×10^{-2}

Table 7.31: Parameter values of the equivalent circuit 1T (lossy metal strip)

From Table 7.31, it is seen that Circuit 1T can only model the T-junction when the TEM lines are treated as lossless lines. For this case, the parameter values are in their typical range. It is because the discontinuity junction is modelled by connecting one end of the three transmission lines together and not modelled by a transmission line (not the case of right-angled bend, see

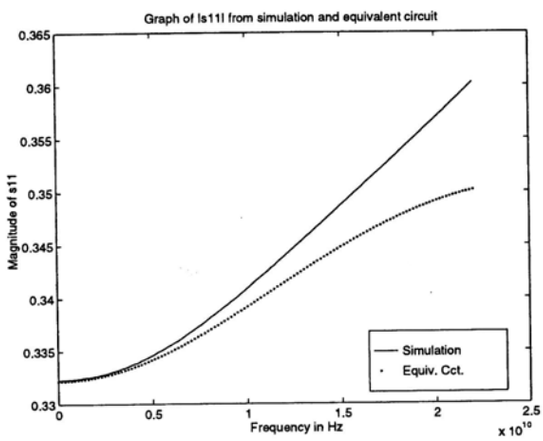

Magnitude of s_{11}

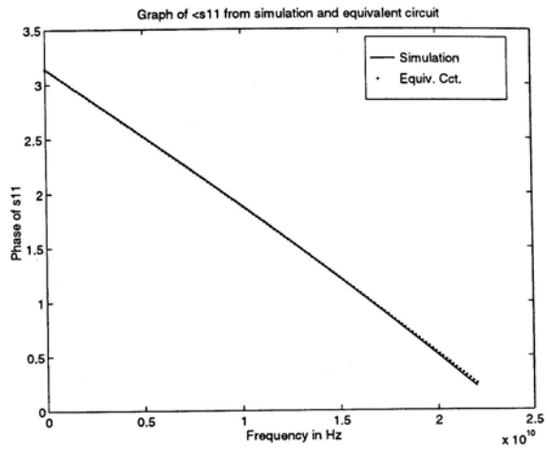

Phase of s_{11}

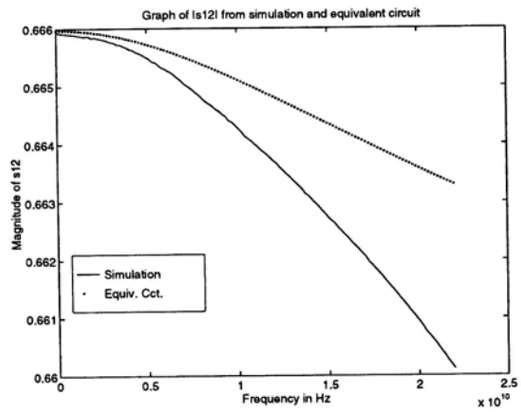

Magnitude of s_{12}

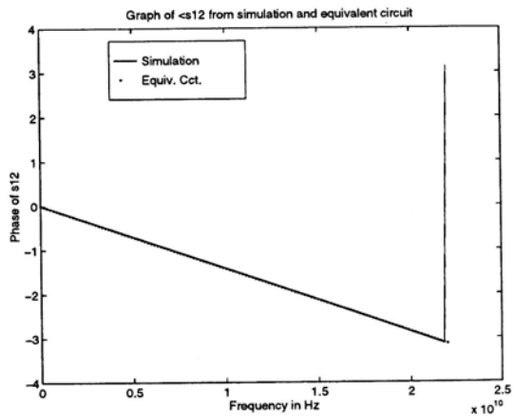

Phase of s_{12}

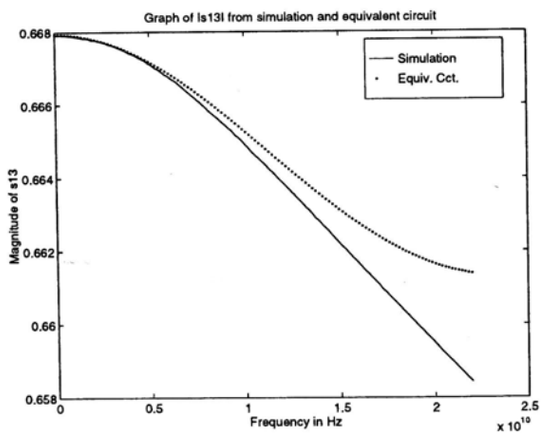

Magnitude of s_{13}

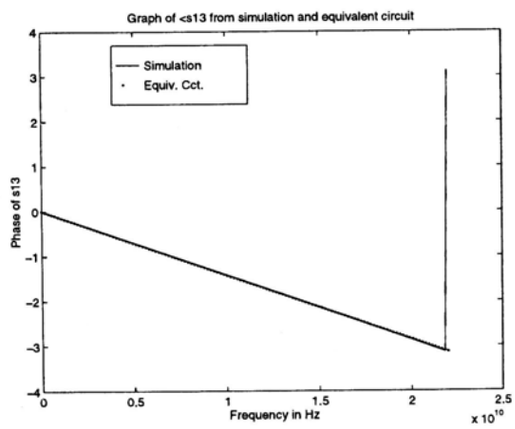

Phase of s_{13}

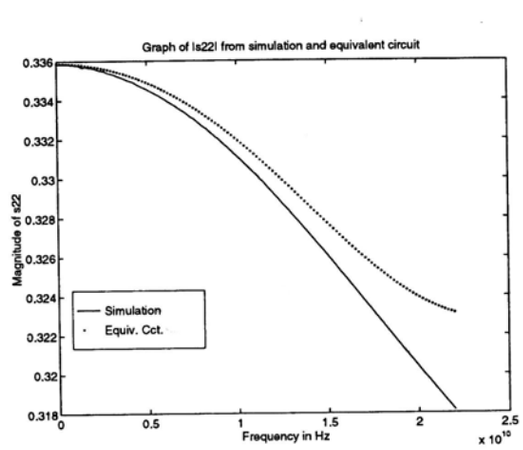

Magnitude of s_{22}

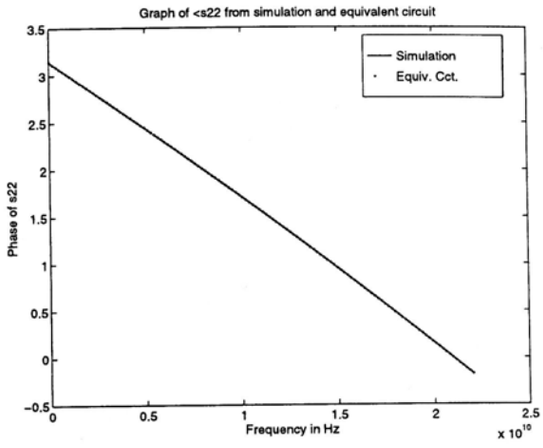

Phase of s_{22}

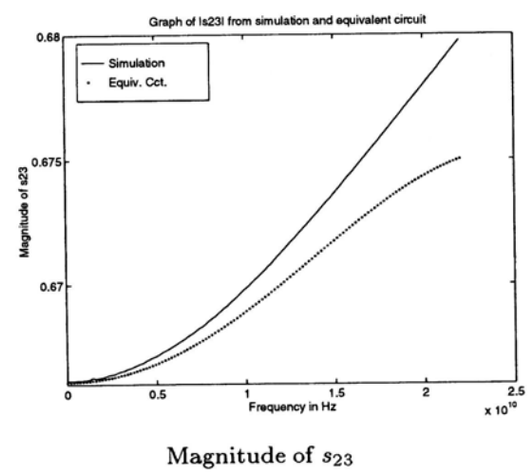

Magnitude of s_{23}

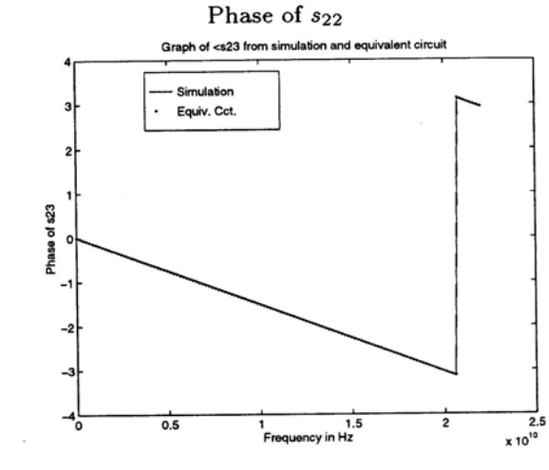

Phase of s_{23}

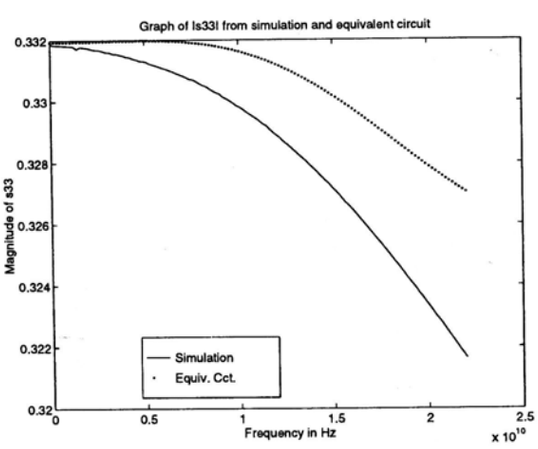

Magnitude of s_{33}

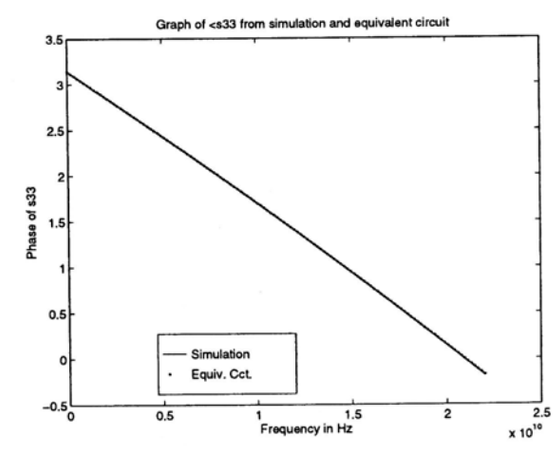

Phase of s_{33}

Figure 7.7: S parameters difference between simulation and circuit 4T, (lossless metal strip), $\frac{h}{w} = 0.6$

Circuit 3L and 4L). So the parameter values are in their typical range even the TEM lines are lossless. When the TEM lines are lossy, optimization results in either negative values or parameter values not in their typical range. The percentage error of the scattering parameters when the TEM lines are lossless are recorded in Table 7.32.

$\frac{h}{w} = 1.0$	s_{11}	s_{12}	s_{23}	s_{22}	s_{23}	s_{33}
err	6.0118	1.1835	1.2588	5.5997	1.3359	5.5734

Table 7.32: Percentage error between the simulated and calculated scattering parameters from circuit 1T, (lossy metal strip)

The degree of fitness between the scattering parameters of the equivalent circuit and the T-junction is shown in Fig. 7.8. It is seen that Circuit 1T lower-estimates the loss of the T-junction especially at high frequency. This loss should be the conductor loss because the skin effect of the lossy metal strip increases with frequency.

Refer to Table 6.21 and 7.31, the relative error of the non-TEM model is smaller to that of the TEM model. So, for a lossy metal strip T-junction, non-TEM Circuit 1T is the choice rather than the TEM one.

Circuit 2T

The same phenomenon (or result) is observed as in Circuit 1T. So it is concluded that Circuit 2T is able to model the T-junction when its TEM lines are lossless lines. Besides, it can be seen that Circuit 2T is better in modelling than Circuit 1T because the percentage error from Circuit 2T is smaller (Table 7.34).

If the TEM model is compared with the non-TEM model by their relative errors (Table 6.21 and 7.33), it is seen that the value of the non-TEM model is smaller. So, the non-TEM Circuit 2T is preferred to model the lossy metal strip T-junction.

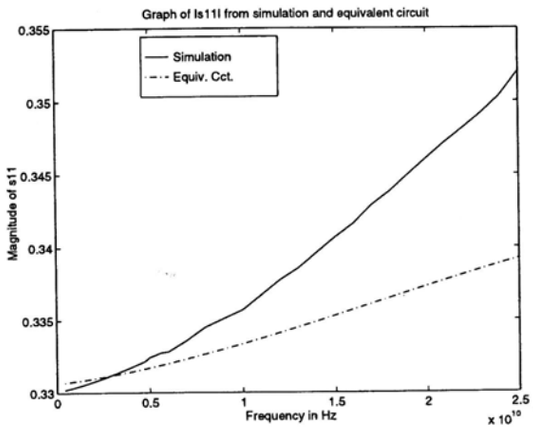

Magnitude of s_{11}

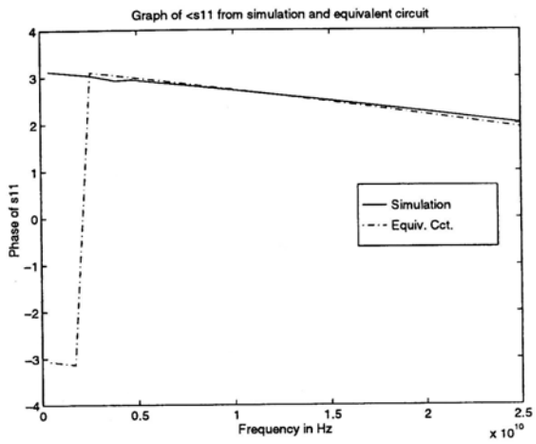

Phase of s_{11}

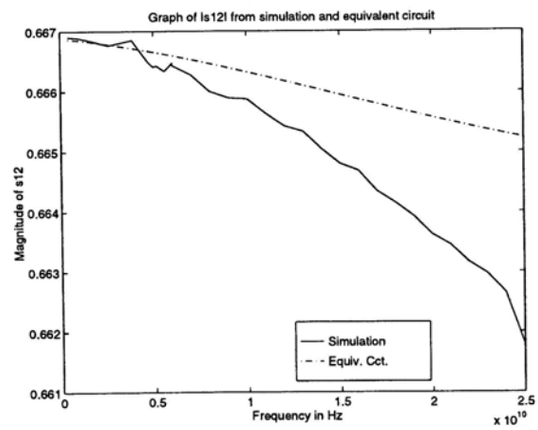

Magnitude of s_{12}

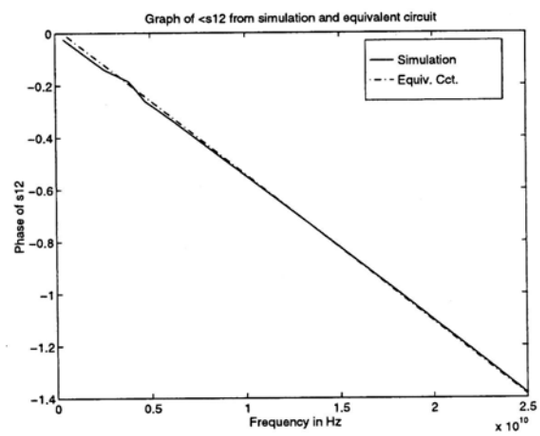

Phase of s_{12}

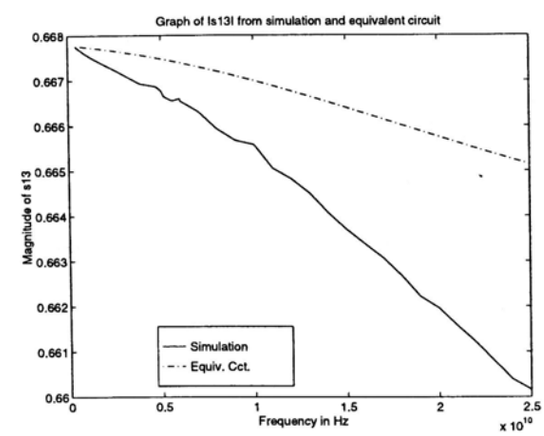

Magnitude of s_{13}

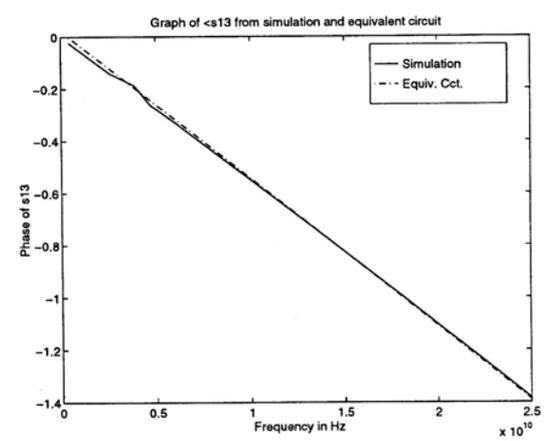

Phase of s_{13}

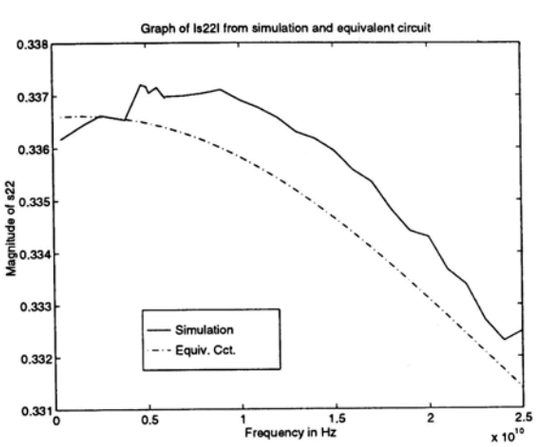

Magnitude of s_{22}

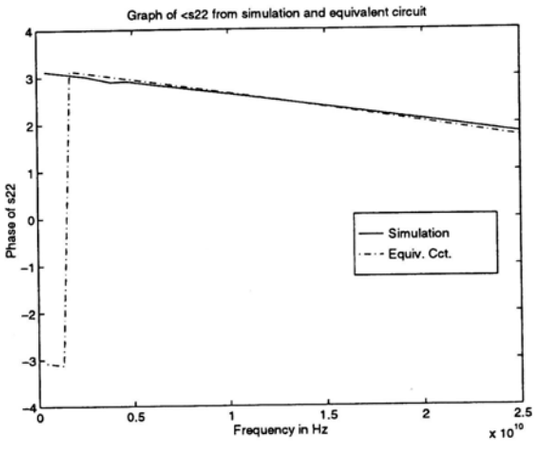

Phase of s_{22}

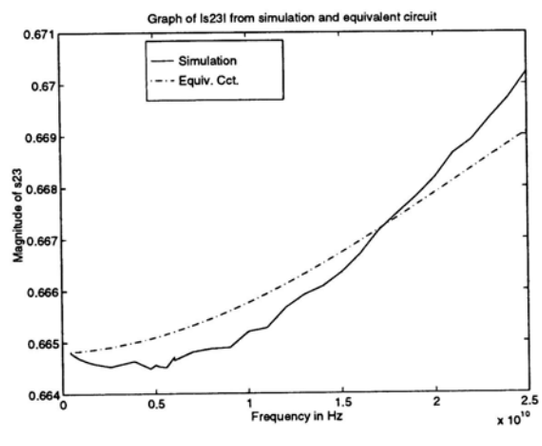

Magnitude of s_{23}

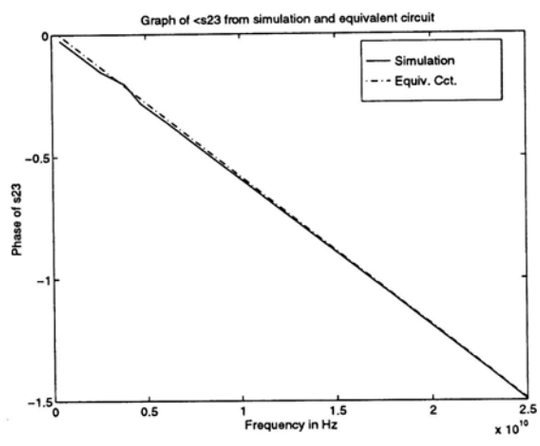

Phase of s_{23}

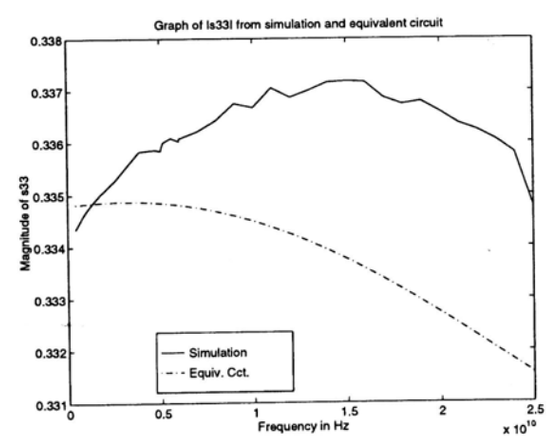

Magnitude of s_{33}

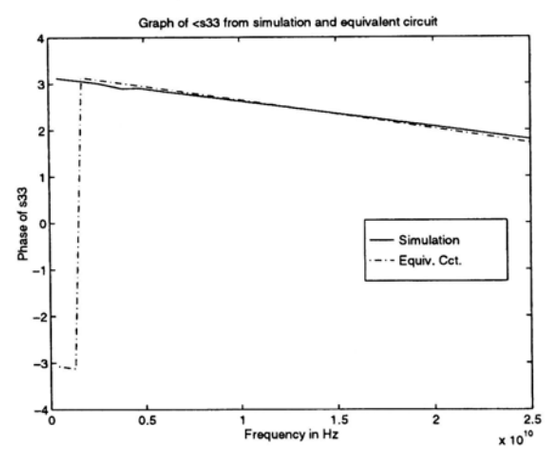

Phase of s_{33}

Figure 7.8: S parameters difference between simulation and circuit 1T (lossy metal strip), $\frac{h}{w} = 1.0$

R	L	G	C	$R_1/\Omega m^{-1}$	L_1/Hm^{-1}	G_1/Sm^{-1}	C_1/Fm^{-1}	l_1/mm
√	√	√	√	−83.834	4.4447×10^{-7}	8.6704×10^{-2}	1.2059×10^{-10}	0.53991
√	√		√	1.0825×10^{-6}	4.3862×10^{-7}	–	1.6572×10^{-10}	0.52273
	√		√	–	4.9398×10^{-7}	–	1.3228×10^{-10}	0.48658

R	L	G	C	$R_2/\Omega m^{-1}$	L_2/Hm^{-1}	G_2/Sm^{-1}	C_2/Fm^{-1}	l_2/mm
√	√	√	√	1.7025	4.6063×10^{-7}	4.0382×10^{-1}	8.9141×10^{-11}	0.44577
√	√		√	26.643	4.7415×10^{-7}	–	1.5080×10^{-10}	0.41515
	√		√	–	5.3666×10^{-7}	–	1.0178×10^{-10}	0.38284

R	L	G	C	C/F	err
√	√	√	√	1.0411×10^{-13}	2.5470×10^{-2}
√	√		√	4.9896×10^{-14}	2.4206×10^{-2}
	√		√	1.0583×10^{-13}	2.5802×10^{-2}

Table 7.33: Parameter values of the equivalent circuit 2T (lossy metal strip)

$\frac{h}{w} = 1.0$	s_{11}	s_{12}	s_{23}	s_{22}	s_{23}	s_{33}
err	5.0510	1.3541	1.4283	5.0612	1.3597	4.9533

Table 7.34: Percentage error between the simulated and calculated scattering parameters from circuit 2T, (lossy metal strip)

Fig. 7.9 shows the degree of fitness of the scattering parameters. It is observed again that Circuit 2T lower-estimates the conductor loss of the T-junction.

Circuit 3T

From Table 7.35, it can be concluded that Circuit 3T can model the T-junction when the TEM lines are treated as lossless lines and the dispersive and loss effect are modelled by the lumped elements. From Chapter 6, there is no modelling result of T-junction with lossy metal strip. It is because negative parameter values are obtained no matter how the initial guess is changed. Table 7.36 records the percentage error of the scattering parameters. It is seen that Circuit 3T is usable to model the T-junction if 5% error can be tolerated.

Since there is no modelling result of Circuit 3T with non-TEM lines, the TEM model is only the choice if Circuit 3T is required. Fig. 7.10 shows the matching performance of the scattering parameters. It is again observed that Circuit 3T with TEM lines still lower-estimates the loss of the T-junction.

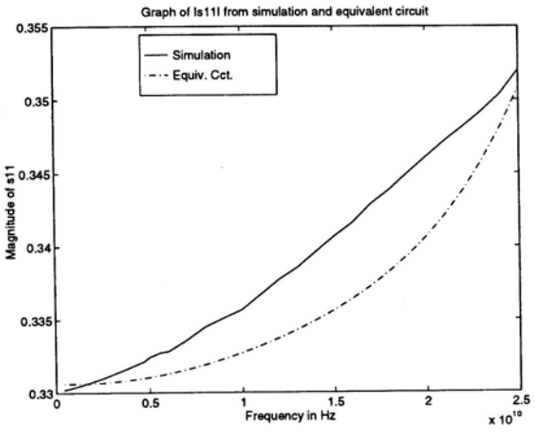

Magnitude of s_{11}

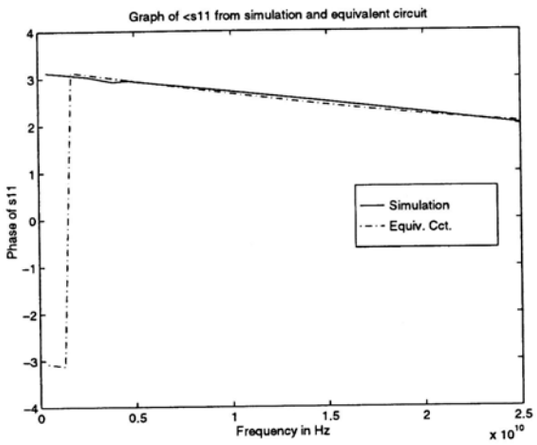

Phase of s_{11}

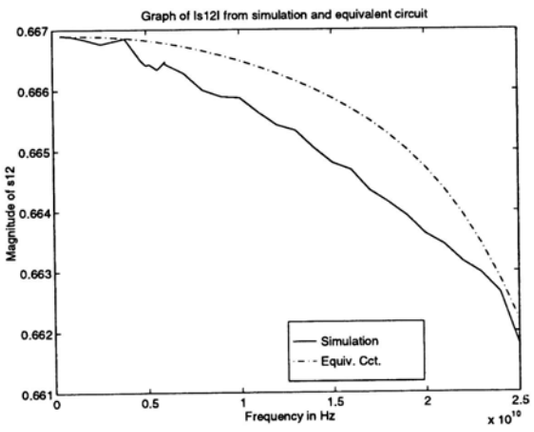

Magnitude of s_{12}

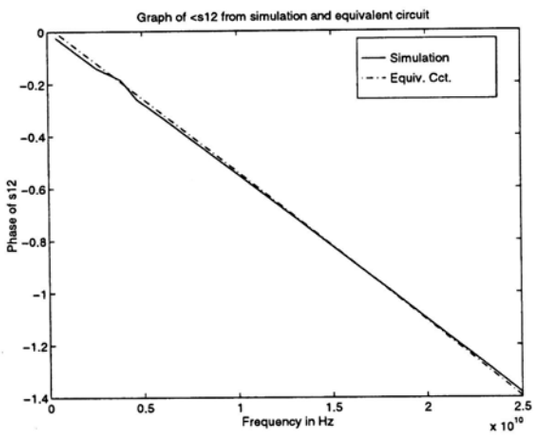

Phase of s_{12}

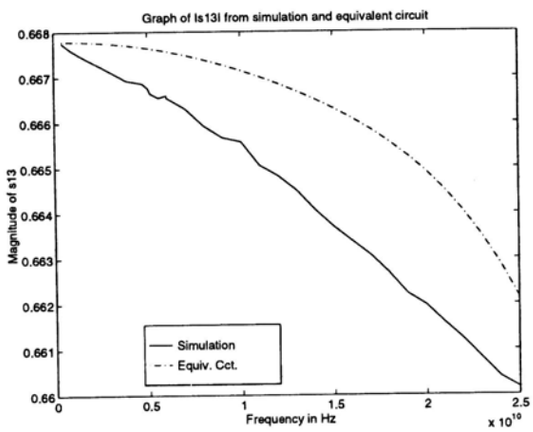

Magnitude of s_{13}

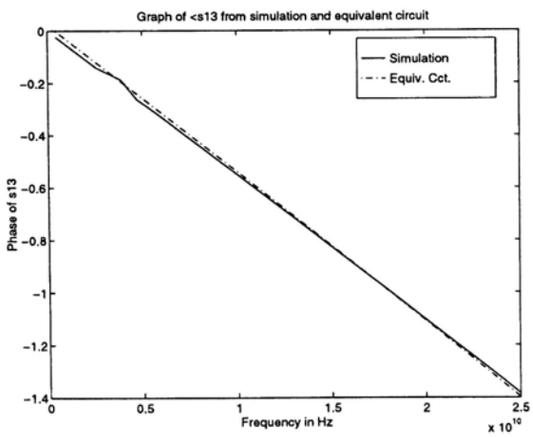

Phase of s_{13}

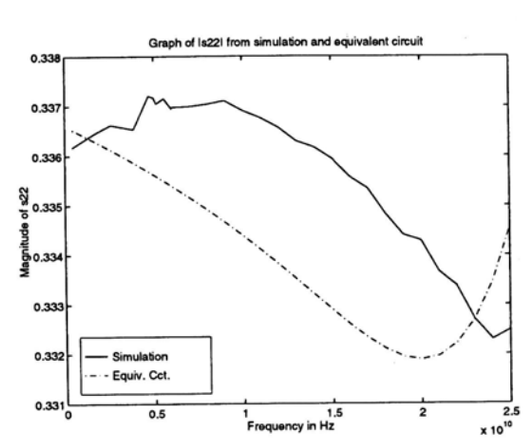

Magnitude of s_{22}

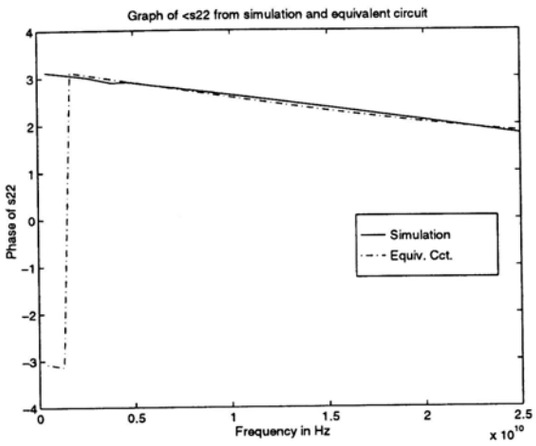

Phase of s_{22}

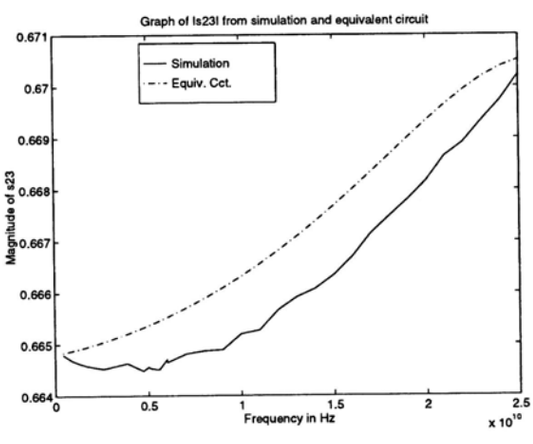

Magnitude of s_{23}

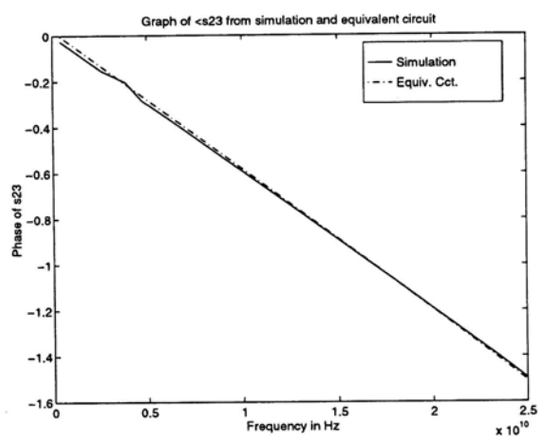

Phase of s_{23}

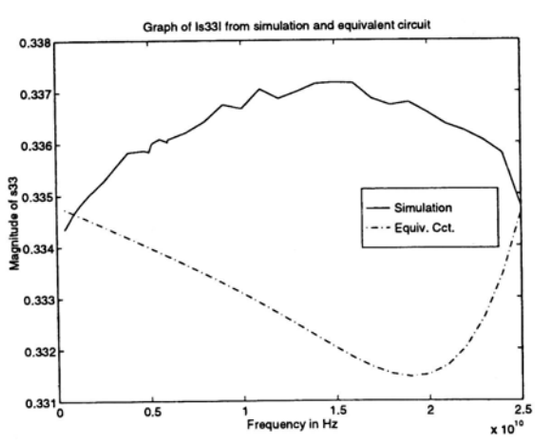

Magnitude of s_{33}

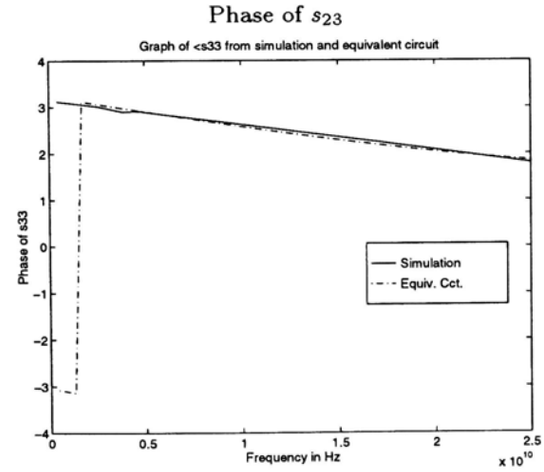

Phase of s_{33}

Figure 7.9: S parameters difference between simulation and circuit 2T (lossy metal strip), $\frac{h}{w} = 1.0$

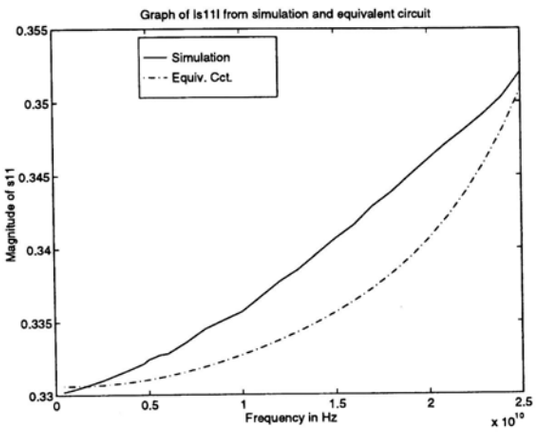

Magnitude of s_{11}

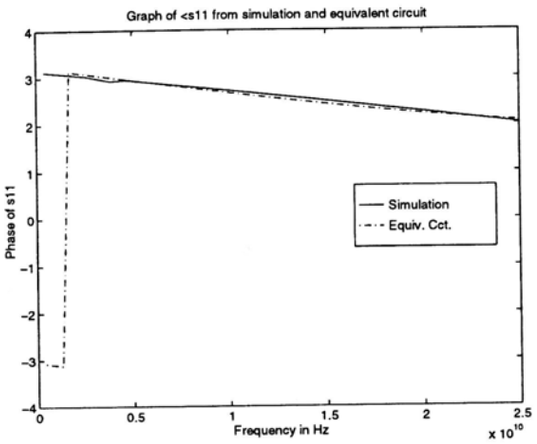

Phase of s_{11}

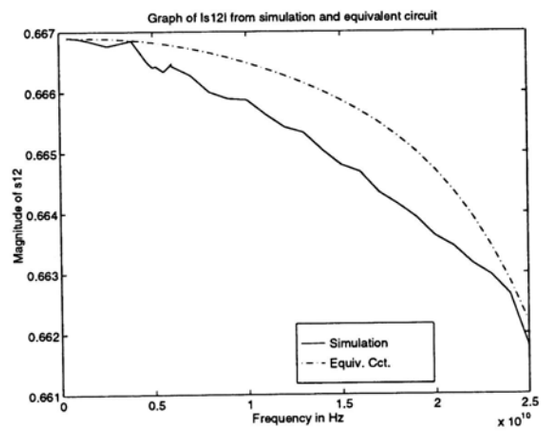

Magnitude of s_{12}

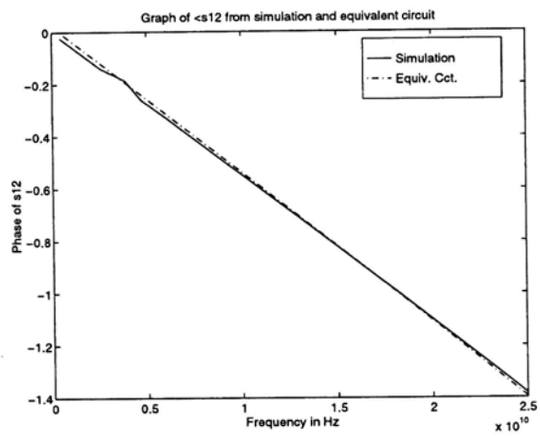

Phase of s_{12}

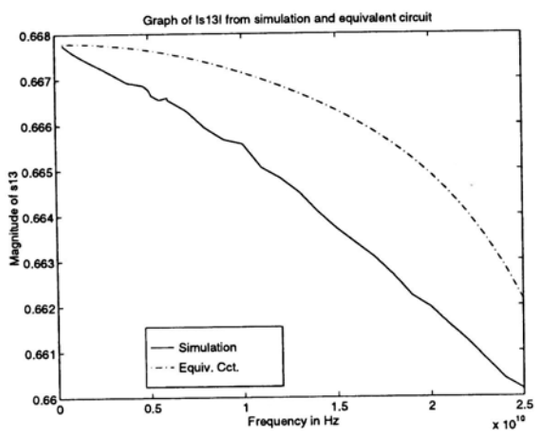

Magnitude of s_{13}

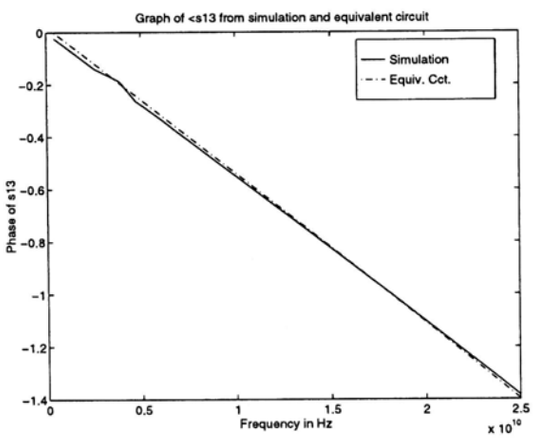

Phase of s_{13}

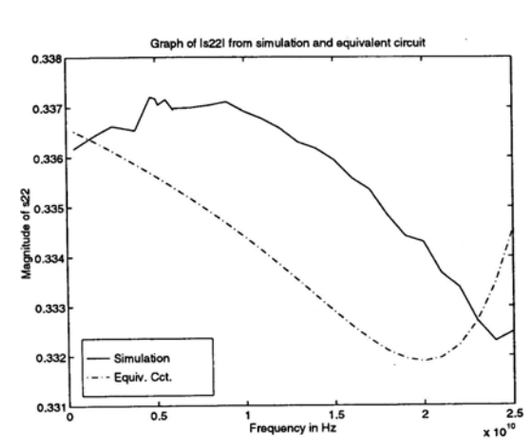

Magnitude of s_{22}

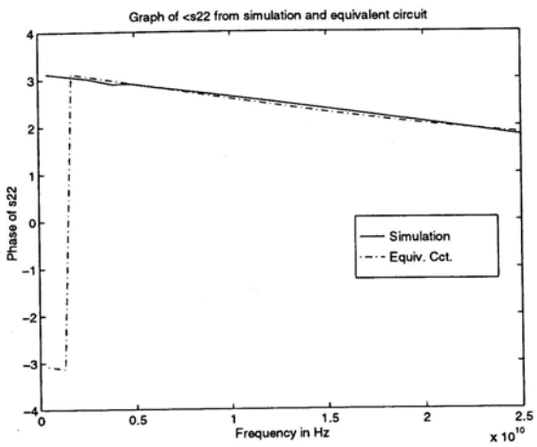

Phase of s_{22}

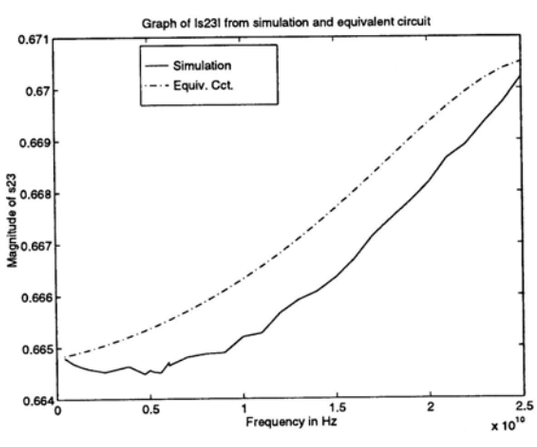

Magnitude of s_{23}

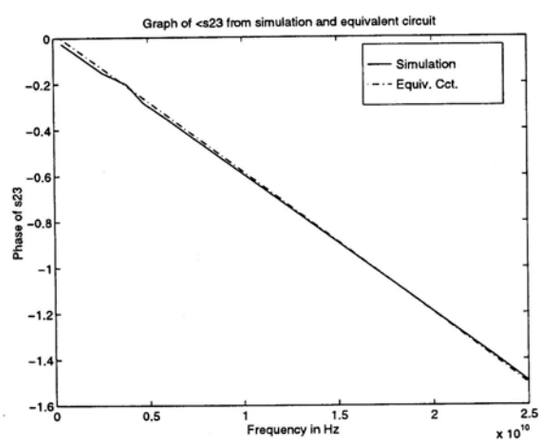

Phase of s_{23}

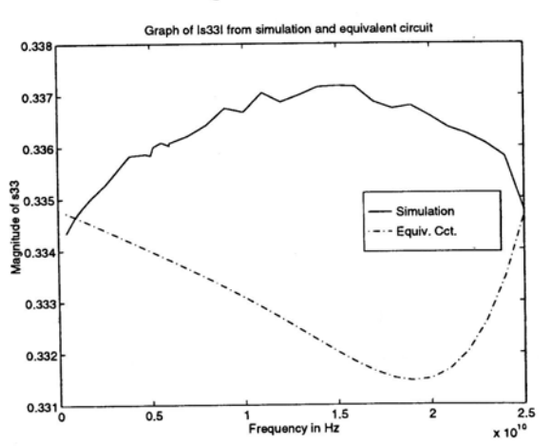

Magnitude of s_{33}

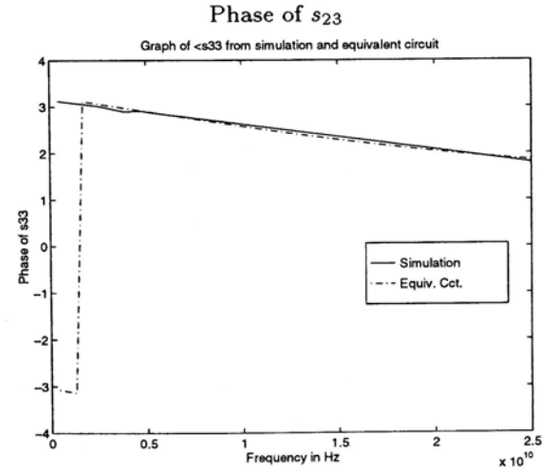

Phase of s_{33}

Figure 7.10: S parameters difference between simulation and circuit 3T (lossy metal strip), $\frac{h}{w} = 1.0$

R	L	G	C	$R_1/\Omega m^{-1}$	L_1/Hm^{-1}	G_1/Sm^{-1}	C_1/Fm^{-1}	l_1/mm
√	√	√	√	−144.43	7.7403×10^{-7}	1.5170×10^{-1}	2.0980×10^{-10}	0.31011
√	√		√	1.9578×10^{-7}	2.4563×10^{-7}	–	3.0128×10^{-10}	0.087869
	√		√	–	1.3811×10^{-6}	–	3.6940×10^{-10}	0.17385

R	L	G	C	$R_2/\Omega m^{-1}$	L_2/Hm^{-1}	G_2/Sm^{-1}	C_2/Fm^{-1}	l_2/mm
√	√	√	√	1.6412	2.9360×10^{-6}	2.5833	5.6738×10^{-10}	0.069413
√	√		√	1.6018×10^{4}	2.3689×10^{-7}	–	8.4353×10^{-10}	0.012196
	√		√	–	2.1314×10^{-6}	–	4.0329×10^{-10}	0.096331

R	L	G	C	L_{eq1}/H	L_{eq2}/H	C_{eq}/F	err
√	√	√	√	-4.2233×10^{-14}	1.5544×10^{-12}	1.0453×10^{-13}	2.5484×10^{-2}
√	√		√	2.5716×10^{-10}	1.9299×10^{-10}	1.9372×10^{-13}	4.0734×10^{-2}
	√		√	2.8153×10^{-13}	1.4389×10^{-13}	1.0619×10^{-13}	2.5823×10^{-2}

Table 7.35: Parameter values of the equivalent circuit 3T (lossy metal strip)

$\frac{h}{w} = 1.0$	s_{11}	s_{12}	s_{13}	s_{22}	s_{23}	s_{33}
err	5.0547	1.3548	1.4291	5.0661	1.3604	4.9581

Table 7.36: Percentage error between the simulated and calculated scattering parameters from circuit 3T, (lossy metal strip)

Circuit 4T

Although the discontinuity region of the T-junction is modelled by connecting one end of the three transmission lines together, Circuit 4T cannot model the T-junction even when the TEM lines are lossless. From Table 7.37, it is seen that the second microstrip line (with length l_2, Fig. 5.4) is very short. It shows that this line is an extra line which means that Circuit 1T is sufficient to model the T-junction.

7.3 Tapered Line

In this section, only the result of the equivalent circuit with three sections of microstrip lines are recorded. Although it is so, we do try the equivalent circuits with different number of sections. However, the optimization results are similar to those with non-TEM lines. That is, the optimization leads to a N-section structure, where $N = 4$, 5, 7, 10, and 20, with the width of the middle section(s)

R	L	G	C	$R_1/\Omega m^{-1}$	L_1/Hm^{-1}	G_1/Sm^{-1}	C_1/Fm^{-1}	l_1/mm
√	√	√	√	−392.80	6.3639×10^{-7}	5.2667×10^{-1}	1.7767×10^{-10}	0.39891
√	√		√	340.34	4.2995×10^{-7}	–	1.7064×10^{-10}	0.51685
	√		√	–	4.5120×10^{-7}	–	1.6974×10^{-10}	0.51675

R	L	G	C	$R_2/\Omega m^{-1}$	L_2/Hm^{-1}	G_2/Sm^{-1}	C_2/Fm^{-1}	l_2/mm
√	√	√	√	5.4020×10^{4}	-9.0934×10^{-6}	-1.7324×10^{-2}	2.9164×10^{-8}	0.0016118
√	√		√	1.4450×10^{-9}	1.3249×10^{-7}	–	8.4613×10^{-9}	0.0027317
	√		√	–	2.3933×10^{-14}	–	9.0448×10^{-9}	0.0028298

R	L	G	C	$R_3/\Omega m^{-1}$	L_3/Hm^{-1}	G_3/Sm^{-1}	C_3/Fm^{-1}	l_3/mm	err
√	√	√	√	−62.004	5.7510×10^{-7}	1.2933	1.0785×10^{-10}	0.35787	2.5460×10^{-2}
√	√		√	401.20	4.6075×10^{-7}	–	1.5728×10^{-10}	0.40746	3.7963×10^{-2}
	√		√	–	4.8243×10^{-7}	–	1.4205×10^{-10}	0.41712	2.4246×10^{-2}

Table 7.37: Parameter values of the equivalent circuit 4T (lossy metal strip)

being narrower than the two end sections. So they are not physical to model the tapered line.

7.3.1 Without Conductor Loss

L_1/Hm^{-1}	G_1/Sm^{-1}	C_1/Fm^{-1}	L_2/Hm^{-1}	G_2/Sm^{-1}
7.2125×10^{-7}	9.8739×10^{-15}	9.3979×10^{-11}	4.4946×10^{-7}	1.7605×10^{-14}

C_2/Fm^{-1}	L_3/Hm^{-1}	G_3/Sm^{-1}	C_3/Fm^{-1}
1.6193×10^{-10}	4.1832×10^{-7}	1.9224×10^{-14}	1.7355×10^{-10}

Table 7.38: LGC values of the equivalent circuit 1t by using the non-TEM microstrip line model

L	G	C	L_1/Hm^{-1}	G_1/Sm^{-1}	C_1/Fm^{-1}	l_1/mm
√	√	√	7.1240×10^{-7}	4.1987×10^{-9}	9.3617×10^{-11}	0.094812
√		√	6.2716×10^{-7}	–	8.8750×10^{-11}	0.076822

L	G	C	L_2/Hm^{-1}	G_2/Sm^{-1}	C_2/Fm^{-1}	l_2/mm
√	√	√	4.7142×10^{-7}	9.7341×10^{-5}	1.6183×10^{-10}	0.22970
√		√	5.6931×10^{-7}	–	1.7290×10^{-10}	0.30899

L	G	C	L_3/Hm^{-1}	G_3/Sm^{-1}	C_3/Fm^{-1}	l_3/mm	err
√	√	√	3.9686×10^{-7}	1.9682×10^{-6}	1.7385×10^{-10}	0.12581	5.7873×10^{-3}
√		√	1.3615×10^{-8}	–	1.3235×10^{-10}	0.059700	5.6896×10^{-3}

Table 7.39: Parameter values of the equivalent circuit 1t (lossless metal strip)

As the previous work does, the optimization is carried out for firstly including the dielectric loss in the equivalent circuit and then not considering it.

Table 7.39 records the optimization results. It is as expected that the optimization result which considers G in Eq. 5.16 is not physical to model the tapered line because their values are too large to describe the actual dielectric loss in the substrate. On the other hand, when G is not taken into account in Eq. 5.16, the transmission line parameters are found comparable to those from non-TEM line model (Table 7.38). Moreover, the percentage error of the scattering parameters are all within 2% (Table 7.40), so it can be concluded that the 3-section lossless TEM line model can model the tapered line.

$w, h = 100\mu m$	s_{11}	s_{21}	s_{22}
Circuit 1t: $err/\%$	1.0604	0.21351	1.1570

Table 7.40: Percentage error between the simulated and calculated scattering parameters (lossless metal strip)

Fig. 7.11 shows the degree of fitness between the scattering parameters of Circuit 1t and those of the tapered line. It is seen that the plots are nearly the same as those of the non-TEM model (Fig. 6.13) because their matching results are very close (Table 6.23 and 7.40). Therefore, both TEM and non-TEM model can be used to approximate the 20% perfect conductor metal strip tapered line.

7.3.2 With Conductor Loss

Since the non-TEM line model even cannot model the tapered line with conductor loss, it is expected that the TEM line model cannot as well. Table 7.41 shows the optimization results. It is seen that either negative parameter values are obtained or the parameter values are not in their reasonable range in the three cases.

7.4 Summary

The equivalent circuits with TEM lines have been used to match the microstrip

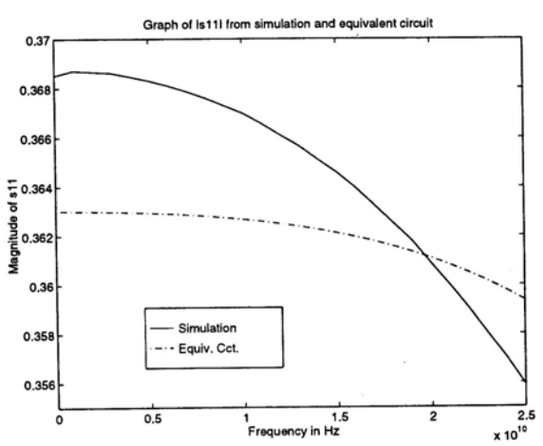

Magnitude of s_{11}

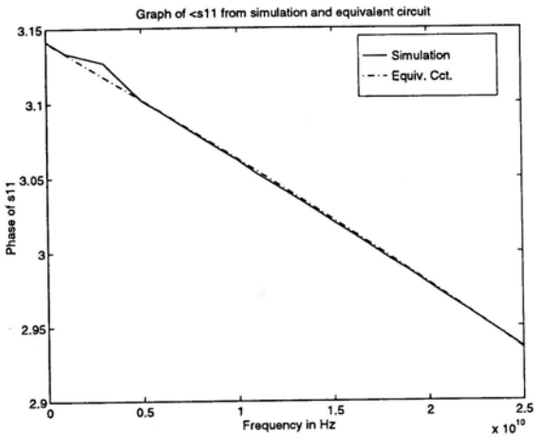

Phase of s_{11}

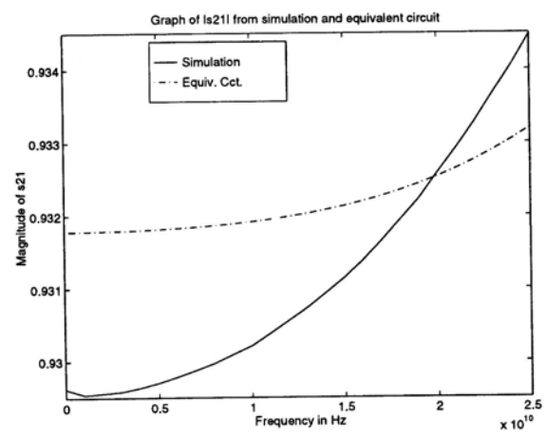

Magnitude of s_{21}

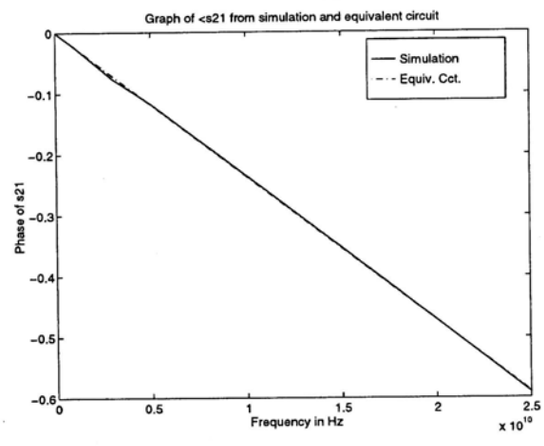

Phase of s_{21}

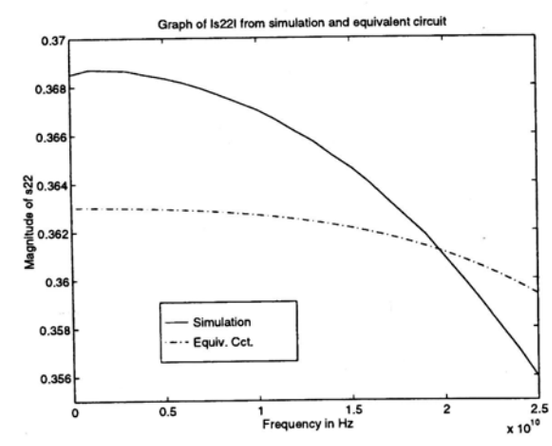

Magnitude of s_{22}

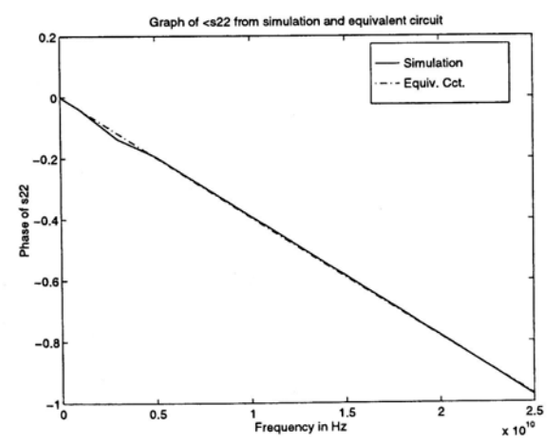

Phase of s_{22}

Figure 7.11: S parameters difference between simulation and circuit 1t (lossless metal strip)

R	L	G	C	$R_1/\Omega m^{-1}$	L_1/Hm^{-1}	G_1/Sm^{-1}	C_1/Fm^{-1}	l_1/mm
√	√	√	√	100.02	7.3118×10^{-7}	-9.2170×10^{-3}	9.1660×10^{-11}	0.098778
√	√		√	100.64	7.0720×10^{-7}	–	9.3540×10^{-11}	0.0990351
	√		√	–	1.9936×10^{-13}	–	-3.6864×10^{-10}	0.10186

R	L	G	C	$R_2/\Omega m^{-1}$	L_2/Hm^{-1}	G_2/Sm^{-1}	C_2/Fm^{-1}	l_2/mm
√	√	√	√	337.90	4.5293×10^{-7}	9.5564×10^{-3}	1.6128×10^{-10}	0.22022
√	√		√	312.76	4.5668×10^{-7}	–	1.6221×10^{-10}	0.10129
	√		√	–	8.0057×10^{-7}	–	3.1126×10^{-10}	0.29423

R	L	G	C	$R_3/\Omega m^{-1}$	L_3/Hm^{-1}	G_3/Sm^{-1}	C_3/Fm^{-1}	l_3/mm
√	√	√	√	−77.730	4.2825×10^{-7}	3.1811×10^{-2}	1.7526×10^{-10}	0.13205
√	√		√	5.1615×10^{-7}	4.2865×10^{-7}	–	1.7641×10^{-10}	0.10124
	√		√	–	1.0998×10^{-6}	–	9.4535×10^{-11}	0.083075

R	L	G	C	err
√	√	√	√	8.1163×10^{-2}
√	√		√	1.5422×10^{-1}
	√		√	2.8564×10^{-2}

Table 7.41: Parameter values of the equivalent circuit 1t (lossy metal strip)

discontinuities through the scattering parameters. Several conclusions are drawn:

- For the right-angled bend with perfect conductor as the metal strip, it is found that the TEM model plus a lumped circuit is quite adequate to model the bend.

- For all other cases, i.e., the right-angled bend with finite conductivity metal strip and the T-junction as well as tapered line with either infinite or finite conductivity metal strip, the non-TEM model is better to model the microstrip discontinuities. Although it is so, the equivalent circuits with TEM lines are adequate to model the three microstrip discontinuities (if there exists) within 10% in error for frequency up to 25GHz. In other words, the TEM model can be included into a CAD package such as SPICE.

Chapter 8

Conclusion

The lumped equivalent circuits, which mainly consist of inductors and capacitors, have been shown in both [JY92] and in Chapter 4 that they are inadequate in modelling the microstrip discontinuities with the signal having picosecond rise time. In this thesis, we have proposed several equivalent circuits to model the three types of microstrip discontinuities: right-angled bend, T-junction, and tapered line. It has been shown in Chapters 6 and 7 that these equivalent circuits are able to model the microstrip discontinuities with wideband frequency spectrum (The maximum frequency being used is up to 25GHz).

The equivalent circuits basically consist of distributed and/or lumped circuit element, so it is necessary to find a good equivalent circuit to model a uniform microstrip line. After several trial and error, the equivalent model shown in section 5.1 has been adopted. By using this model, the performance of the proposed equivalent circuits are good. The relative errors of the scattering parameters between the microstrip discontinuities and the corresponding equivalent circuits are found to be less than 10%, which is tolerable from the engineering point of view. So these equivalent circuits can be used in CAD designing tools to help reduce the VLSI design and simulation time.

Besides using the non-TEM lines in the wideband equivalent circuits to model the microstrip discontinuities, TEM lines have also been used to do the modelling. It is found that in most cases they are able to model the microstrip

discontinuities. However, the performance is worse than the non-TEM model's in general. Although it is so, the equivalent circuits with TEM lines are still preferred because these models can easily be included into some existing CAD packages such as SPICE (In SPICE, only transmission lines with constant $RLGC$ values are accepted.).

The research project consists of two stages. The first stage is to use the HFSS software to calculate the scattering parameters of the microstrip junctions. The software employs the finite element method to solve the field distribution inside the geometry. It is experienced that it takes very long time for the software to calculate a set of scattering parameters of a given geometry. So full wave analysis is not suitable in the engineering design except that the exact solution is needed. Our approach (finding equivalent models) is one of the choices and the results obtained are acceptable in the engineering sense.

The second stage is to find the wideband equivalent circuits to model the microstrip junctions by using some numerical optimization technique. Since the method is a purely numerical approach, the optimization results may not give any physical meaning. For example, negative values of the circuit parameters may result during minimizing the cost function. Moreover, the parameter values may not be practical. For instance, the width of the metal strip of the right-angled bend is $250\mu m$ but that of the equivalent circuit may be found to be some tens times larger. All of these abnormal phenomena may be due to the cost function being trapped into a local minimum[1] or the initial guess being wrongly estimated. The latter problem can be solved by trying different initial guesses. The former problem may not be easy to solve because the Least-Marquardt algorithm does not ensure to find a global minimum. So the numerical results can be adopted only when they are comparable to the physical dimension of the geometry or the typical values.

[1]It is experienced that the cost functions of some equivalent circuits seem to have many nearly same-valued local minima (like a plateau) so that the optimization is difficult to perform.

In this thesis, we have just shown that the wideband equivalent circuits are able to model the three microstrip junctions with picosecond rise time signal. To make these wideband equivalent circuits more applicable, prototypes of the microstrip discontinuities, the usual material used in the VLSI design, and different geometries of the microstrip discontinuities should be made to obtain their scattering parameters. Then the optimization is done with these scattering parameters. The found parameter values of the equivalent circuits can be stored as a lookup table in some CAD designing tools with the design rules of the microstrip discontinuities, so that they can be easily called for later use. This is one of the future directions in continuing the research.

References

[AA80] P. Anders and F. Arndt. "Microstrip Discontinuity Capacitances and Inductances for Double Steps, Mitered Bends with Arbitrary Angle, and Asymmetric Right-Angle Bends". *IEEE Trans. on Microwave Theory and Techniques*, vol. MTT–28(no. 11):pp. 1213–1217, Nov. 1980.

[Bog90] Eric Bogatin. "A Closed Form Analytical Model for the Electrical Properties of Microstrip Interconnects". *IEEE Trans. on Components, Hybrids, and Manufacturing Technology*, vol. 13(no. 2):pp. 258–266, Jun. 1990.

[DCC90] T. Vu Dinh, B. Cabon, and J. Chilo. "New Skin-Effect Equivalent Circuit". *Electronic Letters*, vol. 26(no. 19):pp. 1582–1584, Sept. 1990.

[DKR+90] A. Deutsch, G. V. Kopcsay, V. A. Ranieri, J. K. Cataldo E. A. Galligan, W. S. Graham, R. P. McGouey, S. L. Nunes J. R. Paraszczak, J. J. Ritsko, R. J. Serino, and D. Y. Shih J. S. Wilczynski. "High-Speed signal Propagation on Lossy Transmission Lines". *Journal of Research and Development*, vol. 34(no. 4):pp. 601–615, July 1990.

[Dwo79] Lawrence N. Dworsky. *"Modern Transmission Line Theory and Applications"*, chapter 5. John Wiley & Sons, New York, 1979.

[FA72] A. Farrar and A. T. Adams. "Matrix Methods for Microstrip Three-Dimensional Problems". *IEEE Trans. on Microwave Theory and Techniques*, vol. MTT–20(no. 8):pp. 497–504, Aug. 1972.

[GE74] A. Gopinath and B. Easter. "Moment Method of Calculating Discontinuity Inductance of Microstrip Right-Angled Bends". *IEEE Trans. on Microwave Theory and Techniques*, vol. MTT–22:pp. 880–883, Oct. 1974.

[GGC81] K. C. Gupta, R. Garg, and R. Chadha. *"Computer-Aided Design of Microwave Circuits"*. Artech House, Dedham, Mass, 1981.

[Ham75] E. O. Hammerstad. "Equations for Microstrip Circuit Design". *Proc. European Microwave Conference Microwave Exhibitors & Publishers Ltd.*, pages pp. 268–272, 1975.

[Hew92] Hewlett-Packard Company. *HP 85180A High-Frequency Structure Simulator*, first edition, May 1992.

[HM93] P. H. Harms and R. Mittra. "Equivalent Circuits for Multiconductor Microstrip Bend Discontinuities". *IEEE Trans. on Microwave Theory and Techniques*, vol. 41(no. 1):pp. 62–69, Jan. 1993.

[HNR93] Jianqing He, Norris S. Nahman, and Sedki M. Riad. "A Causal Skin-Effect Model of Microstrip Lines". *IEEE MTT-S Digest*, pages pp. 865–868, 1993.

[Hof87] R. K. Hoffmann. *"Handbook of Microwave Integrated Circuits"*. Artech House, 1987.

[Jac89] Robert W. Jackson. "Full-Wave, Finite Element Analysis of Irregular Microstrip Discontinuities". *IEEE Trans. on Microwave Theory and Techniques*, vol. 37(no. 1):pp. 81–89, Jan. 1989.

[Jin93] Jianming Jin. *"The Finite Element Method in Electromagnetics"*. John Wiley & Sons, 1993.

[JY92] Ronald H. Johnston and Ming Yang. "A Comparison of Microstrip Line Discontinuity Models with Measured Data". *IEEE Trans. on Microwave Theory and Techniques*, pages pp. 1337–1340, 1992.

[Mar63] D. W. Marquardts. "An Algorithm for Least-Square Estimation of Non-Linear Parameters". *J. SIAM*, vol. 11(no. 2):pp. 431–438, Jun. 1963.

[Med92] Max W. Medley. *"Microwave and RF Circuits: Analysis, Synthesis and Design"*. Artech House, 1992.

[NG78] B. M. Neale and A. Gopinath. "Microstrip Discontinuity Inductances". *IEEE Trans. on Microwave Theory and Techniques*, vol. MTT–26(no. 10):pp. 827–831, Oct. 1978.

[NH72] Norris S. Nahman and Donald R. Holt. "Transient Analysis of Coaxial Cables Using the Skin Effect Approximation $A + B\sqrt{s}$". *IEEE Trans. on Circuit Theory*, vol. 19(no. 5):pp. 443–451, Sept. 1972.

[PB83] Protap Pramanick and Prakash Bhartia. "An Accurate Description of Dispersion in Microstrip". *Microwave Journal*, pages pp. 89–92, Dec. 1983.

[SB73] P. Silvester and P. Benedek. "Microstrip Discontinuity Capacitances for Right-Angle Bends, T Junctions, and Crossings". *IEEE Trans. on Microwave Theory and Techniques*, vol. MTT–21(no. 5):pp. 341–346, May 1973.

[SB75] P. Silvester and P. Benedek. "Correction to 'Microstrip Discontinuity Capacitances for Right-Angle Bends, T Junctions, and Crossing".

IEEE Trans. on Microwave Theory and Techniques, vol. MTT–23:pp. 456, May 1975.

[TG75] A. F. Thomson and A. Gopinath. "Calculation of Microstrip Discontinuity Inductances". *IEEE Trans. on Microwave Theory and Techniques*, vol. MTT–23:pp. 648–655, Aug. 1975.

[YEL90] Jiann-Shiun Yuan, William R. Eisenstadt, and Juin J. Liou. "A Novel Lossy and Dispersive Interconnect Model for Integrated Circuit Simulation". *IEEE Trans. on Components, Hybrids, and Manufacturing Technology*, vol. 13(no. 2):pp. 275–280, June 1990.